UNIVERSITÉ DE SHERBROOKE
Faculté de génie
Département de génie civil

CONCEPTION DES BIOSYSTÈMES D'OXYDATION PASSIVE DU MÉTHANE CONSIDÉRANT LEUR RÉPONSE À L'EFFET DE BARRIÈRE CAPILLAIRE

DESIGN OF PASSIVE METHANE OXIDATION BIOSYSTEMS CONSIDERING THEIR RESPONSE TO THE PRESENCE OF CAPILLARY BARRIER EFFECT

Thèse de doctorat
Spécialité: géotechnique environnementale

Bahar AHOUGHALANDARI

Jury: Alexandre R. CABRAL (directeur)
Serge LEROUEIL
Mathieu NUTH
Serge-Étienne PARENT

Sherbrooke (Québec) Canada Septembre 2016

تقدیم به مهر جاودان

مادرم،

و پدرم،

و به پاس شکیب ارجمندشان

RESUMÉ

La construction des biosystèmes d'oxydation passive du méthane (BOPM) est une option économique et durable pour réduire les émissions de méthane des sites d'enfouissement de déchets et des effets subséquents du réchauffement climatique. Les BOPM sont constitués de deux couches principales: la couche d'oxydation du méthane (MOL) et la couche de distribution du gaz (GDL). L'oxydation du méthane se produit dans la MOL par les réactions biochimiques des bactéries méthanotrophes, et la GDL est construite sous la MOL pour intercepter et distribuer les émissions fugitives de biogaz à la base de la MOL. Fondamentalement, l'efficacité d'un BOPM est définie en fonction de l'efficacité d'oxydation du méthane dans la MOL. Par conséquent, il est indispensable de fournir des conditions adéquates pour les activités bactériennes des méthanotrophes. En plus des paramètres environnementaux, l'intensité et la distribution du biogaz influencent l'efficacité des BOPM, et ils peuvent rendre le matériau de la MOL - avec une grande capacité d'accueillir les activités bactériennes - inutilisables en termes d'oxydation du méthane sur place. L'effet de barrière capillaire le long de l'interface entre la GDL et la MOL peut provoquer des émissions localisées de méthane, due à la restriction ou la distribution non-uniforme de l'écoulement ascendant du biogaz à la base de la MOL. L'objectif principal de cette étude est d'incorporer le comportement hydraulique non-saturé des BOPM dans la conception des BOPM, afin d'assurer la facilité et la distribution adéquates de l'écoulement du biogaz à la base de la MOL. Les fonctions de perméabilité à l'air des matériaux utilisés pour construire la MOL des BOPM expérimentaux au site d'enfouissement des déchets de St-Nicéphore (Québec, Canada), ainsi que celles d'autres de la littérature technique, ont été étudiés pour évaluer le comportement d'écoulement non-saturé du gaz dans les matériaux et pour identifier le seuil de migration sans restriction du gaz. Ce dernier seuil a été introduit en tant que un paramètre de conception avec lequel le critère de conception recommandé ici, c'est-à-dire *la longueur de la migration sans restriction de gaz* (LMSG), a été défini. La LMSG est considérée comme la longueur le long de l'interface entre la GDL et la MOL où le biogaz peut migrer à travers la MOL sans restriction. En réalisant des simulations numériques avec SEEP/W, les effets de la pente de l'interface, des paramètres définissant la courbe de rétention d'eau, de la fonction de la conductivité hydraulique du matériau de la MOL sur la valeur de la LMSG (représentant la facilité d'écoulement du biogaz à l'interface) et de la distribution de l'humidité (et par conséquent celle du biogaz) ont été évalués. Selon les résultats des simulations, la conductivité hydraulique saturée et la distribution des tailles de pores du matériau de la MOL sont les paramètres les plus importants sur la distribution de l'humidité le long de l'interface. Ce dernier paramètre influe également sur la valeur du degré de saturation et donc la facilité du biogaz à la base de la MOL. La densité sèche du matériau de MOL est un autre paramètre qui contrôle la facilité d'écoulement ascendant du biogaz. Les limitations principales de la présente étude sont associées au nombre de matériaux de MOL testés et à l'incapacité de SEEP/W de considérer l'évapotranspiration. Toutefois, compte tenu des hypothèses raisonnables dans les simulations et en utilisant les données de la littérature, on a essayé de réduire ces limitations. En utilisant les résultats des expériences et des simulations numériques, des étapes et des considérations de conception pour la sélection du matériau de MOL et de la pente d'interface ont été proposées. En effet,le comportement hydraulique non-saturé des matériaux serait intégré dans les nécessités de conception pour un BOPM efficace, de sorte que la capacité maximale possible d'oxydation du méthane du matériau de la MOL soit exploitée.

Mots clés : biosystèmes d'oxydation passive du méthane, le comportement hydraulique non-saturé, simulation numérique, le comportement d'écoulement du gaz, perméabilité à l'air

ABSTRACT

Implementation of passive methane oxidation biosystems (PMOB) is a cost-effective and sustainable solution to eliminate the methane emissions of landfills to the atmosphere and ensuing global warming effects. PMOBs consist of two main layers: methane oxidation layer (MOL) and gas distribution layer (GDL). The oxidation of methane occurs in MOL through the biochemical reactions of methanotrophic bacteria, and GDL is constructed beneath the MOL to intercept and distribute the fugitive biogas emissions at the base of MOL. Basically, the efficiency of a PMOB is defined based on the methane oxidation efficiency in MOL. Therefore, it is indispensable to provide adequate conditions for the bacterial activities of methanotrophs. In addition to the environmental parameters, the intensity and the distribution of the biogas reaching the MOL material influence the efficiency of PMOBs, and they may cause the MOL material possessing great capacity to host the bacterial activities to be unserviceable in terms of in-field methane oxidation. The capillary barrier effect along the GDL-MOL interface may provoke localized surface methane emissions, resulted from the restricted and/or non-uniform distribution of upward flow of biogas at the base of MOL. The main focus of present study is to incorporate the unsaturated hydraulic behavior of PMOBs into the design of PMOBs, providing adequate ease and distribution of upward flow of biogas at the base of MOL. The air permeability functions of the materials used to construct the MOL of experimental PMOBs at the St-Nicephore landfill (Quebec, Canada), along with other materials from the technical literature, were studied to evaluate the unsaturated gas flow behavior of the materials and to identify the threshold of unrestricted gas migration. This latter threshold was introduced as a design parameter based on which the recommended design criterion herein, i.e. *the length of unrestricted gas migration* (LUGM), was defined. LUGM is considered as the length along the GDL-MOL interface along which biogas can migrate upwards without restriction. Performing sets of numerical simulations in SEEP/W, the effect of slope of interface and the parameters defining the water retention curve and hydraulic conductivity function of MOL material on value of LUGM (representing the ease of upward flow of biogas at the interface) and distribution of moisture (and therefore biogas) along the GDL-MOL interface were assessed. The saturated hydraulic conductivity and the pore size distribution of the MOL material were the most influencing parameters in distribution of moisture along the interface. The latter parameter influences also the value of degree of saturation and therefore, the ease of biogas at the base of MOL. Dry density of MOL material is another parameter that controls the ease of upward flow of biogas. The main limitations of the present study are associated with the number of tested MOL materials and the inability of SEEP/W in considering the evapotranspiration. However, considering reasonable assumptions in simulations and using the data from the literature, it was attempted to reduce the limitations. Based on the results of experiments and numerical simulations, some design steps and considerations for selection of the MOL material and the slope of interface were suggested that incorporate the unsaturated hydraulic behavior into the design necessities for an efficient PMOB so that the maximum possible methane oxidation capacity of MOL material is exploited.

Keywords: passive methane oxidation biosystems, unsaturated hydraulic behavior, numerical simulation, gas flow behavior, air permeability

REMERCIEMENTS

Je souhaite transmettre mes sincères remerciements à :

Alexandre Cabral, mon directeur de recherche, pour tous les moments où il m'accompagnait comme un grand frère, pour la joie qu'il me donnait comme un ami précieux, pour avoir enlevé des obstacles sur mon chemin comme un père, et pour tout ce que je suis « speechless » à décrire…

Lalé et *Behna* (mes sœurs), *Sirous* (mon frère), *Babak* (mon beau-frère), *Marzié* (ma belle-sœur) et *Arshida* & *Arnika* (mes nièces) avec qui ma vie possède des belles couleurs et d'agréables fragrances…

Jean-Guy Lemelin, le technicien du laboratoire de mécanique de sols et géoenvironnement, qui ne me laissait jamais baisser les bras, qui encourageait ma « ténacité » et qui me ramenait vers des résultats fiables…

Serge Leroueil, professeur titulaire à l'Université Laval, qui n'hésitait jamais à collaborer avec nous et à nous fournir ses expériences précieuses de plusieurs dizaines d'années…

Tous mes amis et mes collègues pour leur présence appréciée dans ma vie : Samaneh Amirpour, Mitra Yousefi, Alireza Asadian, Elham Narimani, Bahman Khabiri, Mahbod Sedaghat, Orod Naghibi, Nasim Daemi, Fahimé Rafiee, Hilda Varshochi, Mathieu Nuth, Valérie Dussault, Yulia Vasianovich, Steeve Ambroise, Philippe Tétreault, Serge-Étienne Parent, Carolina Lopera, Sebastian Sanchez, Éliane Ndanga, Éric Bivumburanyiki, Marlon Capanema, Rocio Segura, Ana Oliveira, Karina Santamaria, mes amis de « les sentiers de l'Estrie », mes amis haïtiens (Christopher, Anglade, Wilson), mes amis brésiliens (Pedro et Guilherme) et quiconque a remplacé même une seconde de ma solitude par sa compagnie…

et finalement à *mon pays l'Iran* qui m'a accueillie sur la terre pour la première fois dans le monde, et qui m'a appris la persévérance pour faire du progrès, tasser les difficultés et créer le maximum possible du minimum existant…

TABLE OF CONTENTS

LIST OF FIGURES

LIST OF TABLES

LIST OF SYMBOLS

CH_4: methane
CO_2: carbon dioxide
O_2: oxygen
NH_4^+: ammonium
NO_3^-: nitrate
v_a: velocity of air flow
k_a: coefficient of air permeability
$\frac{\partial h_a}{\partial y}$: pore-air pressure gradient
P_s: absolute outlet air pressure
P_e: absolute inlet air pressure
Q: volumetric air flow rate
A: cross-sectional area of the sample
Δx: sample's height
g: acceleration of gravity (m/s^2)
μ: dynamic viscosity of air at ambient temperature
ν: cinematic viscosity of air at ambient temperature
M: empirical parameter of the Ball et al. [1988] equation
N: empirical parameter of the Ball et al. [1988] equation
θ_a: volumetric air content
$\theta_{a\text{-}occ}$: volumetric air content at occlusion
$\theta_{a\text{-}pocc}$: volumetric air content at pre-occlusion
S_r: degree of saturation
G_s: specific gravity of soil grains
C_u: coefficient of uniformity
D_{10}: effective diameter
f_{oc}: organic matter content
w: water content
w_{opt}: optimum water content
ρ_d: dry density
$\rho_{d\text{-}max}$: maximum dry density
K: gas intrinsic permeability
ψ: suction
k_{sat}: saturated hydraulic conductivity
k-fct: hydraulic conductivity function
θ_w: volumetric water content
θ_r: residual volumetric water content
θ_s: saturated volumetric water content
$\theta_{w\text{-}occ}$: volumetric water content at occlusion
$\theta_{w\text{-}pocc}$: volumetric water content at pre-occlusion
$\theta_{w\text{-}max}$: maximum volumetric water content
$\Delta\theta_w$: difference between maximum and minimum values of θ_w along the interface
a: curve fitting parameter for the van Genuchten [1980] model
n: curve fitting parameter for the van Genuchten [1980] model

m: curve fitting parameter for the van Genuchten [1980] model
k_w: hydraulic conductivity

LIST OF ABBREVIATIONS

English:

GHG: greenhouse gas
PMOB: passive methane oxidation biosystems
GWP: global warming potential
MOL: methane oxidation layer
GDL: gas distribution layer
LUGM: length of unrestricted gas migration
WRC: water retention curve
MSW: municipal solid waste
k_a-function: air permeability function
AEV: air entry value
CB: capillary barrier
GSD: grain size distribution
$LUGM_i$: length of unrestricted gas migration within a segment
$LUGM_{sc}$: length of unrestricted gas migration along the sand-compost within a segment
SPP: Standard Proctor path
FDP: field density path
SACC: soil-air characteristic curve

Français:

CRE: courbe de retention d'eau
BOPM: biosystèmes d'oxydation passive du méthane
LMSG : la longueur de la migration sans restriction du gaz

CHAPTER 1. INTRODUCTION

1.1. General context and problematic

Every year, the biodegradation of organic wastes in landfills produces thousands of tons of biogas. The biogas produced in landfills contents 45-60% dioxide carbon (CO_2) and 40-55% methane (CH_4), both known as greenhouse gases (GHG) and responsible for climate change [IPCC, 2001]. Reduction of GHG emissions is a commitment to prevent the disaster of global warming, and several countries are trying to find solutions to reduce the dangerous anthropogenic interface of GHG with the climate system. Implementation of biogas collection systems and final covers are the most common solutions to eliminate the biogas emissions from landfills. However, neither of these systems is 100% efficient and therefore, some fugitive biogas would emit to the atmosphere.

Passive methane oxidation biosystems (PMOBs) are sustainable and cost-effective engineered systems that aim at reducing CH_4 fugitive emissions, i.e. the produced biogas not captured by gas collection systems or emitted from cracks and other preferential paths within the final cover. In PMOBs, CH_4 is oxidized into CO_2. Since the global warming potential (GWP) of CH_4 is 25 times greater than the GWP of CO_2, there is a net advantage to employ technologies that oxidize fugitive CH_4 emissions into CO_2. PMOBs are, indeed, parts of the landfill final cover, which may coat the whole surface of the cover, or may be locally incorporated into the existing cover – required by the regulations – to eliminate the observed fugitive emissions.

Methane oxidation occurs in the near surface methane oxidation layer (MOL) of PMOBs. This is where a group of naturally occurring and ubiquitous bacteria, the methanotrophs, oxidize CH_4 into CO_2 through the biochemical reactions. In addition to MOL, a layer of coarse-grained material is constructed beneath the MOL, which is called gas distribution layer (GDL). GDL aims at intercepting fugitive emissions and distributing them at the base of MOL. The idea is to avoid emissions concentrated in preferential pathways, which may lead to the formation of hotspots. In other words, good PMOB design requires fugitive emissions intercepted by the GDL to be uniformly distributed as possible [Cabral et al., 2010b;

Fredenslund et al., 2010; Gebert et al., 2011a; Pokhrel et al., 2011; Rachor et al., 2011; Scheutz et al., 2011; Ndanga et al., 2015].

Several environmental and biological studies report on factors controlling or influencing CH_4 oxidation in PMOBs, such as temperature, CH_4/O_2 ratio, pH, moisture, nutritional sources, vegetation and the texture of the MOL material [e.g. Einola et al., 2007; Ait-Benichou et al., 2009; Huber-Humer et al., 2009; Gebert et al., 2011a; Scheutz et al., 2011; Capanema and Cabral, 2012; Chi et al., 2012; He et al., 2012; Roncato and Cabral, 2012; Ndanga et al., 2015; Tate, 2015]. The share of air-filled pores [Gebert et al., 2011a; Rachor et al., 2011] and the distribution of CH_4 at the base of MOL [Cabral et al., 2010a; Fredenslund et al., 2010; Scheutz et al., 2011] influence the CH_4/O_2 ratio within the MOL and CH_4 loading (concentration and flux of methane) at the base of MOL. These two are of particular concern for this study.

The share of air-filled pores, which depends on the dry density and degree of saturation of MOL materials, controls the ease of gas flow through the soil pores [Langfelder et al., 1968; Springer et al., 1998; Maciel and Jucá, 2000; Marinho et al., 2001; Jucá and Maciel, 2006; Tang et al., 2011]. In PMOBs, the precipitation, the choice of initial dry density of MOL material and the settlements in MOL affect the amount of available air-filled pores for downward flow of O_2 and upward flow of CH_4 within the MOL. Moreover, the capillary barrier effect along the interface between GDL and MOL may cause the accumulation of seepage in MOL, non-uniform distribution of moisture along the GDL-MOL interface of inclined PMOBs and the occlusion of air-filled pores, which could provoke the restricted upward flow of biogas at the base of MOL. The capillary barrier effect results from the contrast between the unsaturated hydraulic behavior of MOL and GDL materials. Consequently, the biogas would be deviated non-uniformly within the GDL toward the available flow paths – with lower degrees of saturation – in MOL.

The greater the available surface for unrestricted upward flow of biogas at the base of MOL, the more efficient the CH_4 oxidation in MOL would be. The upward flow of biogas through the preferential pathways may create local surface biogas emissions with concentrations greater than that accepted by regulations, i.e. hotspots, especially at upslope of inclined PMOBs.

1.2. Definition of research project

The field measurements and numerical analyses performed on three experimental inclined PMOBs in Canada, Germany and Netherlands prompted the present study. The resulting observations are as follows:

- *St-Nicephore, Quebec, Canada (PMOB2)*: non-uniform distribution of CH_4 concentrations in surface scans, i.e. greater concentrations at upslope than that associated with downslope. The surface emissions, however, were all lower than 500 ppm, the accepted range by Quebec regulations [Cabral et al., 2010b].

- *Germany and Netherlands*: reports of persistent presence of hotspots at upslope of both PMOBs in Germany [Bohn and Jager, 2011] and Netherlands [Röwer et al., 2012].

- *Numerical analysis*: degrees of saturation greater than 85% (considered as the occlusion of air-filled pores) along the interface between MOL and GDL of the latter two PMOBs in steady-state simulations using SEEP/W [Tétreault et al., 2013].

Since 2006, sets of field and laboratory measurements have been performed to evaluate the efficiency of several experimental PMOBs constructed at the St-Nicephore landfill, where very low surface methane concentrations and high efficiencies in methane oxidation and odor reduction were reported [e.g. Jugnia et al., 2008; Ait-Benichou et al., 2009; Abdolahzadeh et al., 2010; Cabral et al., 2010b; Capanema and Cabral, 2012; Roncato and Cabral, 2012; Lakhouit et al., 2014; Ndanga et al., 2015]. However, the field measurements of PMOB2, conducted by Cabral et al. [2010b], showed high average values of degree of saturation (75% - 90%) in MOL close to the GDL-MOL interface. The results of laboratory-scale column experiments on the material used to construct the MOL of the German PMOB showed 100% methane oxidation efficiency. In addition, the profile of field tests indicated that the MOL material can provide an adequate milieu for methane oxidation. The moisture contents, however, were higher at downslope of the PMOB than that given by the upslope [Bohn and Jager, 2011]. Performing sets of laboratory column tests, high methane oxidation efficiencies

were obtained for the MOL material of the PMOB constructed in the Netherlands [Gebert et al., 2011b]. Moreover, the field measurements showed that the methane oxidation efficiencies were ~85% over the majority of the surface [Röwer et al., 2012], although the methane concentrations were significantly increasing toward the upslope [Geck et al., 2012]. These observations show that, in addition to providing the environmental requirements for biological activities of methanotrophs, it is essential to design the PMOBs considering the unsaturated hydraulic parameters that influence the ease and the distribution of upward flow of biogas at the base of MOL. Otherwise, the biological capacity of the MOL material to oxidize the CH_4 would not be exploited adequately, and the materials remain unserviceable.

The present research project studies the flow of biogas within the MOL, influenced by unsaturated hydraulic behavior of the MOL material when superimposed over a coarser layer (GDL), which creates a capillary barrier effect along the GDL-MOL interface. In order to identify the threshold of unrestricted gas flow, the variation in coefficient of air permeability with degree of saturation was assessed for the materials used to construct the MOL of two experimental PMOBs at the St-Nicephore landfill (Quebec, Canada). The air permeability function was studied along with the water retention curves (WRCs) and the Standard Proctor curves of the materials. Indeed, the gas flow behavior, unsaturated hydraulic behavior and compaction behavior of the materials were evaluated simultaneously. Performing a parametric study, PMOB2 was simulated using unsaturated flow finite element modelling to study the effect of the slope of interface and parameters defining the WRC and hydraulic conductivity function of MOL material on value and distribution of moisture along the interface. The biogas flow behavior at GDL-MOL interface of an experimental PMOB constructed in Denmark was also evaluated. The interface of this PMOB has a jagged form, assuming that a permanent available pathway on top of each segment would be provided for upward flow of biogas, while the bottom parts are restricted due to the seepage accumulation. Performing sets of numerical simulations in SEEP/W, the validity of this assumption was assessed.

1.3. Objectives

Considering the necessity to provide the required ease and distribution of biogas at the base of MOL, the present study aimed mainly at responding the following question:

How to define a design criterion that incorporates the capillary barrier effect, the ease and the distribution of biogas at the base of MOL into the design of PMOBs?

In order to answer the question of the research, it was hypothesised that all the taken steps should converge on maintaining the widest possible surface at the base of MOL where gas migration upwards is unrestricted. Assuming PMOBs as semi-finite media, the length along the GDL-MOL interface – measured horizontally – where biogas can hypothetically migrate without restriction was denominated *length of unrestricted gas migration* (LUGM). It is proposed to adopt LUGM as one of the main design criteria, which should possess the greatest possible value in a good design of PMOB. Therefore, the objectives of the present study are defined as:

1) Identifying the threshold of unrestricted gas migration in MOL to be used as the end of the LUGM, using air permeability function or other accessible and easy-to-use geotechnical tools, such as WRC and Standard Proctor curve.

2) Evaluating the effect of unsaturated hydraulic behavior of the MOL material, including parameters defining WRC and hydraulic conductivity function, on distribution of moisture along the GDL-MOL interface.

3) Presenting design steps and recommendations, which help the choice of MOL material aiming at the longest possible LUGM and reducing the risk of hotspot creation.

1.4. Statement of originality

To the author's knowledge, this is one of the first studies that introduce hydraulic aspects of unsaturated flow of seepage and biogas in the design of PMOBs, by considering the importance of the capillary barrier effect along the GDL-MOL interface. It is also the first to introduce a design criterion for PMOBs, the one that is based on a coherent set of steps taken to achieve the main goal of a PMOB. The design criterion takes the form of the parameter LUGM, which translates the required ease of upward flow of biogas at the base of MOL. In

addition, the more influencing unsaturated hydraulic parameters of MOL material on value and distribution of moisture along the GDL-MOL interface were identified. The author believes that the design criterion and considerations presented herein, along with environmental requirements, would form a more comprehensive guideline for design of PMOBs.

1.5. Structure of the document

The present thesis consists of 6 chapters:

Chapter 2: A literature review is presented, which explains a brief theoretical basis on methane production in landfills and the role of passive methane oxidation biosystems in eliminating the methane emissions to the atmosphere. In addition, the principles of gas flow in unsaturated soils and capillary barrier effect are presented to clarify more elaborately the specific context of the present research project.

Chapter 3: It presents one of the submitted journal papers composed from the results obtained during the present research project. Sets of laboratory experiments were performed to obtain the air permeability functions, water retention curves and Standard Proctor curves of the materials used to construct the MOL of two experimental PMOBs at the St-Nicephore landfill (Quebec, Canada). The onset of abrupt decrease in coefficient of air permeability with volumetric air content was identified on air permeability functions, and was suggested as the design parameter to define quantitatively the LUGM. This latter threshold on air permeability function was correlated to the degree of saturation at air entry value of WRC and at line of optima in Standard Proctor curve. Moreover, the relationship between the shapes of air permeability function, WRC and Standard proctor curve were assessed to establish a methodology for obtaining the design parameter in the absence of air permeability function.

Chapter 4: This chapter includes the results of a parametric study submitted as a journal paper. Numerical simulations, using the finite element software SEEP/W, were conducted to evaluate the effect of the slope of interface and the parameters defining the WRC and hydraulic conductivity function of MOL material on value and distribution of moisture along

the GDL-MOL interface. Several values of variables were used and the ease and the level of uniformity in distribution of upward flow of biogas were studied, using the design parameter and design criterion presented in chapter 3. The reference simulation was an experimental PMOB at the St-Nicephore landfill (PMOB2) whose MOL material was evaluated in chapter 3.

Chapter 5: The results of transient-state SEEP/W simulations, performed on two experimental PMOBs constructed in Germany and Denmark, are presented. The design parameters were identified, using the methodology suggested in chapter 3. The German PMOB, where upslope hotspot was reported, was simulated using the data provided for the precipitation and GDL and MOL materials. There results were compared with those given by steady-state analysis conducted by Tétreault et al. [2013]. The innovative design of the Danish PMOB, i.e. jagged form of the GDL-MOL interface, was evaluated. Due to the lack of actual data of the site, the characteristics of the GDL and the MOL materials of PMOB2 (St-Nicephore, Quebec, Canada) were used in simulations. In order to enhance the performance of the Danish PMOB and approaching the aim of the idea behind constructing a jagged interface, the MOL was substituted by a two-layer MOL whose methane oxidation efficiency was studied by Ndanga et al. [2015]. In all analyses, the value of LUGM and the distribution of the volumetric water content along the GDL-MOL interface were assessed.

Chapter 6: A summary of the conclusions obtained from the laboratory experiments and the parametric study is presented in this chapter. In addition, some recommendations for future studies are presented to develop a more comprehensive documentation on the subject, with fewer limitations.

Appendix: A summary of several types of permeameter suggested in the technical literature to measure the coefficient of air permeability is presented in Appendix A. In addition, the new design of permeameter, used in the air permeability experiments of the present study, is described. Appendix B presents a conference paper, which was published based on the preliminary results obtained during the air permeability tests on the sand-compost mixture used to construct the MOL of PMOB2. Finally, Appendix C consists of a short report of numerical simulations performed to analyze the design of domestic wastewater refinement systems in Canada. The main objective was, in fact, the evaluation of the influence of

capillary barrier effect on occlusion of air-filled pores and biological activities of the aerobic bacteria inhabiting in the enviro-septic pipes and responsible for sewage refinement.

CHAPTER 2. LITERATURE REVIEW

2.1. Biogas production in landfills

Landfilling is a major element in municipal solid waste (MSW) management, which basically aims at protecting the environment against hazardous effects of the waste. Shortly after MSW disposal, the anaerobic degradation of the waste commences whose product, among others, is the biogas composed of 45-60% methane and 40-55% carbon dioxide. Both these latter gases are known as greenhouse gases (GHG), contributing to climate change. The global warming potential of CH_4 is 25 times greater than that given by CO_2 on a weight basis over a 100-year time period. The waste degradation can begin 3 months after the waste decomposition and it lasts over 20-50 years [Zamoranoa et al., 2007]. On 2005, the atmospheric concentration of CH_4 exceeded the natural range of the last 650,000 years, i.e. 320 to 790 parts per billion, which was determined from the ice cores [IPCC, 2001]. 3-10% of the anthropogenic CH_4 emissions belong to the landfills. In 2009, U.S. landfills were the third largest source of human-related CH_4 emissions and responsible for 17 % of overall [USEPA, 2011]. Forced by Kyoto protocol, several countries have to find the alternatives to mitigate CH_4 emissions.

Three main mechanisms define the reduction of methane emissions in landfills: microbial, physical and chemical. Microbial mechanism means the oxidation of methane by microorganisms, physical is the temporary storage of CH_4 in pores or being dissolved in water, and finally chemical mechanism is the process of slowing-down and bypass of gas flux [Huber-Humer et al., 2009]. Spokas et al. [2006] proposed a mass balance equation for the fate of the CH_4 produced by landfills, as follows:

$$CH_4 \text{ produced} = CH_4 \text{ emitted} + CH_4 \text{ collected} + CH_4 \text{ oxidized} + CH_4 \text{ migrated} + \Delta CH_4 \text{ stored} \quad (2\text{-}1)$$

The collected and the oxidized CH_4 parts of Equation (2-1) belong to the installation of biogas collection systems and landfill covers, which play a key role in eliminating the biogas emissions directly to the atmosphere. Figure 2-1 shows the illustration of Equation (2-1).

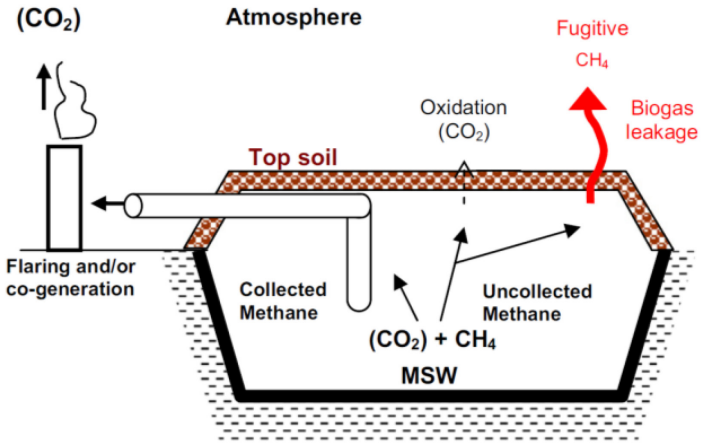

Figure 2-1: Fate of methane in a landfill cell, adapted from Staub et al. [2011]

Four steps can be defined for the typical landfill life, based on which the required system of biogas elimination will be selected: step A) operation, step B) post-operation, step C) aftercare, and step D) long-term custodial care. During step A, i.e. disposal and compaction of the waste, daily cover or a light geosynthetic layer without oxidation ability is installed. Some partial collection of biogas may be performed in modern landfills. Intermediate covers are installed during step B, to cover a section where waste will not be disposed for at least 1 year. Once the capacity of the landfill to accept the waste is attained, i.e. step C, a permanent final cover is constructed. During step D, the active monitoring of the landfill is not required any more, since no significant hazard for the environment is assumed [Barlaz et al., 2009; Spokas and Bogner, 2011; Staub et al., 2011]. Biogas collection systems are more efficient and cost effective while the decomposition of waste generates a large amount of methane. Therefore, according to the US Clean Air Act New Source Performance Standards (NSPS), the biogas collection systems must be installed within the first few years of step C or within 5 years after the last disposal of the waste, whichever occurs earlier [Barlaz et al., 2009; Spokas and Bogner, 2011]. These systems are composed of vertical wells and horizontal perforated pipes, where the collected CH_4 will be flared and therefore, oxidized to CO_2, or will be combusted to produce electricity and heat energy. According to IPCC [2001], the CO_2 emitted during biogas flaring in biogas collection systems and/or aerobic oxidation of CH_4 in cover systems

is not included in the emission calculation. However, flaring can release harmful products for the health into the atmosphere [Hettiarachchi et al., 2009]

When the rate of biogas generation is not sufficiently high for an efficient flaring – such as in old or abandoned landfills – the operation of biogas collection systems are technically and economically challenging [Huber-Humer et al., 2008; Scheutz et al., 2009a; Scheutz et al., 2009b; Chiemchaisri et al., 2010]. Consequently, biogas collection systems are ceased during the passive phase, i.e. step D, and hence, the biogas would be released to the atmosphere. Although the rate of biogas production decreases gradually, the quantity of long-term release of biogas could be considerable and harmful for the environment [Cabral, 2012]. Therefore, constructing the covers with the ability of methane oxidation, in the absence or in combination with biogas collection systems, would increase the capacity of CH_4 mitigation and the cost efficiency of the implemented systems to eliminate the hazards of the landfills. However, neither of these methods is 100% efficient in avoiding the migration of produced methane by the landfill to the atmosphere.

2.2. Passive methane oxidation biosystems

Oxidation of CH_4 into CO_2 through the implementation of biosystems is considered as a cost-effective method, which targets further reduction in fugitive emissions. The methanotrophic bacteria, inhabiting in constituting soil layers of the biosystems, oxidize the methane through aerobic biological processes. Equation (2-2) shows the biochemical reaction associated with the aerobic oxidation of CH_4:

$$CH_4 + 2O_2 \rightarrow CO_2 + 2H_2O + \text{heat} \qquad (2\text{-}2)$$

6-96% of the methane produced in a landfill could be oxidized by biosystems [He et al., 2012]. However, it still remains some fugitive emissions around gas collection or leachate drainage systems [Scheutz et al., 2011]. Passive methane oxidation biosystems (PMOBs) are indeed, engineered systems to enhance the natural oxidation of methane in landfills, to eliminate fugitive methane emissions, i.e. emissions not captured by biogas collection systems, or to control the emissions in old and small landfills where the installation of biogas

collection systems is not an economical choice. PMOBs can be used in landfills with great or low rate of CH_4 production [Huber-Humer et al., 2009; He et al., 2012], and they are constructed during the long-term custodial care [Staub et al., 2011]. Several studies reported very high methane oxidation efficiencies both in laboratory-scale experiments and in experimental field plots [e.g. Huber-Humer et al., 2009; Scheutz et al., 2009a; Cabral et al., 2010b; Rachor et al., 2011; Capanema and Cabral, 2012; He et al., 2012; Roncato and Cabral, 2012; Ndanga et al., 2015].

There are 3 types of PMOBs: 1) biocovers, 2) biowindows, and 3) biofilters. Biocovers replace the entire upper part of the semi-permeable existing cover (Figure 2-2a). Biowindows replace locally the existing cover and enhance the biogas transport to host the CH_4 oxidation process (Figure 2-2b). Biofilters are placed at the end of the biogas collection system to lead the biogas to the biofilter unit (Figure 2-2c) [Scheutz et al., 2011; Staub et al., 2011]. All types of PMOBs consist of two main layers: the near surface methane oxidation layer (MOL) where the CH_4 oxidation by methanotrophic bacteria occurs and the underlying gas distribution layer (GDL), which intercepts fugitive emissions and distributes them as uniformly as possible at the base of the MOL. Generally, the organic rich materials such as composts, sewage sludge, peat, etc., are used in the MOL material to enhance the growth of methanotrophic bacteria. The GDL consists preferably of coarse grained materials, in order to facilitate the distribution and the upward flow of biogas.

Several parameters control the methane oxidation efficiency of PMOBs, including the texture, temperature, moisture content, NH_4^+ and NO_3^- contents, vegetation, pH and CH_4/O_2 mixing ratio in MOL. Therefore, in order to enhance the methane oxidation efficiency of PMOBs, the MOL material should possess great organic matter content and water retention capacity, coupled with low thermal conductivity, good temperature insulation ability and enough porosity and air-filled pore volume [Huber-Humer et al., 2009; He et al., 2012].

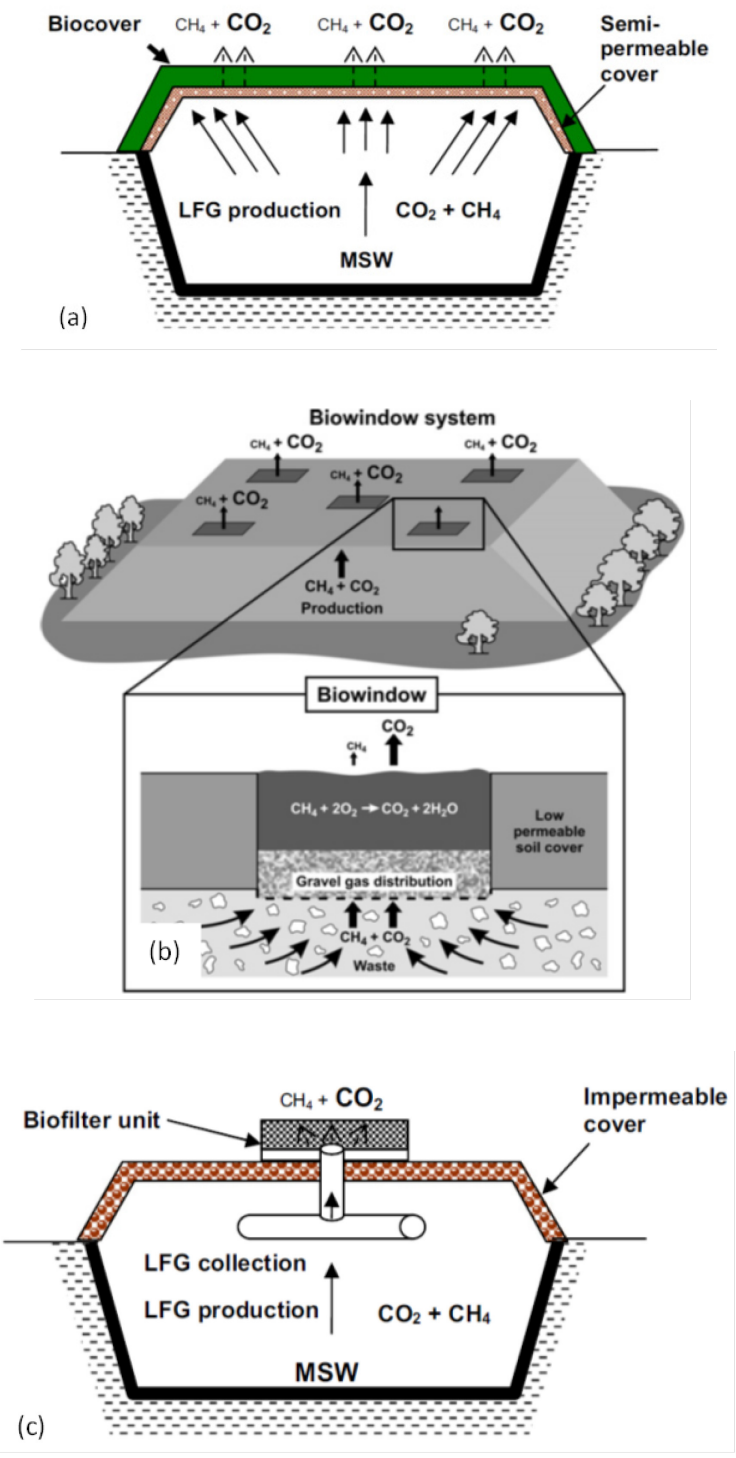

Figure 2-2: General concept of: (a) biocovers, adapted from Staub et al. [2011], (b) biowindows, adapted from Scheutz et al. [2011], and (c) biofilters, adapted from Staub et al. [2011]

The CH_4/O_2 mixing ratio, the flux of oxygen and CH_4 loading at the base of MOL play a vital role in methane oxidation activity of methanotrophs [Hrad et al., 2012]. The CH_4 oxidation increases linearly with a simultaneous increase in oxygen and methane concentrations,

meaning that a balance between the upward flow of methane and downward flow of oxygen is required. A CH_4/O_2 ratio of 1:3 is necessary for an efficient methane oxidation [He et al., 2012]. Under limited O_2 concentrations, active methanotrophs, inhabiting in the upper layers, do not develop and hence, the aerobic methane oxidation is limited [Chi et al., 2012]. The greater flux of oxygen than the CH_4 flux reduces the quality of gas in biogas collection system and increases the risk of fire inside the landfill [Jung et al., 2009]. In addition, under the great CH_4 loading at the base of MOL, methanotrohps cannot oxidize the methane fast enough and therefore, the methane directly emits to the atmosphere. The lower the CH_4 loading, the more the methanotrophs will be capable to oxidize the upward flow of biogas [Jung et al., 2009; Fredenslund et al., 2010; Gebert et al., 2011a; Pokhrel et al., 2011; Rachor et al., 2011; Scheutz et al., 2011; Ndanga et al., 2015].

In order to sustain the microbial activity of methanotrophs in PMOBs, the moisture content of MOL material equal to 10–20% is required [Chanton et al., 2011; Spokas and Bogner, 2011]. However, the upward flow of CH_4 and downward flow of O_2 are influenced by the moisture, and excessive moisture may limit the transport of CH_4 and O_2 within the MOL: the greater the degree of saturation, S_r, the lower the flux of CH_4 and O_2.

Consequently, in a good design of PMOB, the distribution and the magnitude of the moisture in MOL material can be considered as important physical parameters, controlling the methane oxidation efficiency by influencing the CH_4/O_2 mixing ratio, the distribution and the value of O_2 and CH_4 loading. GDL is basically constructed to help the distribution of methane at the base of MOL. Nonetheless, the capillary barrier effect along the GDL-MOL interface and ensuing accumulation of seepage may restrict the upward flow of biogas or disturb the distribution of biogas along the interface.

2.3. Flow of gas through unsaturated soils

In unsaturated soils, air can be in the form of a continuous phase or occluded air bubbles. The flow of free air (advection) through the unsaturated soils occurs when the air phase is continuous. The main mechanisms for flow of occluded air bubbles, however, are the diffusion and dissolved air flow by advection. The occluded air bubbles are air bubbles

distributed in soil phase and their continuous path is broken. The form of the air phase, i.e. continuous or occluded, is controlled by soil properties, water content and degree of saturation [Fredlund and Rahardjo, 1993; Lu and Likos, 2004; Fredlund et al., 2012]. Air flow systems in unsaturated soils are shown in Figure 2-3.

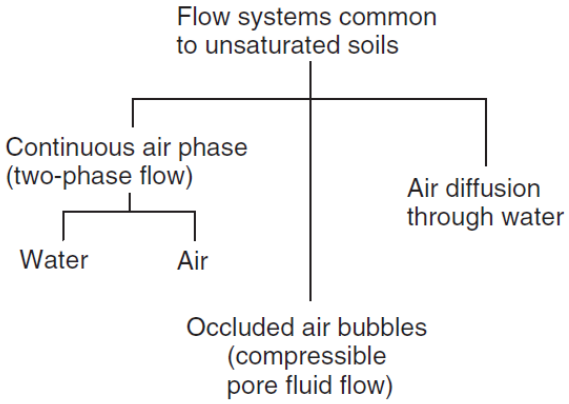

Figure 2-3: Air flow systems in unsaturated soils, adapted from Fredlund et al. [2012]

Concentration, density or pressure gradients govern the flow of free air through the continuous air phase of unsaturated soils. The pressure gradient is commonly considered as the only driving potential for the flow of free air. The gaseous diffusion is a process formed by a concentration gradient. In PMOBs, the dominant flow mechanism of CH_4 is more complicated. Indeed, depending on degree of saturation of materials, pressure gradient and concentration gradient, CH_4 would preferably flow by advection [Huber-Humer et al., 2008] or by diffusion [Pokhrel et al., 2011]. Since the process of waste biodegradation continues over time and the produced biogas can build up gradually, the gas pressure would be higher inside the landfill. Therefore, it can be speculated that the pressure gradient can be the primary driving force for upward flow of biogas [Vangpaisal and Bouazza, 2004; Barral et al., 2010]. Changes in ambience temperature or pressure can also result in greater pressure gradients [Rajesh et al., 2014].

In order to describe the flow of air through porous media, Fick's law or Darcy-type formulation can be used. Using the first Fick's law, a formulation for the gas flow can be obtained similar to Darcy's law [Fredlund et al., 2012]. This formulation is as follows:

$$v_a = -k_a \frac{\partial h_a}{\partial y} \quad (2\text{-}3)$$

$\frac{\partial h_a}{\partial y}$ is the pore-air pressure gradient, v_a is the velocity of air flow and k_a is the coefficient of air permeability. The coefficient of air permeability, under steady-state condition, for a gas that behaves in a similar manner to an ideal gas is calculated using Equation (2-4):

$$k_a = \frac{2 \times Q \times \mu \times \Delta x \times P_s \times g}{(P_e^2 - P_s^2) \times A \times \nu} \quad (2\text{-}4)$$

where P_s (Pa) is the absolute outlet air pressure, P_e (Pa) is the absolute inlet air pressure, Q is the volumetric air flow rate (m^3/s), A is the cross-sectional area of the sample (m^2), Δx is the sample's height (m), g is the acceleration of gravity (m/s^2), μ is the dynamic viscosity of air at ambient temperature (Pa.s), and ν is the cinematic viscosity of air at ambient temperature (m^2/s).

Coefficient of air permeability can be measured at several degrees of saturation (resulting from pairs of several initial dry density and water content values) and suctions, in order to obtain the air permeability function in the form of k_a (S_r), k_a (ψ) or k_a (θ_a), where ψ is the suction and θ_a is the volumetric air content. θ_a is defined as the ratio of the volume of air-filled pores to the total volume of a representative sample of the soil.

The general trend of the air permeability function shows that the coefficient of air permeability is largely influenced by the volume and the arrangement of the soil macropores. The k_a values decrease as the volumetric air content decreases (or S_r increases). At a particular θ_a value, where the air-filled pores become occluded and the air flows by the gas diffusion mechanism, an abrupt reduction in k_a value occurs. In addition, the more continuous and the less tortuous the air-filled pores are, the greater the k_a value would be. The onset of abrupt change in k_a values was reported to occur at suctions larger than air entry value (AEV) [e.g. Springer et al., 1998; Jucá and Maciel, 2006; Fredlund et al., 2012] or at optimum water content [e.g. Langfelder et al., 1968; Marinho et al., 2001].

Ball et al. [1988] suggested an exponential formulation between k_a and θ_a, which is similar to the Ahuja et al. model [1984] to relate the hydraulic conductivity and volumetric water content. The Ball et al. equation [1988] is shown in Equation (2-5) where M and N are empirical parameters. N is a pore continuity index, which represents the influence of θ_a, pore tortuosity and the surface area of the particles in k_a value.

$$k_a = M\theta_a^N \tag{2-5}$$

The air flow behavior through the soil can also be described by gas intrinsic permeability, *K*, which is independent of the nature of the migrating fluid and related to the nature of porous medium. Reichenauer et al. [2011] recommended the minimum value of 5×10^{-13} m^2 for the gas intrinsic permeability of the material used to construct MOL.

At a given void ratio, the intrinsic permeability measured to air in the dry sample should be similar to that with water in the saturated sample. However, Muskat [1937] reported large discrepancies between air intrinsic permeability and water intrinsic permeability. Klinkenberg [1941] explained that the interconnections between the pore capillaries and the gas molecules facilitate the flow of gas molecules through the pores. Therefore, the gas intrinsic permeability would be larger than water intrinsic permeability. This phenomenon, which is known as "Klinkenberg effect" or "gas slippage", occurs when the diameter of pore capillaries is comparable to the mean free path of the gas, where the gas molecules collide with the walls of the pores more than with other gas molecules. Subsequently, the Darcy's law with the assumption of zero flow at walls seems to be invalidated by Klinkenberg effect, since the gas flow velocity at walls is not zero when the gas slippage occurs (Figure 2-4) [Fredlund et al., 2012]. Klinkenberg effect is more probable in fine grained porous media whose permeability is lower, and it is negligible at very large gas pressures [Wu et al., 1998]. In addition, the lower the degree of saturation, the more clear the Klinkenberg effect would be [Estes and Fulton, 1956].

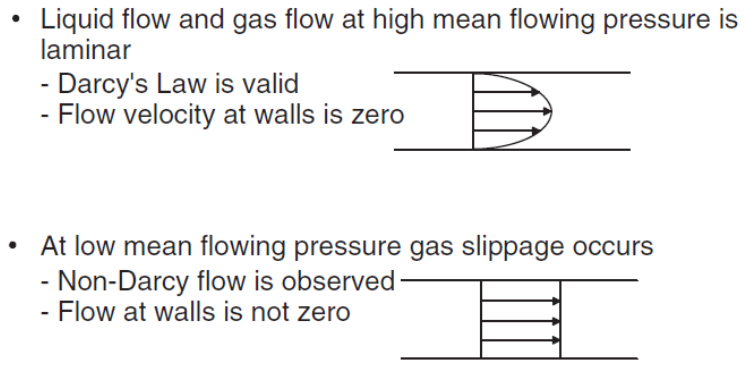

Figure 2-4: Validity of Darcy's law for flow of gas in soils, at great or low mean gas pressure, adapted from Fredlund et al. [2012]

2.4. Capillary barrier effect

The capillary barrier effect (CBE) is formed along the interface of two superimposed layers of porous materials possessing contrasting unsaturated hydraulic properties. Indeed, within a particular range of suction values, the hydraulic conductivity value of the upper layer (moisture retention layer, MRL) is greater than that associated with the bottom layer (capillary break layer, CBL). Therefore, when the seepage reaches the top of the MRL, the MRL retains the seepage by capillary forces and limits the percolations toward the CBL[Lu and Likos, 2004].

The sharper the difference between pore size distribution and particle size of the two layers, the more efficient the capillary barrier would be. Proper drainage of the MRL, through the implementation of drainage systems or imposing the inclination, helps maintaining the relatively high suction values along the interface within the range of functional CBE. The combination of gravity force and the CBE along an inclined CBL-MRL interface results in a two dimensional lateral seepage in MRL. Subsequently, the suction would be decreasing and S_r would be increasing toward the downslope. Starting from a particular point (or region), denominated as *breakthrough point*, the capillary forces and the ensuing CBE are not functional anymore and the vertical percolation toward the CBL commences. The horizontal distance from the upslope, along which the CBE is efficient, is known as *diversion length* (DL).

Several equations were suggested to calculate the DL under the steady-state condition, which consider the value of DL as a function of hydraulic conductivity functions (*k-fct*) of the MRL and CBL materials, the slope the CBL-MRL interface and the infiltration rate. The DL may end where the downward flow through the CBL-MRL interface is equal to the steady seepage flow rate [Ross, 1990], which corresponds to the suction at CBL-MRL equal to the water entry value (WEV) of the CBL material [Steenhuis et al., 1991; Walter et al., 2000; Vachon et al., 2015]. The WEV is defined as the suction at which the seepage starts entering the macro-pores of the soil.

The CBE can be used to construct the final cover of landfills to prohibit the infiltrations into the landfill and ensuing leachate production [Stormont, 1996; Khire et al., 2000; Bussière et al., 2003a; Aubertin et al., 2006; Parent and Cabral, 2006; Abdolahzadeh, 2011], or to limit the acid-generation in mine tailings by restricting the downward diffusion of oxygen [Yanful, 1993; Wilson et al., 1995; Williams et al., 1997; Bussière et al., 2003b; Dagenais et al., 2005; Adu-Wusu and Yanful, 2006]. In final landfill covers with capillary barrier effect (CCBE), the design aims at providing the longest possible DL associated with the maximum seepage rates, required by the legislations. For oxygen barriers, the CBE should be efficient enough to yield great S_r values along the CBL-MRL interface and therefore, occluded air-filled pores and low enough coefficient of oxygen diffusion.

The requirements for the design of a PMOB with sufficient methane oxidation efficiency results in superimposing two soil layers, i.e. MOL and GDL, whose unsaturated hydraulic behavior would create the CBE along the GDL-MOL interface. For example, the *k-fct*s of the materials used to construct the MOL and the GDL of an experimental PMOB at the St-Nicephore landfill (Quebec, Canada) are shown in Figure 2-5. For suctions greater than ~4.5 kPa, the hydraulic conductivity of MOL material is greater than that associated with GDL material. Therefore, the CBE would be formed along the GDL-MOL interface and the MOL would retain the seepage, until the WEV of the GDL material is attained.

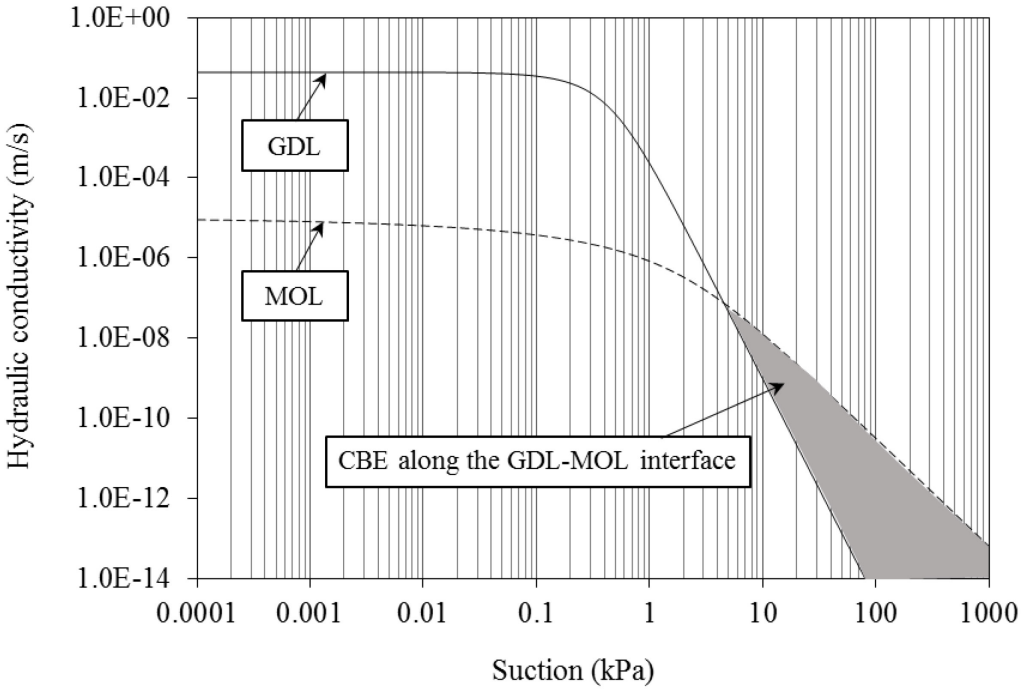

Figure 2-5: Hydraulic conductivity functions of the MOL and GDL materials, used to construct the experimental PMOB2 at the St-Nicephore landfill

Although the formation of CBE along the GDL-MOL interface of PMOBs may enhance the prohibition of percolations reaching the wastes, it increases the risk of occlusion of air-filled pores in MOL material attributed to the accumulation of moisture in MOL along the interface. Subsequently, the biogas would emit directly to the atmosphere through the regions with lower S_r values or preferential paths created by cracks. The methanotrophs cannot oxidize these latter emissions due to the CH_4 fluxes and concentrations higher than the capacity of methanotrophs or the lack of enough moisture for microbiologic activities. These local fugitive emissions may possess CH_4 methane concentrations greater than that accepted by legislations, and they are known as hotspots. The persistent presence of upslope hotspots have been reported during several years of field investigations on PMOBs constructed in Germany [Bohn and Jager, 2009] and the Netherland [Geck et al., 2012; Röwer et al., 2012].

CHAPTER 3. A NEW DESIGN CRITERION FOR PASSIVE METHANE OXIDATION BIOSYSTEMS

Avant-propos

Titre: Design of Passive Methane Oxidation Biosystems: Considerations about Compaction and Hydraulic Characteristics on Biogas Migration

Auteurs et affiliation:

Bahar Ahoughalandari: étudiante au doctorat, Université de Sherbrooke, Faculté de génie, Département de génie civil

Alexandre R. Cabral: professeur titulaire, Université de Sherbrooke, Faculté de génie, Département de génie civil

Serge Leroueil: professeur titulaire, Université Laval, Département de génie civil et de génie des eaux

Date de soumission: 31 mai 2016

Revue: Geotechnical and Geological Engineering Journal (Springer)

Titre français: La conception des biosystèmes d'oxydation passive du méthane : les considérations de compaction et des caractéristiques hydrauliques sur la migration du biogaz

Contribution au document:

This paper contributes to achieving the first objective of the research project, i.e. identification of the threshold of unrestricted gas migration in MOL to be used as the end of the LUGM. The air permeability functions, WRCs and Standard Proctor curves of the materials used to construct the MOL of two PMOBs at the St-Nicephore landfill (Quebec, Canada) were studied simultaneously. Depending on the behavior observed in WRCs or air

permeability functions of the materials, the threshold of the unrestricted gas migration was identified. Therefore, the *length of unrestricted gas migration* (LUGM) ends when this threshold is attained.

Résumé français :

L'effet de barrière capillaire le long de l'interface entre les deux couches principales des biosystèmes d'oxydation passive de méthane (BOPM), c'est-à-dire la couche d'oxydation du méthane (MOL) et la couche de distribution de gaz (GDL), peut provoquer une restriction sur l'écoulement ascendant du biogaz à la base de la MOL. Cela diminue l'efficacité de l'oxydation du méthane du BOPM et augmente les chances de produire des « hotspots ». Dans cette étude, les critères de la conception sont introduits afin de faciliter d'écoulement du biogaz. La courbe de rétention d'eau (CRE), la fonction de perméabilité à l'air (k_a-fonction) et la ligne d'optima (sur la courbe Proctor Standard) des matériaux utilisés pour la construction de la MOL de deux BOPMs expérimentaux au site d'enfouissement des déchets à St-Nicéphore (Québec, Canada) ont été obtenues au laboratoire. En outre, les caractéristiques principales d'autres matériaux de la littérature ont été exploitées. Par la suite, les critères de conception ont été définis en utilisant les degrés de saturation aux lignes d'optima et la tendance des k_a-fonctions et celle des CREs. En considérant ces critères de la conception des BOPMs, le risque des émissions élevées et localisées du méthane, attribuées à la migration bloquée de gaz à l'interface entre la GDL et la MOL, devrait être réduit.

Abstract: The capillary barrier effect along the interface between the two main layers constituting the passive methane oxidation biosystems (PMOB), namely the methane oxidation layer (MOL) and gas distribution layer (GDL), may result in restricted upward flow of biogas at the base of MOL. This decreases the methane oxidation efficiency of the PMOB and increases the chances of hotspot creation. In this study, design criteria are introduced to assess the ease of biogas flow. Laboratory experiments were conducted to obtain the water retention curve (WRC), air permeability function (k_a-function) and line of optima (on Standard Proctor curve) of the materials used to construct the MOL of two experimental PMOBs at the St-Nicephore (Quebec, Canada) landfill. In addition, the main characteristics for other materials were obtained from the literature. Design criteria were then defined based on the degree of saturation at the lines of optima and the pattern of k_a-functions and WRCs. Considering these criteria in the design of PMOBs may help reduce the risk of high surface methane emissions, localized near the top of the slope of PMOBs, caused by restricted gas migration at the GDL-MOL interface.

Keywords: passive methane oxidation biosystems, gas flow behaviour, capillary barrier effect, water retention curve, Standard Proctor curve

3.1. Introduction

Passive methane oxidation biosystems (PMOBs) are considered as cost-effective solutions to reduce fugitive CH_4 emissions, i.e. emissions not captured by gas collection systems. Generally, a PMOB consists of two main layers: the near surface methane oxidation layer (MOL), where methanotrophic bacteria oxidize CH_4 into CO_2, and the underlying gas distribution layer (GDL), mainly composed of coarse-grained materials. The main function of the GDL is to intercept fugitive emissions and distribute them as uniformly as possible at the base of the MOL, as illustrated schematically in Figure 3-1. The methane oxidation efficiency of PMOBs depends on several environmental and operational conditions, including the uniformity of the CH_4 loading (upward flow of fugitive biogas) at the base of the MOL. Greater uniformity facilitates the work of methanotrophic bacteria, which results in greater CH_4 oxidation efficiencies [Cabral et al., 2010a; Fredenslund et al., 2010; Scheutz et al., 2011].

The contrast between the unsaturated hydraulic properties of the constituent materials forming the MOL and GDL leads to the formation of a capillary barrier along their interface, which prevents water to flow from the MOL into the GDL. Consequently, the infiltration of meteoric water into a sloped PMOB and ensuing unsaturated flow would result in an increasing degree of water saturation (S_r) from the top of the slope to the bottom, along the GDL-MOL interface. Since S_r is a key parameter in controlling gas flow behaviour through unsaturated soils, the upward migration of fugitive biogas may be diverted within the GDL towards the drier (upslope) parts of the biosystem. This may eventually lead to the creation of a hotspot, i.e. a region of high CH_4 fluxes [Cabral et al., 2010a; Bohn and Jager, 2011; Röwer et al., 2012] and surface CH_4 concentrations that can be higher than acceptable by legislation.

Several environmental and biological aspects of methane oxidation in PMOBs have been well documented in the technical literature [Einola et al., 2007; Ait-Benichou et al., 2009; Huber-Humer et al., 2009; Gebert et al., 2011a; Scheutz et al., 2011; Capanema and Cabral, 2012; Chi et al., 2012; He et al., 2012; Roncato and Cabral, 2012; Ndanga et al., 2015; Tate, 2015]. Likewise, the literature abounds with studies that document and analyze air flow through unsaturated soils [Blackwell et al., 1990; Fredlund and Rahardjo, 1993; Vaughan, 2003; Lu and Likos, 2004; Fredlund et al., 2012], the influence of water content on the coefficient of air permeability [Langfelder et al., 1968; Springer et al., 1998; Maciel and Jucá, 2000; Marinho et al., 2001; Jucá and Maciel, 2006; Tang et al., 2011], and the design of oxygen barriers to prevent acid mine drainage [Yanful, 1993; Cabral et al., 2000; Bussière et al., 2003b; Mbonimpa et al., 2003; Maqsoud et al., 2011]. On the other hand, very little has been published about the effects of capillary barriers on CH_4 oxidation. For example, Tétreault et al. [2013] conducted a series of numerical simulations to assess the behaviour of two sloped PMOBs whose MOL and GDL formed capillary barriers. Their results showed that moisture content values were high all along the interfaces, which explained the concentrated fluxes usually found near the top of the two large-scale experimental plots. This behaviour was also observed by Berger et al. [2005], who constructed and monitored the behaviour of an inclined PMOB in the laboratory. In order to minimize the pore obstruction by water associated with the capillary barrier effect, Kjeldsen et al. [2013] constructed an experimental PMOB with a jagged ("zig-zag shape") GDL-MOL interface. With this very innovative design, the pores in MOL close to the interface and near every crest would be dry enough to allow unrestricted upward flow of biogas.

Despite the various field experiments presented in the technical literature, proper design criteria for PMOBs taking into consideration the capillary barrier effect and its consequences on upward biogas flow are still lacking. The focus on such criteria would be to help maximize upward biogas flow and uniformity of biogas distribution at the GDL-MOL interface. This can be translated into maintaining the longest possible length, taken horizontally, along the GDL-MOL interface where gas migration upwards is unrestricted and CH_4 loading is as uniform as possible. This length is referred herein as the *length of unrestricted gas migration* (LUGM).

Samples from the MOLs of two experimental PMOBs constructed at St-Nicephore (Quebec, Canada) landfill were analyzed in the laboratory in order to determine their main geotechnical parameters and subsequently to assess gas flow under unsaturated conditions at various initial dry density and water content values. Design parameters – associated with the design criterion LUGM – are proposed based on simple geotechnical tools, such as the water retention curve (WRC) and compaction (Standard Proctor) curve. Ultimately, design steps are considered based on the line of optima of the compaction curve, alone or combined with the WRC and air permeability function, when the latter two are available.

The main limitation of the proposed methodology to obtain the fundamental parameters used in the design of PMOBs is associated with the limited number of materials actually characterized in order to develop design criteria. However, the methodology was also applied to materials whose main characteristics were obtained from the literature.

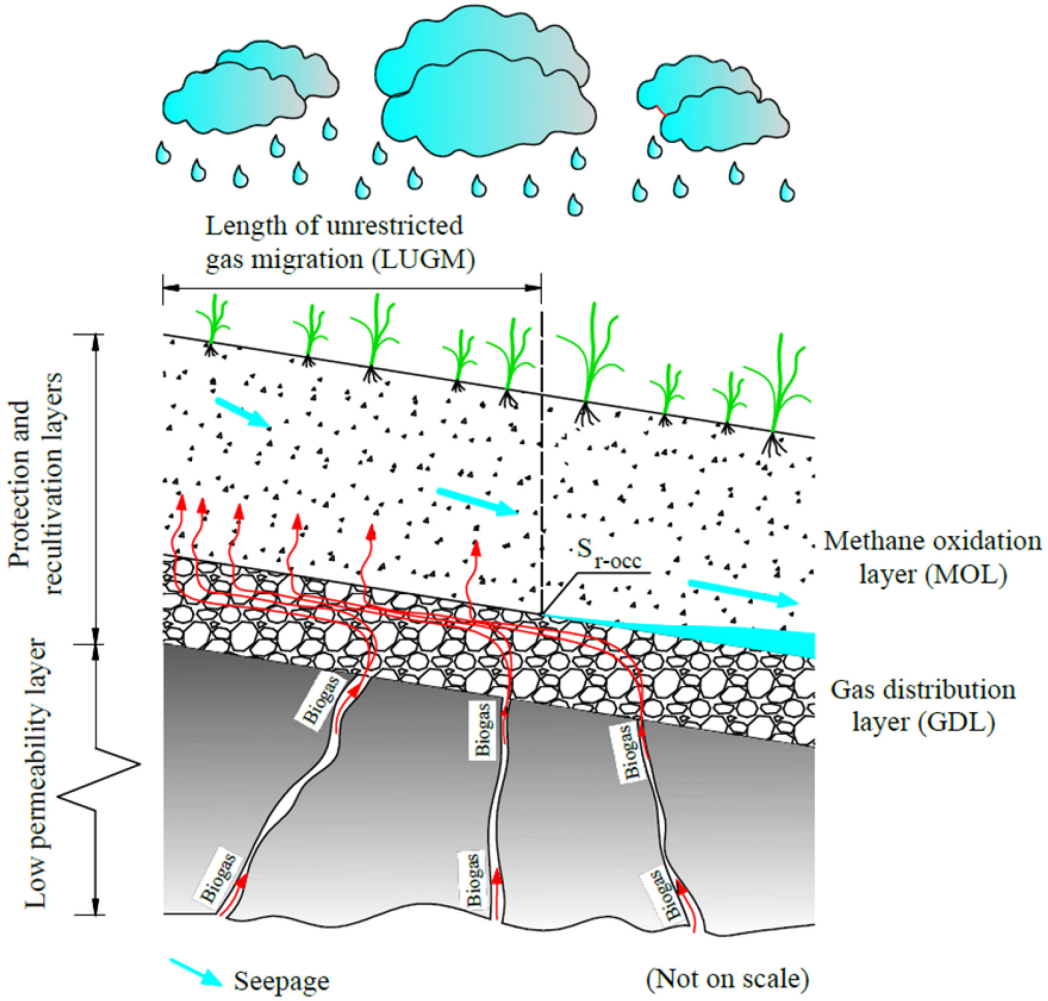

Figure 3-1: Schematic layout of a PMOB

3.2. Materials and methods

3.2.1. Materials

The material used to construct the MOL of the first experimental PMOB was a mixture of five volumes of compost and one volume of coarse sand (D_{10} = 0.07mm, D_{85} = 0.8mm, and the coefficient of uniformity (C_u) = 4.3) with the following characteristics: organic matter content (f_{OC}) equal to 17.8% $g_{o\text{-}m}/g_{dry\text{-}soil}$; specific gravity ($G_s$) equal to 2.24; optimum water content (w_{opt}) and maximum dry density ($\rho_{d\text{-}max}$) equal to 43% and 1080 kg/m^3, respectively (Standard

Proctor). The MOL of the second PMOB was constituted of uniform sand (D_{50} = 0.15mm and C_u = 2.25) with G_s = 2.71, w_{opt} ~ 12.0%, $\rho_{d\text{-}max}$ = 1750 kg/m^3.

The sand-compost mixture has been reported to show high methane oxidation capacity both in laboratory and field conditions [Cabral et al., 2010b; Roncato and Cabral, 2012]. The fine sand was selected by Ndanga et al. [2015] to be used in a multi-layer MOL that showed very high methane oxidation efficiencies both in laboratory-scale column experiments and in the field.

3.2.2. Testing

The Standard Proctor test for both materials was performed according to ASTM-D698 [2012]. Several test points were chosen to obtain the WRC and coefficient of air permeability (k_a) of the materials for a wide range of initial dry density (ρ_d) and water content values (circles in Figure 3-2). The compaction effort and method to prepare samples to determine the WRC and k_a were different from those used to obtain the compaction curve (Standard Proctor).

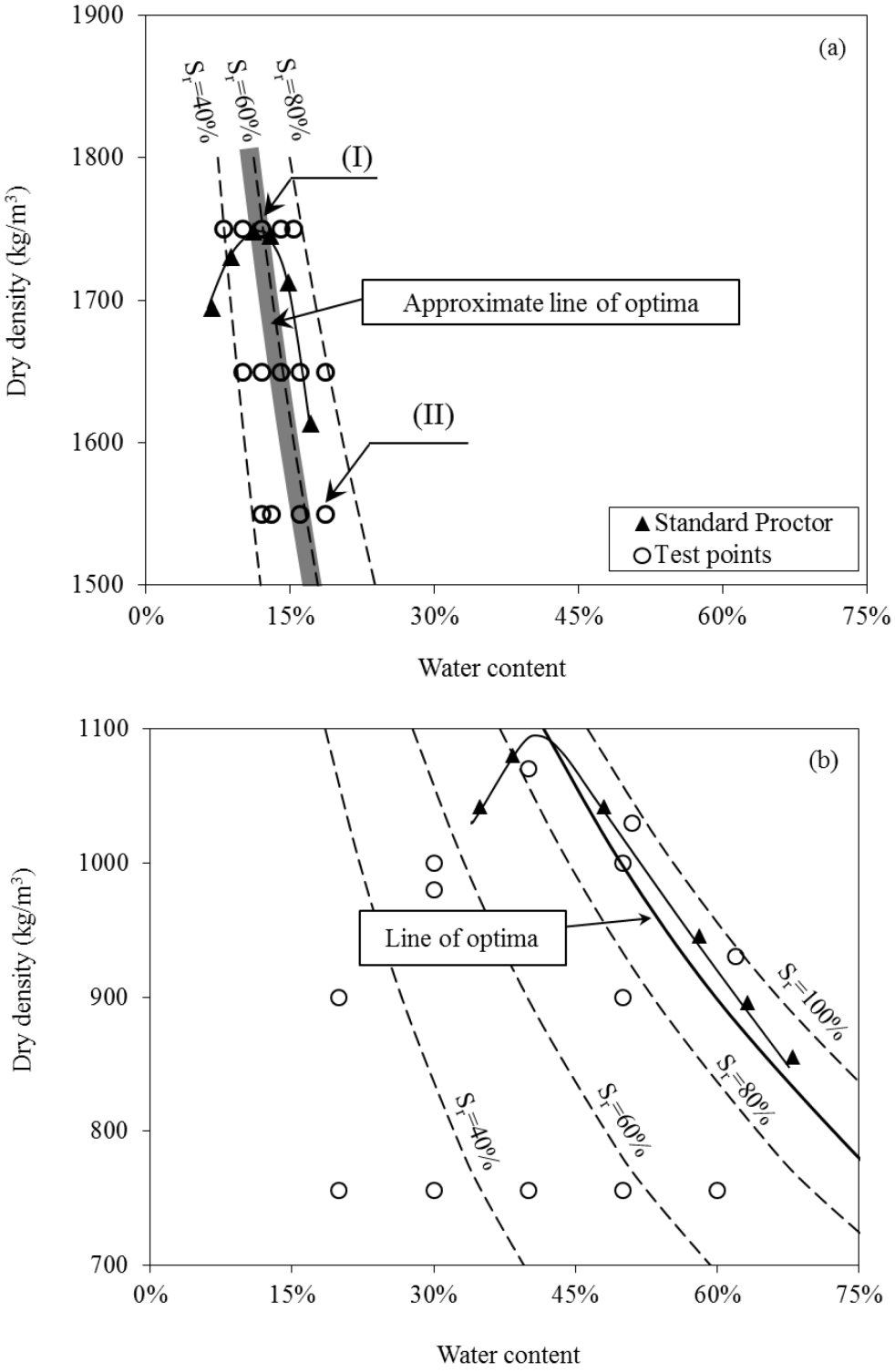

Figure 3-2: Standard Proctor curves and test points of (a) fine sand, and (b) sand-compost mixture

Test points to determine k_a and WRC were selected along 3 constant dry density paths (1550 kg/m^3, 1650 kg/m^3 and 1750 kg/m^3) for the fine sand. In the case of the sand-compost mixture, the test points were selected as follows: 4 initial water content and ρ_d values superimposing the Standard Proctor curve (herein denominated "Proctor path") and 3 constant dry density paths (750 kg/m^3 (in situ value), 900 kg/m^3 and 1000 kg/m^3). Samples with the required amount of water were kept in plastic bags for at least 48 hours before testing to allow the homogenization of moisture.

a. Water retention curve

The WRCs were obtained using the modular laboratory instrument HYPROP (UMS GmbH) and following its manual [HYPROP-UMS, 2013]. With this instrument, it is possible to determine the WRC (drying path) of a vertical soil column based on the evaporation method proposed by Wind [1968].

b. Coefficient of air permeability

The coefficient of air permeability was measured using a soap flow meter connected to the inlet of a triaxial cell. Each sample was compacted in a membrane surrounded by a rigid mold adapted to the triaxial cell. This mold is equipped with two holes on both sides, through which vacuum is applied during sample preparation to ensure that the flexible membrane sticks adequately to the mold and to the sample, thereby preventing air from flowing between the membrane and the sample. Once the sample preparation is completed, vacuum application is discontinued, but the mold remains in place. The mold was found to be an excellent substitute for the required confining pressure during the air permeability experiments. Several tests were performed to verify this assertion. In order to avoid any air leakage, both ends of the sample were sealed with two O-rings. Finally, the coefficient of air permeability for each test point (circles in Figure 3-2) was calculated for differential air pressure values ranging from 0.5 to 5.0 kPa, in increments of 0.5 kPa, as follows:

$$k_a = \frac{2 \times Q \times \mu \times \Delta x \times P_s \times g}{(P_e^2 - P_s^2) \times A \times \nu} \qquad 3\text{-}1$$

where k_a is the coefficient of air permeability (m/s), P_s (Pa) is the absolute outlet air pressure, P_e (Pa) is the absolute inlet air pressure, Q is the volumetric air flow rate (m^3/s), A is the cross-sectional area of the sample (m^2), Δx is the sample's height (m), g is the acceleration of gravity (m/s^2), μ is the dynamic viscosity of air at ambient temperature (Pa.s), and ν is the cinematic viscosity of air at ambient temperature (m^2/s).

In addition, the gas intrinsic permeability (m^2) of the porous medium, which is independent of the nature of the migrating gas, was calculated as follows:

$$K = \frac{k_a \times \nu}{g} \qquad 3\text{-}2$$

3.3. Results

3.3.1. Fine Sand

Figure 3-3 presents the WRCs of fine sand samples at each of the three values of ρ_d (Figure 3-2a) and two initial water content values: one dry and the other wet side of the line of optima. WRCs of the remaining test points (circles in Figure 3-2a) led to results quite similar to those shown in Figure 3-3 and are therefore not presented. As can be observed, for all dry density values in Figure 3-3, the air entry values (AEVs) of the sand are easily identifiable: they correspond to the suction values where the samples start to desaturate abruptly. It is noteworthy that the samples underwent negligible reduction in S_r for suction values lower than their respective AEVs. As expected, Figure 3-3 shows that the AEV increases from ~3 kPa to ~5 kPa with the increase in initial ρ_d from 1550 kg/m^3 to 1750 kg/m^3. Otherwise, AEVs for this material are approximately the same for both the dry and wet sides of optima.

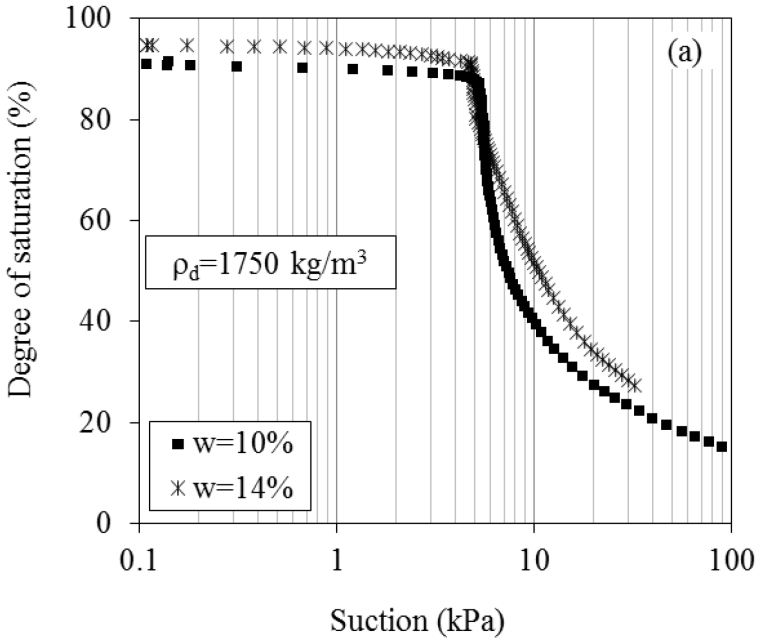
(a)
Degree of saturation (%)
100
80
60
40
20
0
0.1
1
10
100
Suction (kPa)
ρd=1750 kg/m3
w=10%
w=14%

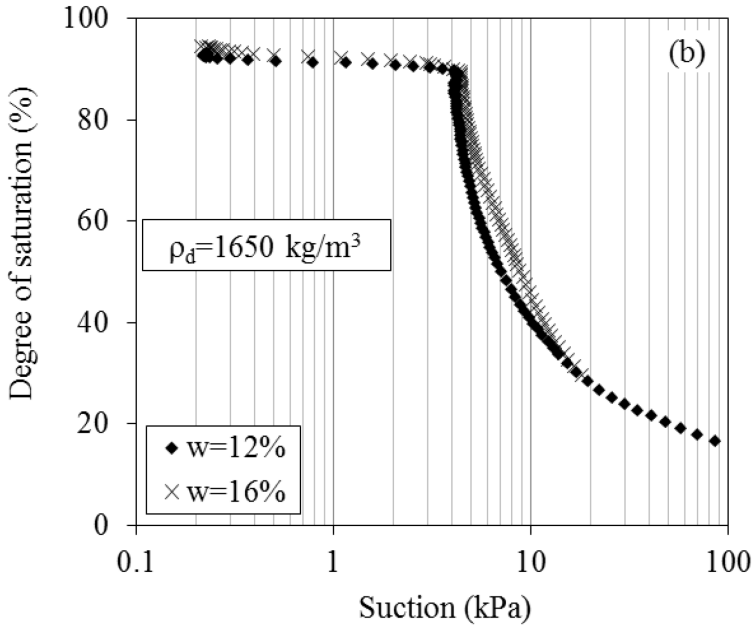
(b)
Degree of saturation (%)
100
80
60
40
20
0
0.1
1
10
100
Suction (kPa)
ρd=1650 kg/m3
w=12%
w=16%

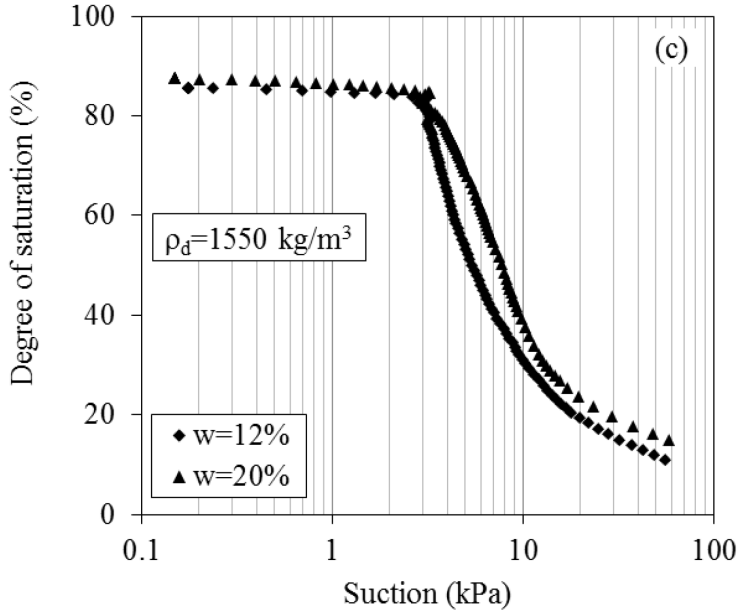

Figure 3-3: WRCs of fine sand samples at two initial water content values (one dry and the other wet of the line of optima) and three different values of initial dry density; (a) 1750 kg/m^3, (b) 1650 kg/m^3 and (c) 1550 kg/m^3

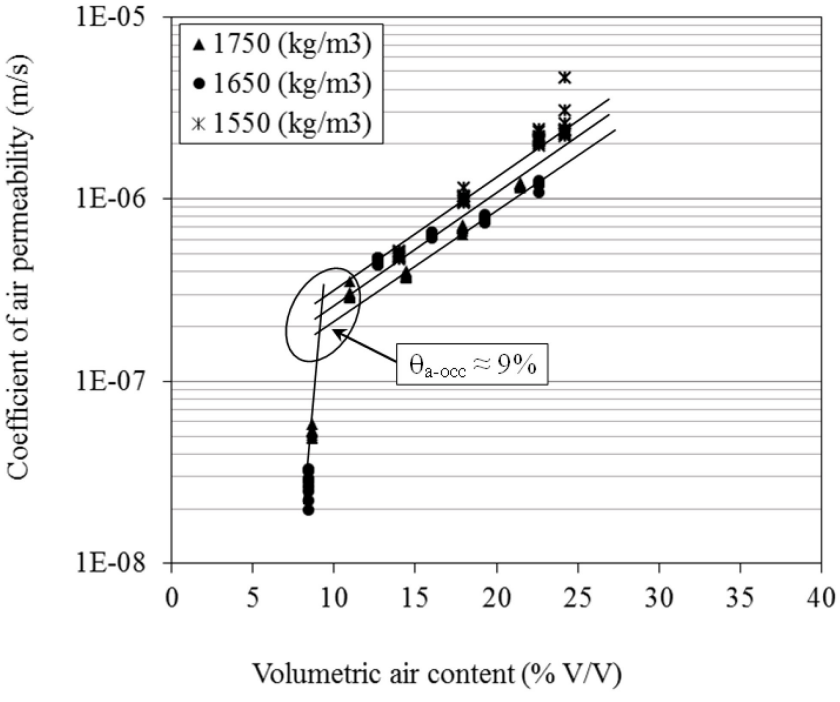

Figure 3-4: Variations in the coefficient of air permeability of fine sand with volumetric air content (θ_a), at several values of differential pressure

The relationship between the measured coefficient of air permeability (k_a) and volumetric air content (θ_a), herein denominated k_a-function, is presented in Figure 3-4 for the three values of ρ_d. θ_a is defined as the ratio of the volume of air-filled pores to the total volume of a representative sample of the soil. Each represents the value of k_a obtained at a particular θ_a and differential pressure value. Variations in volumetric air content (θ_a) are attributed to the simultaneous changes in initial ρ_d and water content of the sample. It is not clearly visible in the plot, but several data points corresponding to several values of differential pressure nearly coincide, indicating that the magnitude of the differential pressure has a minor effect on k_a.

Figure 3-4 shows that the logarithm of k_a decreases linearly between θ_a = 25% and ~9%. For θ_a < 9%, an abrupt decrease in k_a is observed. The θ_a associated with this abrupt change in k_a (in fact it is the threshold of detectable air flow during the experiments) is denominated herein "occlusion value", or $\theta_{a\text{-}occ}$. Therefore, $\theta_{a\text{-}occ} \approx 9\%$. This value corresponds to S_r between 70% and 75%, which are greater than the S_r associated with the line of optima (55%-60%; Figure 3-2a). Therefore, $\theta_{a\text{-}occ}$ occurrs on the wet side of the line of optima. The change in k_a with θ_a in the region indicated by an ellipse in Figure 3-4 appears very abrupt. Instead, there is probably a *transition zone* for the region defined by $8.5\% < \theta_a < 11\%$, for which air permeability tests were not performed. In any case, the radius of curvature of this latter *transition zone* would be small.

According to Figure 3-4, at a given θ_a, the k_a tends to decrease as ρ_d increases, but the differences are rather small for engineering purposes. For example, the tests singled out by arrows (I) and (II) in Figure 3-2a have nearly the same θ_a (≈ 15%), and k_a (I) ≈ $4x10^{-7}$ m/s and k_a (II) ≈ $5x10^{-7}$ m/s, respectively.

Since the ambient temperature was constant during air permeability tests, Figure 3-4 can also represent the pattern of gas intrinsic permeability variations with θ_a. Accordingly, it is possible to use the data shown in Figure 3-4 to assess the flow behaviour of CH_4 - instead of air.

3.3.2. Sand-compost mixture

Figure 3-5 presents the WRCs for the sand-compost mixture. Very small differences were observed between WRCs obtained for the "test points" on each initial dry density path, indicated in Figure 3-2b. Therefore, only representative WRCs are presented. The 2 WRCs in Figure 3-5a were obtained with samples prepared at two initial dry density and water content values along the Standard Proctor curve; one on the dry side and the other on the wet side. Those presented in Figure 3-5b were obtained with samples compacted to attain the initial ρ_d of a PMOB tested at the St-Nicephore landfill, i.e. 750 kg/m^3.

The AEVs are not as well defined as they were for the fine sand. Indeed, S_r started to decrease slowly for suction values lower than the value associated with the commencement of the desaturation zone. Accordingly, the radii of curvature around the AEVs are bigger than those observed in WRCs obtained with the fine sand. AEV values were ~1 kPa for the samples compacted at ρ_d = 750 kg/m^3 and greater than 3 kPa for $\rho_d \approx$ 1000 kg/m^3.

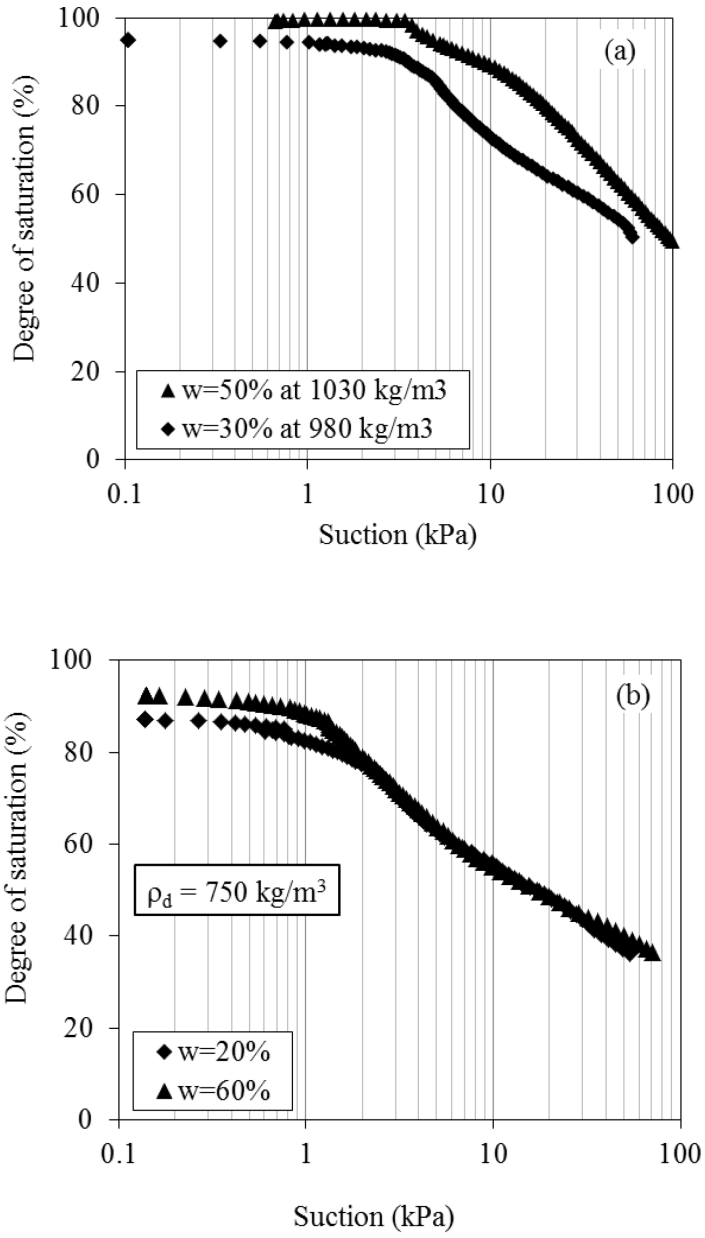

Figure 3-5: WRCs of sand-compost mixture samples at two initial water content values (dry and wet ofoptima) and at: (a) Standard Proctor dry densities (about 1000 kg/m^3), and (b) in situ ρ_d (750 kg/m^3)

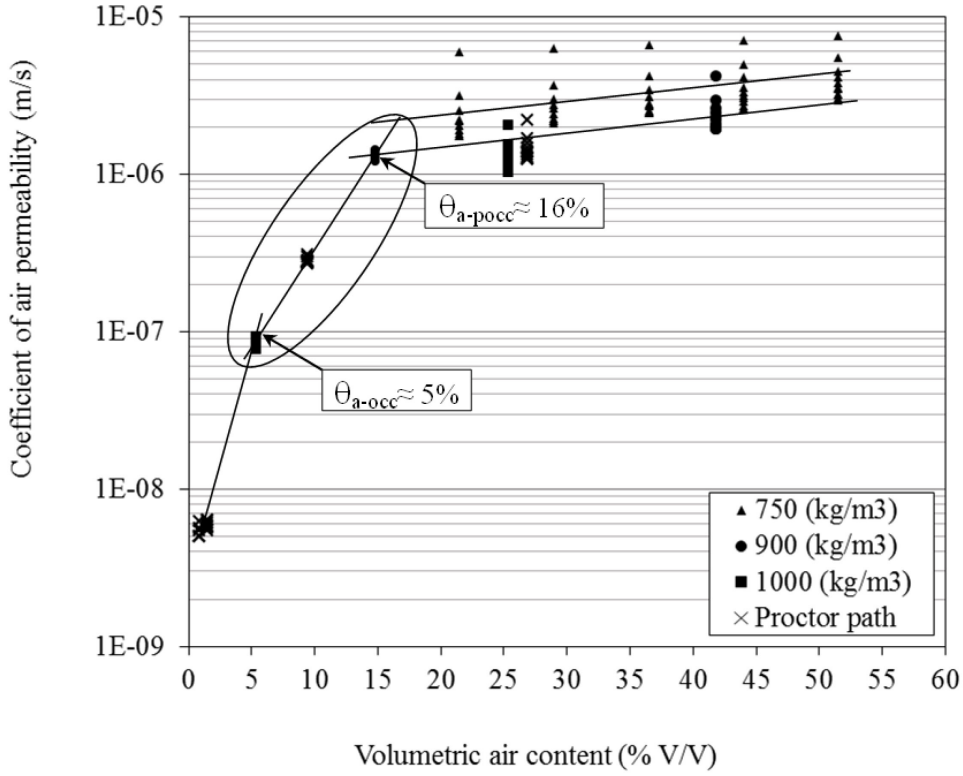

Figure 3-6: Variations in coefficient of air permeability of sand-compost mixture with volumetric air content (θ_a) at several differential pressure values

The k_a-function of the sand-compost mixture is shown in Figure 3-6 where, for each test point, the k_a value was also measured at several differential pressure values. As in the previous case, data points corresponding to several values of differential pressure coincide. In this case as well, considering that tests were performed at constant ambient temperature, the plot in Figure 3-6 can also represent the pattern of gas intrinsic permeability.

The curve can be subdivided into three zones whose borders are associated with two volumetric air content values. The first one is $\theta_a \approx 5\%$, which delimits the zone where the obtainment of k_a was challenging (the soap bubble inside the flowmeter is virtually immobile). In this case, $\theta_a \approx 5\%$ is herein denominated as $\theta_{a\text{-}occ}$. The second border is defined by $\theta_a \approx 16\%$. Above this value, k_a does not vary as much with changes in θ_a. This value is defined here as the pre-occlusion value, or $\theta_{a\text{-}pocc}$. In the case of the sand-compost, a *transition zone* can therefore be identified between $\theta_{a\text{-}pocc}$ and $\theta_{a\text{-}occ}$ (ellipse in Figure 3-6).

For the sand-compost, $\theta_{a\text{-}pocc}$ corresponds to S_r between 73% and 77%, which is lower than the S_r associated with the line of optima (~90% in Figure 3-2b), whereas $\theta_{a\text{-}occ}$ occurs when S_r

lies between 91% and 92%, i.e. approximately the S_r at the line of optima (and also the S_r value associated with AEV; Figure 3-5b).

Springer et al. [1998] also identified 3 zones in the k_a-function obtained following tests with silty sand samples compacted by dropping and stabbing on a constant dry density path. The first zone was identified as the zone of emergence of air permeability at air entry value. The second was associated with the maximum rate of air permeability variation until the gravitational drainage ceased, and the third was associated with the lowest rate of changes for lower values of volumetric water content (therefore greater values of volumetric air content on a constant dry density path).

3.4. Discussion

3.4.1. Relationships between the shapes of the Standard Proctor Curve, WRC and k_a-function

The establishment of a relationship between unsaturated air and water flow has been the focus of several studies published in the literature. For example, Ball et al. [1988] adapted an exponential relationship between hydraulic conductivity and water-filled porosity to relate the air permeability to the air-filled porosity, and validated it experimentally using samples of silty and clayey loam. Ba-Te et al. [2005] obtained a relationship in the form of $k_a = f(\psi)$, where ψ is the suction, by substituting the fitting equation of the WRC (S_r versus suction) into an empirical relationship between air permeability and degree of saturation. They validated this relationship using data sets from Singapore residual soils and Japanese soils. Kamiya et al. [2006] developed an apparatus to measure k_a, S_r and suction, simultaneously. Their results show a clear similarity between the shapes of WRC and k_a-suction curves for a river silty sand and three types of sandy soils. Ultimately, such relationships – in fact, the parameters that describe the shape of the curves – may be used to infer where $\theta_{a\text{-}occ}$ (and/or $\theta_{a\text{-}pocc}$) is located, which is an essential step in determining the *length of unrestricted gas migration* (LUGM), and assessing the level of uniformity in the distribution of gas flow within this length at the base of the MOL.

Materials tested in this study:

The relationships between WRCs, k_a-functions and Standard Proctor curves were identified in the cases of the fine sand and sand-compost mixtures tested in this study. For both materials, the shapes of WRC in the vicinity of the AEV (Figure 3-3 and Figure 3-5) show similarities with the corresponding k_a-functions in the vicinity of $\theta_{a\text{-}occ}$ for fine sand (Figure 3-4) and between $\theta_{a\text{-}pocc}$ and $\theta_{a\text{-}occ}$ for sand-compost (Figure 3-6). When there is a *transition zone* in the vicinity of the AEV, one of the design parameters could be $\theta_{a\text{-}pocc}$. If desaturation comes abruptly, further considerations (see discussion further in the text) are needed to define the design parameter.

It can be observed that the wider the horizontal distance between the S_r isolines on the Standard Proctor curves (Figure 3-2), the steeper the slope of the desaturation zone in the WRCs (Figure 3-3 and Figure 3-5, or Figure 3-7), and the steeper the slope of k_a-functions where $\theta_a > \theta_{a\text{-}occ}$ (fine sand; Figure 3-4) or $\theta_a > \theta_{a\text{-}pocc}$ (sand-compost; Figure 3-6). It can be observed in Figure 1 that the Standard Proctor curve for the sand-compost mixture spans over a much greater range of water content values than that of the fine sand. Accordingly, the S_r isolines of degree of saturation are wider apart in the case of sand-compost. This means that from the isoline associated with $S_{r\text{-}occ}$, a reduction of 20% in S_r for the fine sand would correspond to a meager decrease of ~5% in water content, whereas for the sand-compost, the same decrease of 20% from the isoline associated with $S_{r\text{-}occ}$ would lead to a ~18% decrease in water content. In practical terms, this means that slight changes in water content in the fine sand may lead to pore occlusion, while the sand-compost mixture requires greater moisture changes to attain occlusion. For fine sand, the WRC along the slope of the desaturation zone is considerably steeper than for the sand-compost mixture. Indeed, a 20% reduction in S_r corresponds to only 4 kPa increase in suction for fine sand (Figure 3-3), whereas suction increases nearly 35 kPa in the case of the sand-compost mixture (Figure 3-5). Furthermore, insofar as θ_a is greater than $\theta_{a\text{-}occ}$ (fine sand; Figure 3-4) or $\theta_{a\text{-}pocc}$ (sand-compost; Figure 3-6), the slope of the k_a-function is steeper for fine sand. Indeed, a 15% reduction of θ_a in fine sand leads to nearly one order of magnitude decrease of k_a, whereas it remains within the same order of magnitude for the sand-compost mixture.

It is noteworthy that the slope of the k_a-θ_a curve, for $\theta_a > \theta_a$ or $\theta_a > \theta_a$, reflects the sensitivity of k_a to changes in θ_a (or S_r under constant dry density conditions). Consequently, the steeper the slope of the k_a-θ_a curve of MOL material in an inclined PMOB, the greater the reduction in k_a as θ_a decreases (and S_r increases) toward the bottom of the slope of the PMOB. In addition, the distribution of k_a along the interface would be less uniform with respect to a PMOB with MOL material possessing a shallower slope of k_a-θ_a curve. Consequently, the slope of the k_a-θ_a curve of the MOL is directly related to the uniformity of upward biogas flow distribution at the base of the MOL.

Materials tested in other studies:

Figure 3-7 presents the WRC of materials tested in several other studies, in addition to representative WRCs of the fine sand (Figure 3-3) and sand-compost (Figure 3-5). As can be observed in Figure 3-7, the AEVs of the landfill cover material (Marinho et al. 2001), the clay [Jucá and Maciel, 2006] and the silty sand [Springer et al., 1998] are not very well defined, as is the case of the sand-compost tested in this study. The shapes of the WRC show that desaturation of these materials occurs gradually, in particular in the region where suction values are lower than those associated with the desaturation zone. Similarly to the fine sand tested in this study, the AEV of the sand tested by Kamiya et al. [2006] is clearly identified and both materials show abrupt desaturation once the AEV is attained.

The steepest desaturation zone observed in Figure 3-7 occurred for the fine sand tested in this study, followed by the sand tested by Kamiya et al. [2006]. The steepness of the desaturation zone of the 3 other materials, namely landfill cover [Marinho et al., 2001], silty sand [Springer et al., 1998] and sand-compost (this study) are rather similar, with the least steep being that of the sand-compost. In comparison with other published cases, the soils tested in the present study are thus extremes.

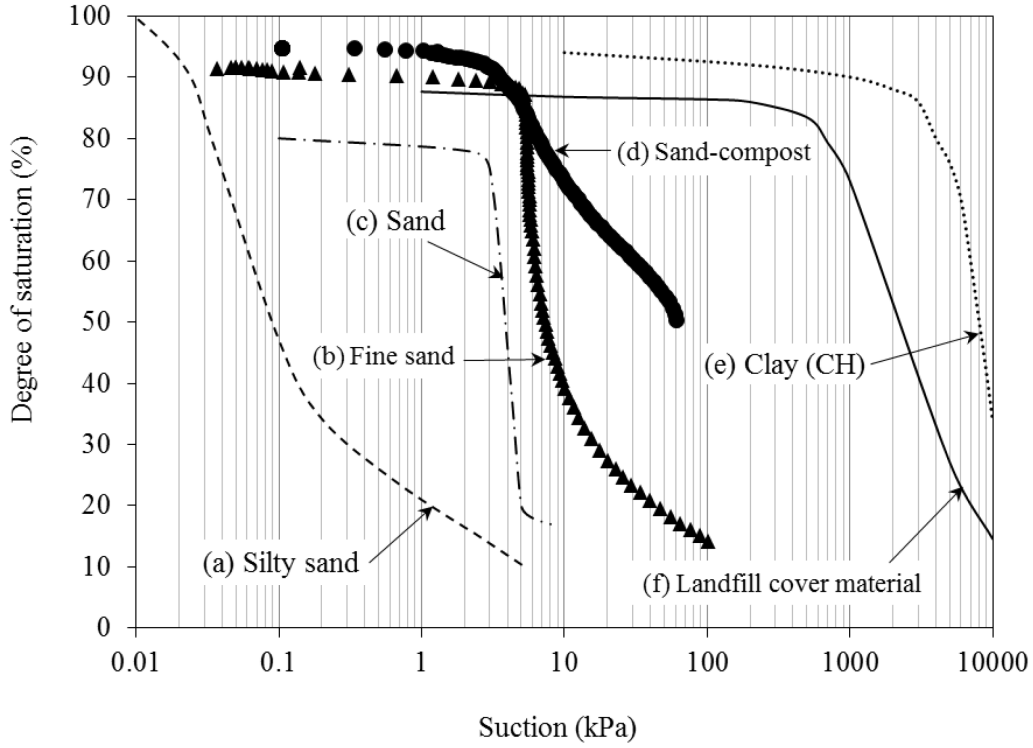

Figure 3-7: The WRCs of (a) silty sand adapted from Springer et al. [1998], (b) fine sand (this study), (c) sand adapted from Kamiya et al. [2006], (d) sand-compost (this study), (e) clay (CH) adapted from Jucá and Maciel [2006], and (f) landfill cover material adapted from Marinho et al. [2001]

Figure 3-8 shows the k_a-functions of the materials whose WRCs were presented in Figure 3-7. In order to obtain the k_a-functions in the form of θ_a-k_a, G_s was assumed equal to 2.67, for the cases where the actual value was not available. This is a very common value for the kinds of materials reported in Figure 3-8. In any case, the variation of G_s within the range for common soils (~2.62-2.74) does not affect the analyses made herein. For the silty sand presented in Figure 3-8a [Springer et al., 1998], the k_a-function is in the form of gas intrinsic permeability versus θ_a, because it was not possible to show it otherwise without making too many additional assumptions. In each figure, the curves were drawn based on the data published by the respective authors. The thick solid line represents the slope of the corresponding k_a-function for θ_a values greater than the onset of the abrupt decrease in k_a, as was considered in this study. For comparison, the slope of k_a-functions of the fine sand (Figure 3-4; for $\theta_a > \theta_{a\text{-}occ}$) and sand-compost mixture (Figure 3-6; for $\theta_a > \theta_{a\text{-}pocc}$) are represented by a dotted line and a dashed line, respectively.

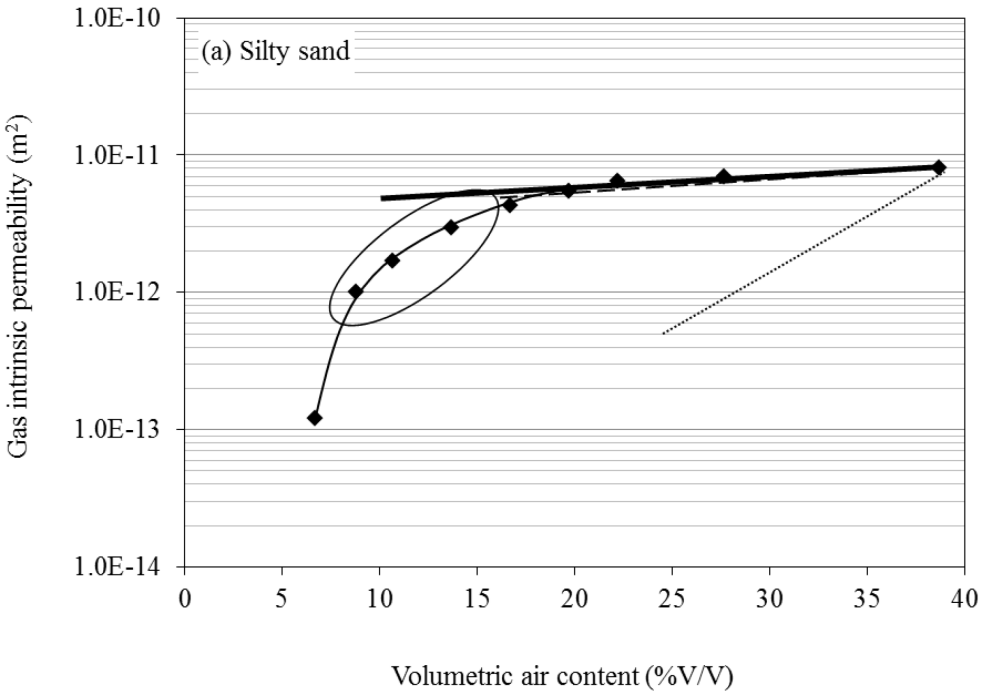
(a) Silty sand
Gas intrinsic permeability (m²)
1.0E-10
1.0E-11
1.0E-12
1.0E-13
1.0E-14
0
5
10
15
20
25
30
35
40
Volumetric air content (%V/V)

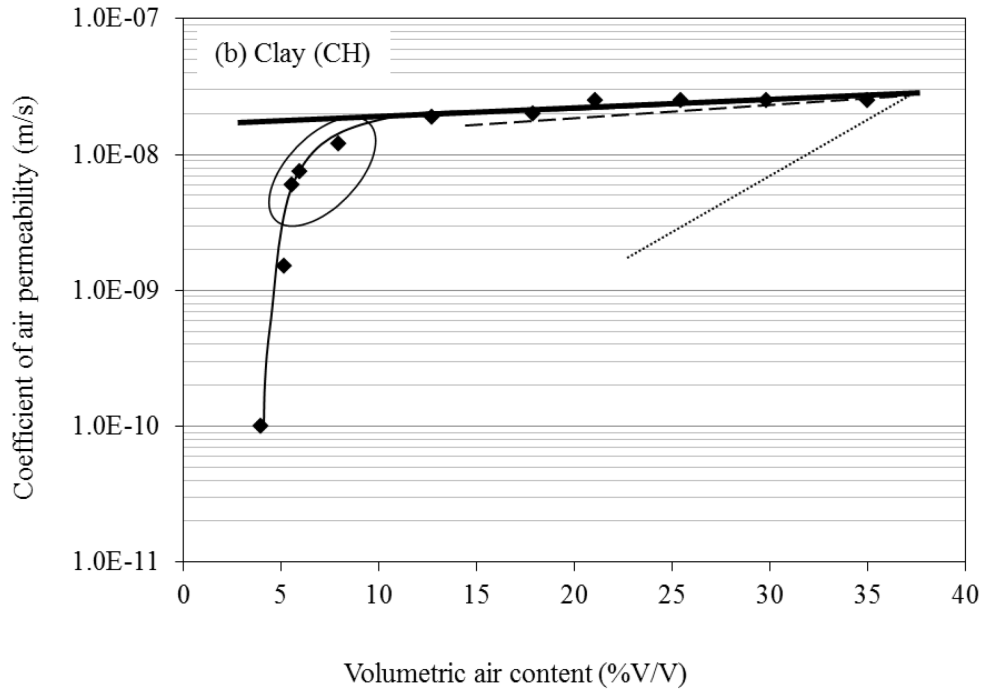
(b) Clay (CH)
Coefficient of air permeability (m/s)
1.0E-07
1.0E-08
1.0E-09
1.0E-10
1.0E-11
0
5
10
15
20
25
30
35
40
Volumetric air content (%V/V)

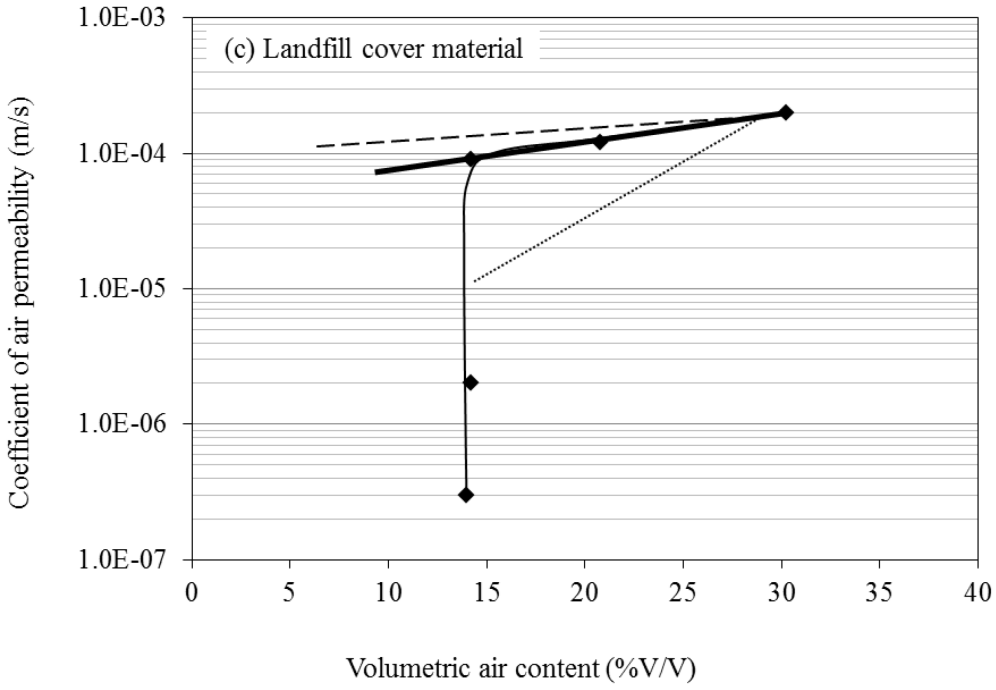

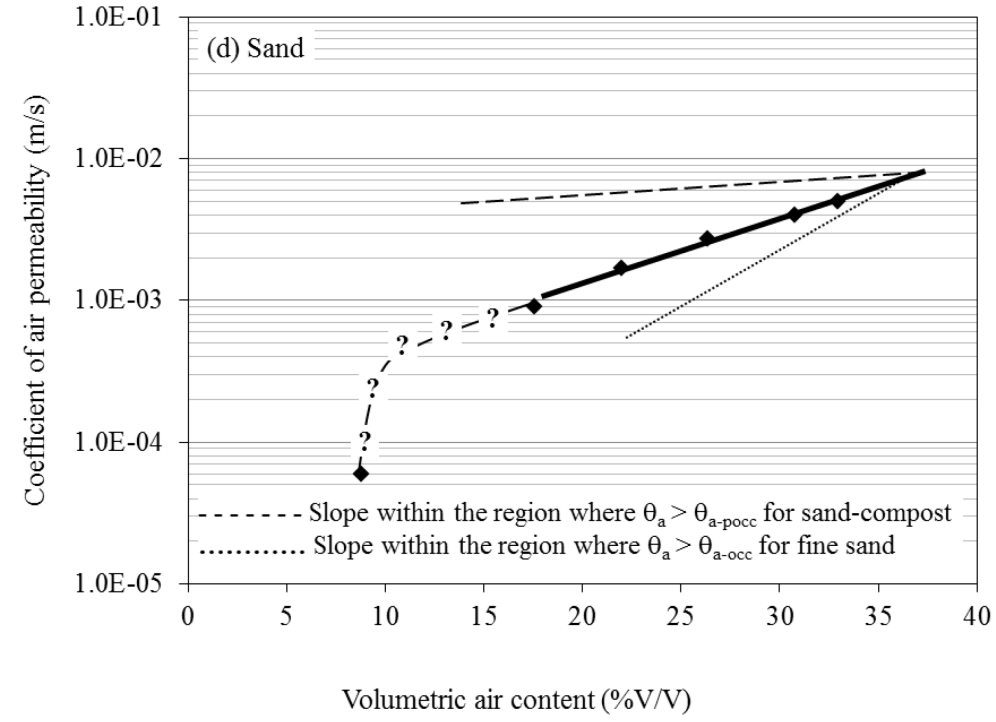

Figure 3-8: The k_a-functions of materials from other studies, adapted from (a) Springer et al. [1998], (b) Jucá and Maciel [2006], (c) Marinho et al. [2001], and (d) Kamiya et al. [2006]

In Figure 3-8a and b, a *transition zone* is observed within the region with $8\% < \theta_a < 17\%$ and $5\% < \theta_a < 12\%$, respectively (indicated by an ellipse). Therefore, $\theta_{a\text{-pocc}}$ would be equal to 12% for the clay and 17% for the silty sand. As far as the landfill cover material is concerned,

despite the gradual desaturation in the vicinity of its AEV (Figure 3-7), a *transition zone* was not identified for its k_a-function (Figure 3-8c). Based on the WRC of the sand tested by Kamiya et al. [2006] (Figure 3-7), one could expect a k_a-function similar to that found for the fine sand of this study, i.e. without a *transition zone*. It is not clear whether there is a transition zone in Figure 3-8d, due to the lack of results in the zone where $10\% < \theta_a < 20\%$.

The steepest slope of the curve, where θ_a is greater than that given by the onset of the abrupt variations in k_a with θ_a, is clearly associated with fine sand, followed by the sand tested by Kamiya et al. [2006] (Figure 3-8a), the landfill cover material (Figure 3-8c) and the sand-compost, the clay (Figure 3-8b), and the silty sand (Figure 3-8d). The latter 3 have very similar slopes. The clay sample studied by Jucá and Maciel [2006] seems to be an atypical clay as far as the slope of the desaturation zone of the WRC is concerned. For this material, however, the variation of k_a with θ_a is minimal for $\theta_a > \theta_{a\text{-}pocc}$, therefore, the k_a-function behaves as expected for a clayey material. Despite the similarity between the slope of the desaturation zones in WRCs of sand-compost of this study and landfill cover material [Marinho et al., 2001], the slope of the k_a-function is slightly steeper for the case of landfill cover material [Marinho et al., 2001] than that associated with sand-compost.

Generally, these results seem to indicate that, with the exception of the landfill cover material, the shape of the WRC in the vicinity of the AEV (Figure 3-7) corresponds to the shape of the k_a-function in the vicinity of the onset of abrupt decrease in k_a or within the region with $\theta_{a\text{-}pocc} < \theta_a < \theta_{a\text{-}occ}$. Moreover, a steep slope of the desaturation zone of the WRC is associated with a steep slope (thick solid line) of the k_a-function.

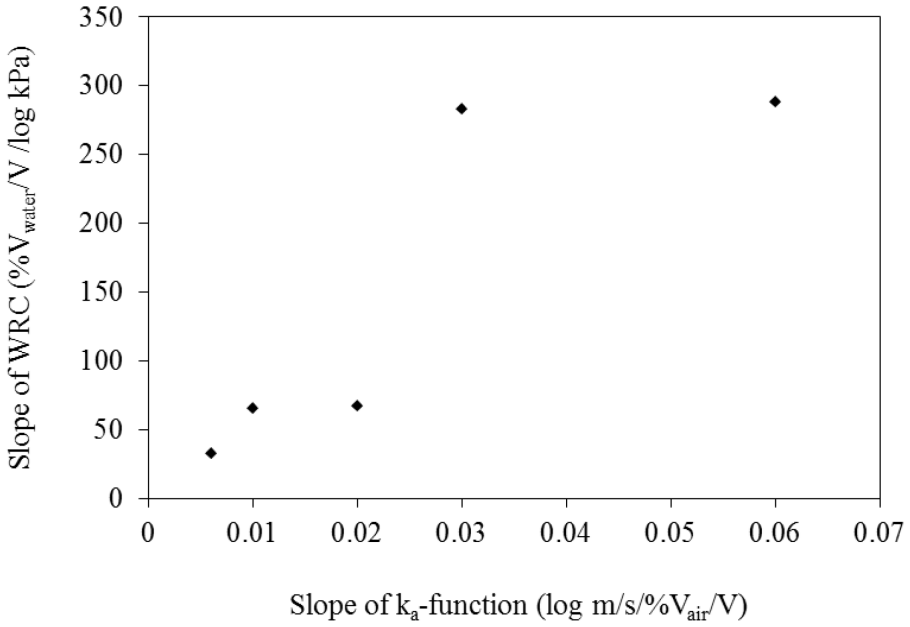

Figure 3-9: Relationship between the slope of desaturation zones of WRCs and the slope of k_a-functions for $\theta_a > \theta_{a\text{-}occ}$ or $\theta_a > \theta_{a\text{-}pocc}$, for materials from other studies and this study

For the materials presented in Figure 3-7, except for the clay studied by Jucá and Maciel [2006], calculations were made to determine the absolute value of the slope of the best fitting line for the desaturation zones of the WRCs and k_a-functions, for θ_a values greater than those at the onset of the abrupt decrease in k_a. The results of these calculations, shown in Figure 3-9, are quantitatively consistent with the conclusions of discussions about Figure 3-7 and Figure 3-8. Indeed, it is possible to observe a clear trend in the relationship between the slopes of the k_a-function and WRC: the greater the slope of WRC, the greater the slope of k_a-function.

Figure 3-10 presents the Standard Proctor curves of the materials tested in this and other studies found in the technical literature. For sake of comparison, the horizontal distances between S_r isolines 20% apart (represented by arrows in Figure 3-10) were measured for a dry density value 200 kg/m^3 lower than the optimum dry density. This arbitrary value was chosen so that the arrows are of reasonable dimensions in the figure. The shortest distance is associated with the fine sand (this study), followed by the landfill cover material [Marinho et al., 2001], the MH-CH [Langfelder et al., 1968] and sand-compost (this study).

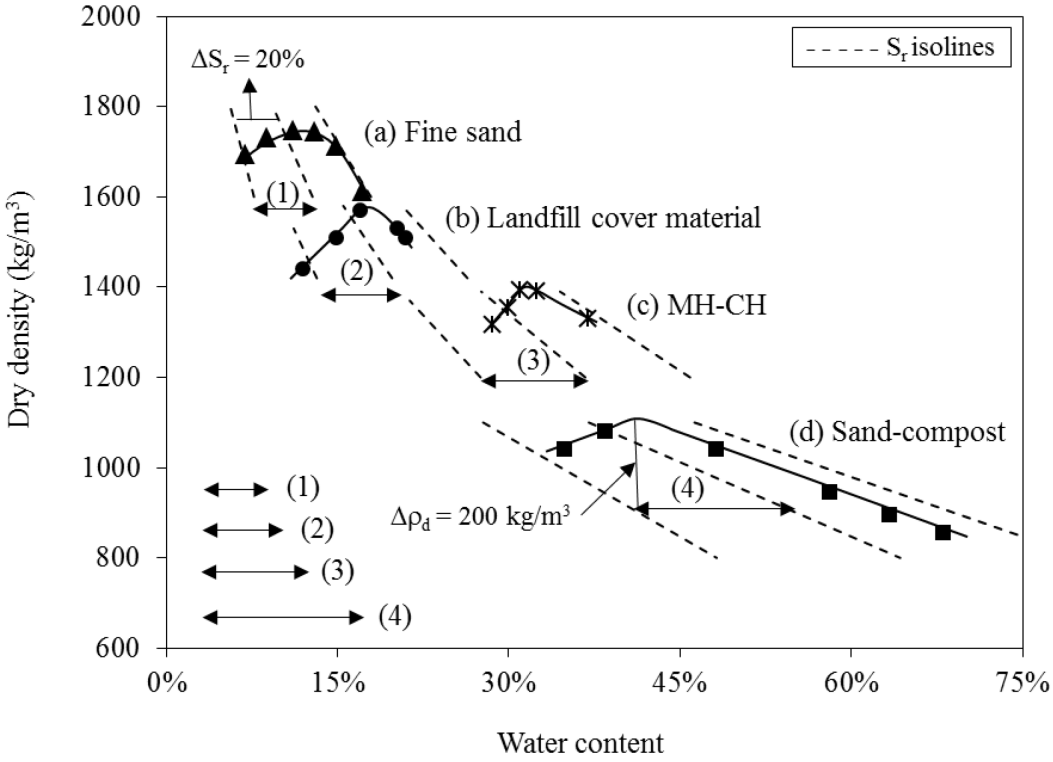

Figure 3-10: Compaction curves of (a) fine sand (this study), (b) Landfill cover material adapted from Marinho et al. [2001], (c) MH-CH adapted from Langfelder et al. [1968], and (d) sand-compost (this study)

In can be observed in Figure 3-11 that the slope of the k_a-function is the steepest for the fine sand, followed by the MH-CH [Langfelder et al., 1968] and the sand-compost. It follows the same order as the horizontal distances between S_r isolines, presented above in Figure 3-10. Based on this limited amount of data, it seems that the shorter the distance between S_r isolines, the steeper the slope of the k_a-function. However, as indicated in Figure 3-11, the slope of the k_a-function of the landfill cover [Marinho et al., 2001] is slightly less steep than that of the MH-CH [Langfelder et al., 1968], despite the fact that the distance between S_r isolines is slightly shorter for the landfill cover material.

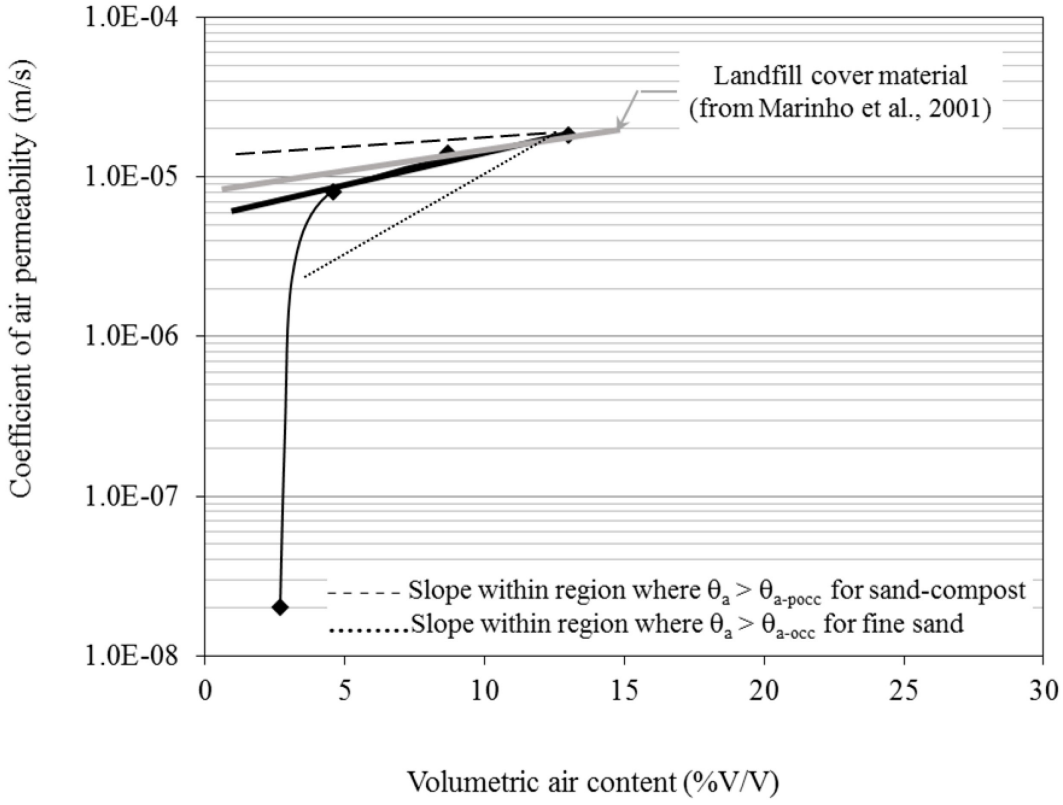

Figure 3-11: The k_a-function of the MH-CH material adapted from Langfelder et al. [1968], accompanied by materials tested in this study

It is well known that the slope of the desaturation zone of WRCs of fine-grained soils is less steep than in the case of coarse-grained soils, while compaction curves of fine-grained materials spread over a wider range of water content values than the compaction curves of coarse-grained materials. The shape of the compaction curve, in addition to the relationship between WRC and k_a-function, may thus be valuable information during an assessment of gas flow behaviour through porous materials used to construct PMOBs. In other words, critical design steps can be accomplished using simple and easy-to-obtain data, such as compaction curves and WRC.

3.4.2. Relationships between $S_{r\text{-}occ}$ values and S_r at the line of optima and S_r at AEV

According to Leroueil and Hight [2013], near the proctor optimum there is a transition in the distribution of pore sizes and arrangement of air-filled pores. Indeed, soils compacted on the dry side of optimum have a bimodal pore-size distribution (i.e. presence of macropores and

micropores), whereas soils compacted on the wet side of optimum have a single family of pores (micropores). Furthermore, the air phase is continuous on the dry side of optimum and occluded − in the form of discontinuous bubbles − on the wet side of optimum.

Results of air permeability tests obtained by Langfelder et al. [1968] with clay or silty samples compacted dynamically (Standard Proctor and other), statically or by kneading, show that close to the optimum water content, slight increases in water content cause several orders of magnitude reduction in the k_a value. Similar findings were obtained by Marinho et al. [2001] and Jucá and Maciel [2006] who tested silty samples. This seems to indicate that occlusion occurs near optimum water content. This was also observed in the case of the sand-compost mixture, where the S_r at the line of optima coincides with occlusion of air pores (see discussion in section 3.3.2), whereas for the fine sand, the $S_{r\text{-}occ}$ value is greater than that given by the line of optima (see section 3.3.1).

In addition, according to the k_a-function (Figure 3-6) and WRCs (Figure 3-5) of the sand-compost mixture, the S_r associated with the AEV provides a reasonable estimate of S_r at pore occlusion. In the case of fine sand, S_r at AEV (Figure 3-3) would not be a good indicator of occlusion, because, the pores would be occluded at a degree of saturation lower than that associated with the AEV (see section 3.3.1). The abrupt decrease of k_a value with decreasing suction (therefore with increasing S_r) when the suction value becomes lower than the AEV has been reported in the literature [e.g. Fredlund et al., 2012]. However, in certain cases, the abrupt decrease in k_a that characterizes occlusion begins at a S_r value lower than that associated with AEV [Kamiya et al., 2006].This seems to indicate that further investigation is required in order to find a more precise indicator of pore occlusion based on WRC.

3.4.3. Design Steps

The above discussion shows that easily available data (such as the Standard Proctor curve and/or WRC) can be used to infer the shape of k_a-function and, eventually the S_r at $\theta_{a\text{-}occ}$ (or at $\theta_{a\text{-}pocc}$). In addition, WRC and Standard Proctor curve can be used to obtain the design parameter required to determine the design criterion LUGM.

For MOLs constituted of materials similar to the fine sand, it is suggested that biogas can flow unrestricted from the top of the slope until the point along the GDL-MOL interface where the volumetric air content reaches the occlusion value, obtained in the manner explained in the remainder of this section. In other words, LUGM would be the length from upslope, taken horizontally, along which θ_a is greater than $\theta_{a\text{-}occ}$. In the case of MOLs constructed with materials similar to the sand-compost mixture, gas flow would be considered reasonably restricted beyond the point along the interface where θ_a becomes lower than $\theta_{a\text{-}pocc}$. The occlusion or pre-occlusion values would be obtained as follows:

a) If the k_a-function has been determined, occlusion is defined as the θ_a at which the soap bubble inside the flowmeter is virtually immobile. It is arbitrary, but it is nonetheless a practical definition. In cases where pre-occlusion can be determined via the k_a-function (e.g. sand-compost mixture; Figure 3-6), using the S_r associated with the pre-occlusion value to define the occlusion and to calculate LUGM leads to a conservative design.

b) In the absence of the k_a-function, for MOL materials that behave in a manner similar to the fine sand, one can resort to the S_r corresponding to the line of optima (of the Standard Proctor) to calculate a conservative occlusion value and LUGM.

c) For materials that behave in a similar manner to the sand-compost mixture (i.e. AEV not well defined), and in the absence of the k_a-function (therefore, without knowledge of $\theta_{a\text{-}pocc}$ and $\theta_{a\text{-}occ}$), using the S_r 10% to 20% lower than the S_r corresponding to the line of optima would lead to volumetric air content in the vicinity of $\theta_{a\text{-}pocc}$, which ensures at least viable biogas migration. The LUGM would be therefore defined based on $\theta_{a\text{-}pocc}$.

This selection was verified based on the results presented by Maciel and Jucá [2000] on sandy clay samples, for which the difference between the S_r at the start and end of what has been defined herein as the *transition zone*, i.e. $\theta_{a\text{-}pocc} > \theta_a > \theta_{a\text{-}occ}$ (see for example, Figure 3-6) was approximately 20%. Likewise, Springer et al. [1998] and Ba-Te et al. [2005] reported nearly 14% and 13% changes in volumetric water content within the *transition zone* for a silty sand and for Japanese fine soils, respectively. Here again, more refined design procedures will

eventually be developed with further studies concerned with the hydraulic behaviour of PMOBs.

3.4.4. Further design considerations

As far as assessment of the level of uniformity in the distribution of gas flow within the LUGM at the base of the MOL is concerned, the slope of k_a-θ_a curves where $\theta_a > \theta_{a\text{-}occ}$ (fine sand) or $\theta_a > \theta_{a\text{-}pocc}$ (sand-compost) corresponds to the slope of the desaturation zone in the WRCs, as discussed in section3.4.1. The slope of the k_a-θ_a curve reflects the sensitivity of k_a to the changes in θ_a (or S_r) and therefore the distribution of k_a in MOL along the GDL-MOL interface. Accordingly, in the absence of k_a-function, it is possible to use the slope of the desaturation zone of the WRC to help in the selection of the MOL material. For example, lesser slopes of the curves lead to greater uniformity of θ_a (therefore S_r) along the GDL-MOL interface. This greater uniformity leads to greater uniformity in biogas distribution at the base of the MOL.

3.5. Conclusions

In this study a key parameter for designing PMOBs, denominated *length of unrestricted gas migration* (LUGM) was defined, and steps to obtain the parameters needed to determine it, were presented. These parameters, i.e. $\theta_{a\text{-}occ}$ and $\theta_{a\text{-}pocc}$, were defined as the threshold of unrestricted upward flow of biogas. The flow of biogas was considered reasonably unrestricted when: 1) $\theta_a > \theta_{a\text{-}occ}$ for MOL materials with uniform grain size distribution, similar to the fine sand tested in this study, and 2) when $\theta_a > \theta_{a\text{-}pocc}$ for MOL materials with k_a-function similar to that given by the sand-compost mixture. Similarities were found between the shapes of k_a-function around $\theta_{a\text{-}occ}$ (and/or $\theta_{a\text{-}pocc}$) and WRC around the AEV, as well as between the width over which the Standard Proctor curve spans and the slope of k_a-function and WRC. It was also shown that in the absence of k_a-function, one can resort to the S_r at the line of optima or S_r at AEV to obtain the value of $\theta_{a\text{-}occ}$ and/or $\theta_{a\text{-}pocc}$. The methodology presented to obtain $\theta_{a\text{-}occ}$ and $\theta_{a\text{-}pocc}$ helps in the selection of the appropriate

material for MOL, the one that would provide the longest possible LUGM, therefore the lowest risk of hotspot creation.

Acknowledgements

This study received financial support from the Natural Science and Engineering Research Council of Canada (NSERC) and Waste Management (WM Quebec Inc.), under the collaborative research and development grant # CRD 379885-08, from the Consortium de recherche et innovations en bioprocédés industriels du Québec (CRIBIQ) and from Discovery Grant #170226. The invaluable help of Jean-Guy Lemelin, technician, must also be acknowledged.

CHAPTER 4. INFLUENCE OF CAPILLARY BARRIER EFFECT ON BIOGAS DISTRIBUTION AT THE BASE OF PASSIVE METHANE OXIDATION BIOSYSTEMS

Avant-propos

Titre: Influence of capillary barrier effect on biogas distribution at the base of passive methane oxidation biosystems: parametric study

Auteurs et affiliation:

Bahar Ahoughalandari: étudiante au doctorat, Université de Sherbrooke, Faculté de génie, Département de génie civil

Alexandre R. Cabral: professeur titulaire, Université de Sherbrooke, Faculté de génie, Département de génie civil

Date de soumission: 12 mai 2016

Revue: Waste Management

Titre français: Influence de l'effet de barrière capillaire sur la distribution du biogaz à la base des biosystèmes d'oxydation passive du méthane : l'étude paramétrique

Contribution au document:

The present paper helped to accomplish the last two objectives of the research project, defined in section1.3. Using the design criterion and the pertaining parameters introduced in chapterCHAPTER 3 3, the results of numerical simulations possessing several variables were interpreted. The contribution of this paper to the thesis is the evaluation of the most important parameters, related to the unsaturated hydraulic behavior of the MOL material and capillary barrier effect along the GDL-MOL interface, in value and distribution of moisture along the

interface. Consequently, the ease and the distribution of upward flow of biogas at the base of MOL would also be assessed. Finally, the selection of MOL material considering the influence of capillary barrier effect on upward flow of biogas would be possible, based on the obtained results in the present paper.

Résumé français:

Parmi les paramètres qui influent sur l'efficacité de l'oxydation du méthane dans les biosystèmes d'oxydation passive de méthane (BOPM), on trouvel'intensité et la distribution du chargement de CH_4 à la base de la couche d'oxydation du méthane (MOL). Les deux sont affectés par l'effet de barrière capillaire créé par la superposition des deux matériaux constituant le BOPM, c'est-à-dire les matériaux de la MOL et la couche de distribution de gaz (GDL). L'effet de barrière capillaire sur l'écoulement non saturé de l'eau a été bien documenté dans la littérature. Toutefois, son effet sur l'écoulement du gaz à travers les BOPM devrait être approfondit. Dans cette étude, des simulations numériques ont été réalisées pour évaluer l'effet des caractéristiques hydrauliques non-saturées du matériau de la MOL sur la valeur et la distribution d'humidité et, par conséquent, sur la facilité et l'uniformité de la distribution de l'écoulement ascendant du biogaz le long de l'interface entre la GDL et la MOL. Les paramètres hydrauliques non-saturés des matériaux utilisés pour construire le BOPM expérimental au site d'enfouissement de déchets à St-Nicéphore (Québec, Canada) ont été adoptés pour construire la simulation référence de l'étude paramétrique. Le comportement de l'écoulement du biogaz pour ce matériau particulier de la MOL a été analysé selon sa fonction de perméabilité intrinsèque au gaz, qui a été obtenue au laboratoire. Les paramètres qui ont davantage influencé le comportement de BOPM, ont été la conductivité hydraulique saturée et la distribution de la taille des pores du matériau de la MOL, dont les effets ont été intensifiés à la suite d'une augmentation de la pente de l'interface. L'effet de la densité sèche initiale a été également évalué. La sélection des matériaux de la MOL qui optimisent ces trois paramètres peuvent empêcher la restriction indésirable dans le flux ascendant de biogaz, ce qui provoque finalement la redirection vers le haut de la pente, où les flux élevés de CH_4 (hotspots) peuvent s'échapper dans l'atmosphère. L'écoulement ascendant non-bloqué du biogaz à travers l'interface entre la GDL et la MOL, et la distribution uniforme de l'humidité et du biogaz couvrant la majorité possible de la longueur de l'interface fourniraient une bonne conception de BOPM. Comment les obtenir, ceci est l'objectif de cet article.

Abstract: The efficiency of methane oxidation in passive methane oxidation biosystems (PMOB) is influenced, among others, by intensity and distribution of the CH_4 loading at the base of the methane oxidation layer (MOL). Both are affected by the capillary barrier that results from the superposition of the two materials constituting the PMOB, namely the MOL and the gas distribution layer (GDL). The effect of capillary barriers on the unsaturated flow of water has been well documented in the literature. However, its effect on gas flow through PMOBs is still poorly documented. In this study, sets of numerical simulations were performed to evaluate the effect of unsaturated hydraulic characteristics of MOL material on the value and distribution of moisture and hence, the ease and uniformity in the distribution of the upward flow of biogas along the GDL-MOL interface. The unsaturated hydraulic parameters of the materials used to construct the experimental field plot at the St-Nicephore landfill (Quebec, Canada) were adopted to build the reference simulation of the parametric study. The behavior of the upward flow of biogas for this particular MOL material was analyzed based on its gas intrinsic permeability function, which was obtained in the laboratory. The parameters that most influenced the behavior of the PMOB were the saturated hydraulic conductivity and pore size distribution of the MOL material, whose effects were intensified as the slope of the interface increased. The effect of initial dry density was also assessed herein. Selection of MOL materials that optimize these three parameters may prevent unwanted restriction in the upward flow of biogas, which ultimately causes redirection towards the top of the slope, where high CH_4 fluxes (hotspots) may escape to the atmosphere. Unrestricted upward flow of biogas across the GDL-MOL interface and uniform distribution of moisture and biogas covering most of its length make up for good PMOB design. How to obtain them is the main object of this paper.

Keywords: Landfill final covers, Passive methane oxidation biosystems, Biogas flow behavior, Capillary barrier effect, Numerical simulation

4.1. Introduction

A capillary barrier (CB) is formed when water flows through two soil layers with contrasting unsaturated hydraulic properties are superimposed. Capillary forces associated with this contrast create a capillary block along the interface, which limits vertical percolation of water

through the interface or reduces gas fluxes, and in the case of inclined CBs, may laterally drain the meteoric seepage.

CBs can be incorporated into the design of final covers for landfills, acid-generating mine tailings and waste-rock dumps. In the case of landfills, the design of the final cover must consider maximum seepage rates imposed by legislation to control the infiltration, therefore leachate generation [e.g. Stormont, 1996; Khire et al., 2000; Bussière et al., 2003a; Aubertin et al., 2006; Vachon et al., 2015]. In the case of mine residues, the goal is to prevent the influx of atmospheric oxygen, thereby preventing the generation of acid mine drainage [Yanful, 1993; Wilson et al., 1995; Williams et al., 1997; Bussière et al., 2003b; Dagenais et al., 2005; Adu-Wusu and Yanful, 2006].

Recently, passive methane oxidation biosystems (PMOBs) have been promoted as a means to reduce fugitive CH_4 emissions (emissions not captured by gas collection systems) from landfills. PMOBs are of particular importance during the aftercare phase, i.e. following the shutdown of active gas collection [e.g. Huber-Humer et al., 2009; Cabral et al., 2010b; Roncato and Cabral, 2012; Sadasivam and Reddy, 2014].

PMOBs are engineered systems installed at the top-most part of the final cover and consist of two main layers: the methane oxidation layer (MOL), localized near the surface and where most CH_4 is oxidized into CO_2 (using atmospheric O_2) by methanotrophic bacteria, and the underlying gas distribution layer (GDL), which intercepts fugitive emissions. The methane oxidation efficiency of PMOBs depends on several parameters, including the CH_4 loading at the base of the PMOB [Cabral et al., 2010b; Fredenslund et al., 2010; Gebert et al., 2011a; Pokhrel et al., 2011; Rachor et al., 2011; Scheutz et al., 2011; Ndanga et al., 2015]. The lower the CH_4 loading, the more the methanotrophs will be capable to oxidize the upward flow of biogas intercepted by the GDL. To reduce the loading, this upward flow has to be distributed over the widest surface possible.

The contrast in unsaturated hydraulic behavior between the MOL and the GDL materials results in CB formation along the GDL-MOL interface [Tétreault et al., 2013; AhouGhalandari et al., 2015]. As a result, the MOL retains water and, therefore, its degree of saturation (S_r) increases where the capillary block occurs, i.e. along the GDL-MOL interface. In an inclined interface, the retained water seeps both laterally and vertically, causing an

increase of S_r towards the bottom of the slope. The ensuing effects of S_r on occlusion of air-filled pores and gas flow has been the object of several studies dealing with unsaturated flow through porous media [e.g. Langfelder et al., 1968; Maciel and Jucá, 2000; Marinho et al., 2001; Jucá and Maciel, 2006]. Beyond a certain point along the sloping interface, the increase in S_r may lead to occlusion of air-filled pores, and therefore create a restriction to the upward flow of biogas. As a consequence, biogas diverts toward the regions of the biosystem with lower S_r located upstream [Tétreault et al., 2013]. This may in turn create a hotspot, i.e. a localized region where surface CH_4 concentrations are higher than acceptable by legislation and where methane oxidation is much less [Bohn and Jager, 2009; Cabral et al., 2010a; Röwer et al., 2012].

It stems from the preceding that an efficient PMOB design would be associated with the longest possible length along the GDL-MOL interface where upward gas migration is unrestricted. This length is herein denominated *length of unrestricted gas migration* (LUGM).

Bohn and Jager [2009] observed the persistent presence of a hotspot upslope a large-scale experimental PMOB constructed in Germany, with a slope of 1V:10H. Similarly, the surface emission measurements performed by Röwer et al. [2012] and Geck et al. [2012] showed upslope hotspots in an experimental PMOB with a slope of 1V:5H, constructed in the Netherlands. Both PMOBs were composed of a two-material recultivation layer (protection and vegetation layers) as MOL, and a two-layer capillary barrier that was constructed to control infiltration, but also acted as GDL. Conducting a series of steady-state numerical simulations on these two PMOBs, Tétreault et al. [2013] concluded that biogas could flow unrestricted through the GDLs, where the degrees of saturation were low, but pore occlusion likely occurred at the GDL-MOL interfaces. Hotspots upstream of the PMOBs most probably resulted from pore occlusion. Kjeldsen et al. [2013] constructed an experimental PMOB with a jagged MOL-GDL interface with the intention of limiting the potentially water clogged interface to the lower parts, leaving the rest free to distribute the CH_4 loading at the base of the MOL.

This very clever idea put forth by Kjeldsen et al. [2013] needs to be further developed, in order to incorporate proper design steps and design parameters. Indeed, there seems to be a need for more rigorous numerical studies on gas flow behavior through PMOBs that includes

consideration of the CB effect and the importance of uniformity of biogas distribution and the ease of upward biogas flow. Such studies would provide tools for selecting MOL and GDL with appropriate geotechnical and hydraulic characteristics and geometrical parameters of PMOB.

The focus of this study was to evaluate how the distribution of biogas along the interface of an inclined PMOB was affected by the slope of the PMOB, and by some of the basic unsaturated hydraulic parameters of the MOL material. A parametric study was conducted using data from an experimental PMOB constructed at the St-Nicephore landfill as a starting point (or *Reference simulation*). Several years of monitoring this PMOB have shown it to be a highly efficient PMOB, capable of oxidizing very high CH_4 loads [Capanema and Cabral, 2012; Roncato and Cabral, 2012].

Transient state numerical simulations were performed using the commercial program SEEP/W [2010]. The main variables in these simulations included, as mentioned previously, the slope of the GDL-MOL interface and the unsaturated hydraulic properties of the MOL material, i.e. water retention curve and the saturated hydraulic conductivity. The simulations made it possible to evaluate the effect of each variable on the distribution of moisture along the GDL-MOL interface and on the magnitude of LUGM.

The tools proposed herein are another necessary step in the development of PMOB design. The study is innovative insofar as it brings the hydraulic aspects and unsaturated flow to the forefront of PMOB design, which have not yet received the attention they deserve. The main limitations of the study are two-fold. The first is related to the lack of consideration of evapotranspiration in the numerical simulations. This limitation was circumvented by considering that a reasonable percentage of the total precipitation actually seeped through the cover and reached the GDL-MOL interface. This is not perfect, but allowed the parametric study to remain within the realm of the possible. The other limitation relates to the characterization of all alternative MOL materials. Unfortunately, this could not be done within the framework of this project.

4.2. Materials and methods

4.2.1. Site configuration

The experimental PMOB numerically analyzed in this study is one of the three PMOBs constructed within the existing final cover of the St-Nicephore landfill, Quebec, Canada to evaluate the methane oxidation efficiency of the designs under field conditions [Capanema and Cabral, 2012; Roncato and Cabral, 2012]. This PMOB, referred to in the literature as PMOB2, measured 2.75 m (W) × 9.75 m (L) with a slope of 3.5%. A drainage system was installed at the lowest point to evacuate percolated water. It consisted of an 80-cm-thick MOL containing a mixture of five volumes of compost and one volume of coarse sand whose main characteristics are the following: specific gravity (G_s) = 2.24, $S_{r\text{-}opt}$ (S_r at line of optima) = 90%, $\rho_{d\text{-}insitu}$ (in situ dry density) = 750 kg/m^3, in situ porosity equal to 0.665 and in situ gravimetric water content on the day of field measurements (w%) = 47%. These values were used in numerical simulations as initial conditions. The material constituting the MOL of PMOB2 (experimental field plot at the St-Nicephore landfill) is denominated herein as *Reference MOL*. The 40-cm-thick GDL was constructed using 12.7-mm clean gravel, which was placed under the MOL.

4.2.2. Hydraulic properties of the materials

The drying water retention curve (WRC) of the *Reference MOL* was determined using the HYPROP apparatus [HYPROP-UMS, 2013], at in situ initial dry density and water content [AhouGhalandari et al., 2015]. For GDL, the WRC was estimated using the Fredlund et al. model [Fredlund et al., 2002], derived from the grain size distribution curve of the material. In the present study, the effect of hysteresis of the WRC was not considered and only the drying curve was used. Saturated hydraulic conductivity (k_{sat}) of the *Reference MOL* was equal to 9×10^{-6} m/s, which was measured according to ASTM D2434-68 [ASTM-D2434-68, 2006] at in situ initial dry density and water content. The k_{sat} of GDL was calculated using the Chapuis equation [2004].

The van Genuchten model [1980] was used to fit the WRC (Equation 4-1), whereas hydraulic conductivity functions (*k-fcts*) were obtained using the van Genuchten [1980] model, based on

the Mualem formulation [1976] (Equation 4-2). The WRC and *k-fct*s obtained were then used during the simulations using SEEP/W (Figure 4-1 and Figure 4-2).

$$\theta_w = \theta_r + \frac{\theta_s - \theta_r}{\left[1 + \left(\frac{\psi}{a}\right)^n\right]^m} \qquad 4\text{-}1$$

$$k_w = k_{sat} \frac{\left[1 - (a\psi^{(n-1)})(1 + (a\psi^n)^{-m})\right]^2}{\left[((1 + a\psi)^n)^{\frac{m}{2}}\right]} \qquad 4\text{-}2$$

θ_w is the volumetric water content, θ_s is the saturated volumetric water content, θ_r is the residual volumetric water content, ψ is suction, a, n, and m are curve fitting parameters and k_w is the hydraulic conductivity.

In order to perform this study, the parameters defining the WRC and *k-fct* of the *Reference MOL* and the slope of the interface were set to vary over a range of values that kept the transformed material within the approximate geotechnical category of the *Reference MOL*. The parameters describing the WRC and *k-fct* of the GDL remained constant for all simulations. Table 4-1 presents the parameters considered in the numerical simulations. The corresponding WRCs and *k-fct*s are shown in Figure 4-1 and Figure 4-2, respectively.

Table 4-1: Hydraulic properties of the materials used in the numerical simulations

Simulation No.	Slope	MOL (sand-compost)					GDL (gravel)				
		a (kPa)	n	k_{sat} (m/s)	θ_s (%m^3/m^3)	θ_r (%m^3/m^3)	a (kPa)	n	k_{sat} (m/s)	θ_s (%m^3/m^3)	θ_r (%m^3/m^3)
(1)	3.5%	2.8	1.28								
(2)	3.5%	2.8	1.5	9×10^{-6}							
(3)	3.5%	4.2	1.28								
(4)	3.5%	2.8	1.28								
(5)	3.5%	2.8	1.5	9×10^{-4}							
(6)	3.5%	4.2	1.28		67.0	0.17	0.5	2.4	4.3×10^{-2}	30.0	0.0
(7)	10%	2.8	1.28								
(8)	10%	2.8	1.5	9×10^{-6}							
(9)	10%	4.2	1.28								
(10)	10%	2.8	1.28								
(11)	10%	2.8	1.5	9×10^{-4}							
(12)	10%	4.2	1.28								

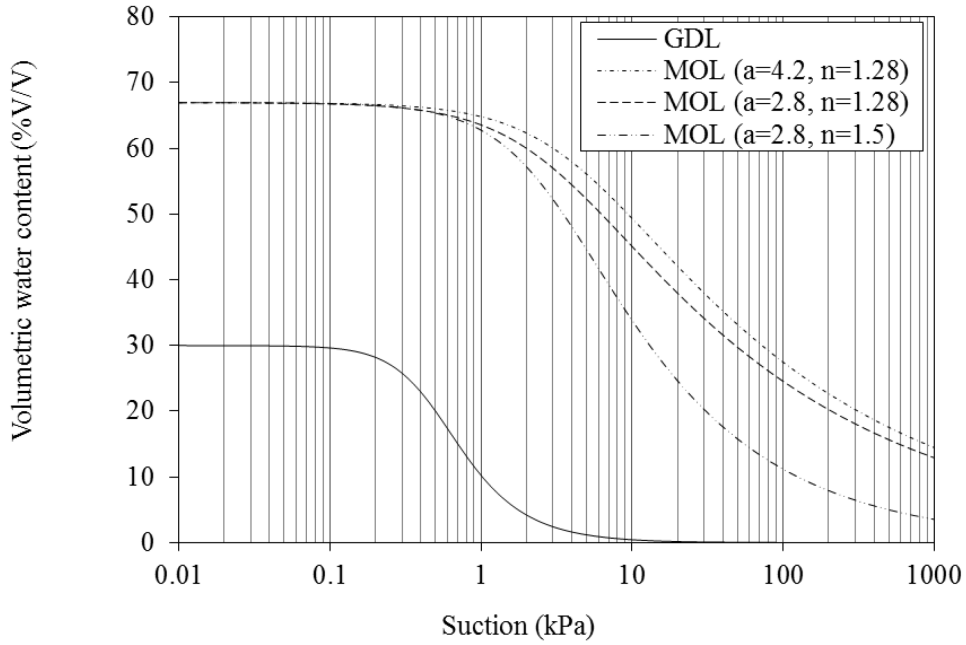

Figure 4-1: Water retention curves of the materials used in the parametric analysis

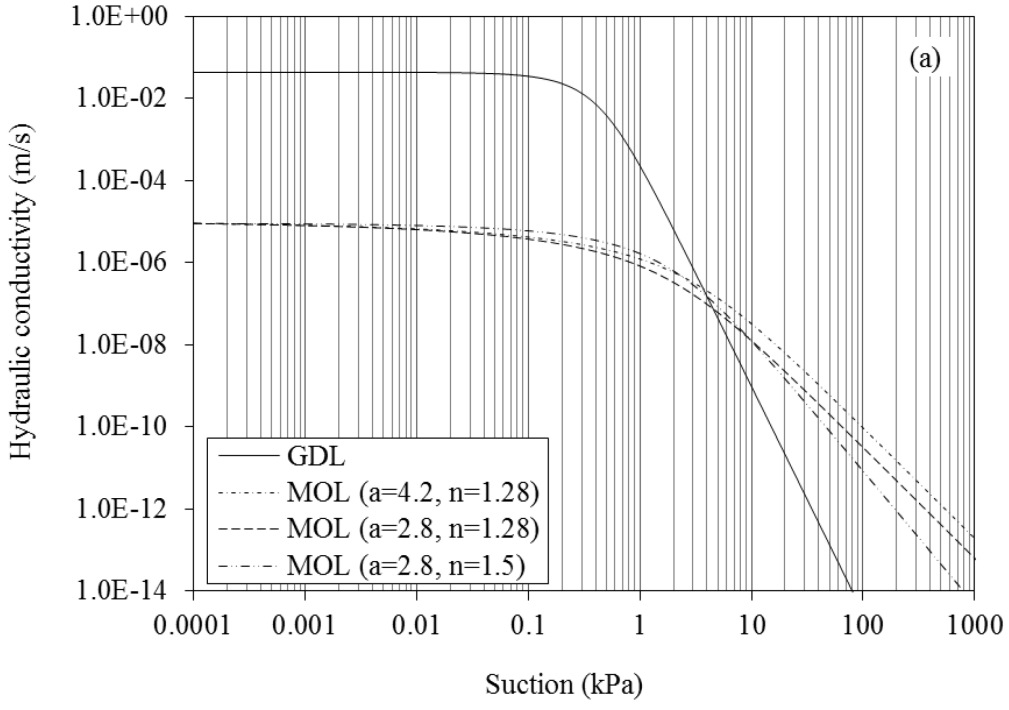

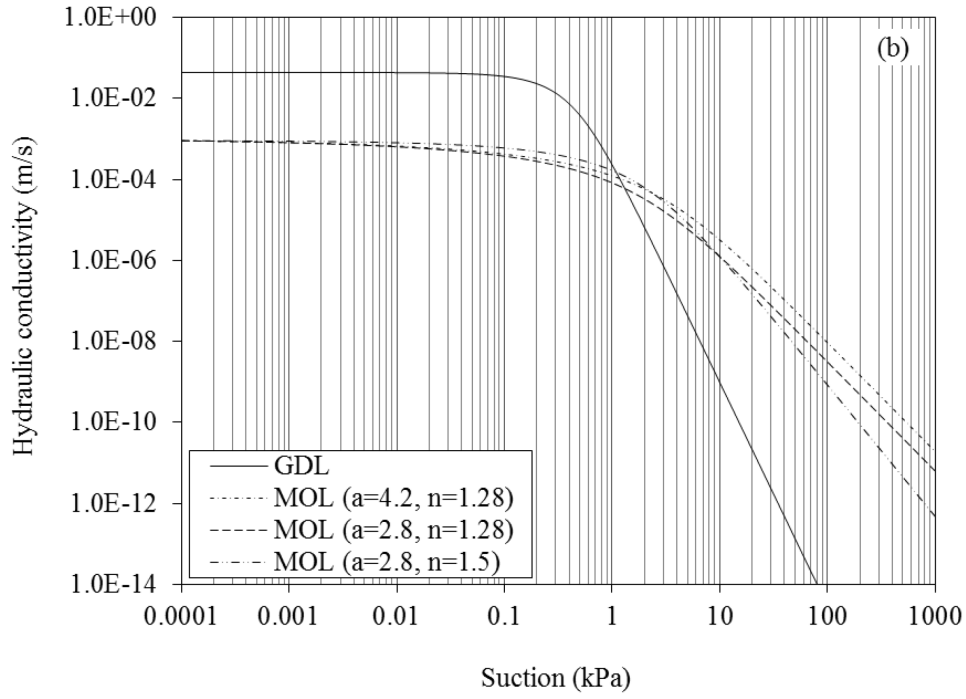

Figure 4-2: Hydraulic conductivity functions of the materials used in the parametric analysis; (a) $k_{sat\text{-}MOL} = 9\times10^{-6}$ m/s, and (b) $k_{sat\text{-}MOL} = 9\times10^{-4}$ m/s

4.2.3. Gas Flow Properties of MOL Material

Performing a series of air permeability tests, using a soap flow meter (Bubble-O-Meter; 1-10-500 ml) connected to the inlet of a triaxial cell, the gas intrinsic permeability (K) of the sand-compost mixture used to build the MOL of PMOB2 was measured at several initial water contents and dry densities (ρ_d). Figure 4-3 shows the test results as K value at each volumetric air content (θ_a). In order to incorporate the gas flow behavior of MOL material in the results of numerical simulations, the Ball et al. model [1988] was adopted as the fitting curve for K-θ_a plot, which was consistent with the experimental data (Figure 4-3).

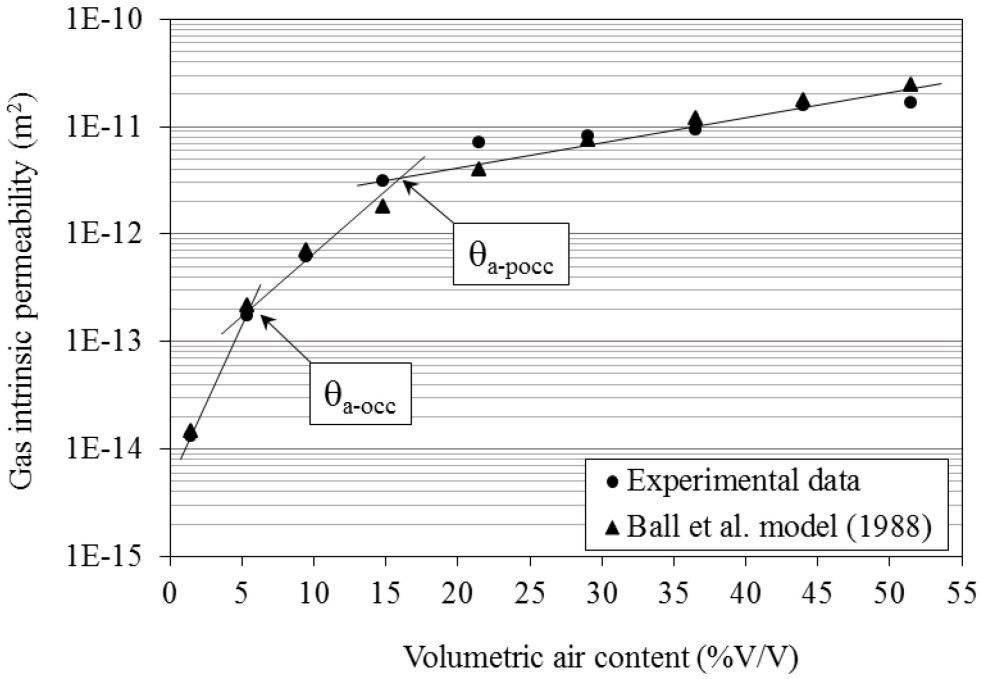

Figure 4-3: Gas intrinsic permeability function of the material used as MOL in numerical simulations

As shown in Figure 4-3, the curve can be subdivided into three regions whose frontiers are $\theta_a \approx 5\%$ and $\theta_a \approx 16\%$, herein defined as occlusion value ($\theta_{a\text{-}occ}$) and pre-occlusion value ($\theta_{a\text{-}pocc}$), respectively. The value of *K* is equal to 3.1×10^{-12} (m^2) at $\theta_{a\text{-}pocc}$ and equal to 1.9×10^{-13} (m^2) at $\theta_{a\text{-}occ}$. For θ_a to be maintained constant, if the dry density increases, the corresponding water content must decrease. Regardless, the value of *K* is not very affected by the dry density if θ_a remains constant. The $\theta_{a\text{-}pocc}$, $\theta_{a\text{-}occ}$ and corresponding *K* values derived from data presented in Figure 4-3, can be used for any given pair of initial dry density and water content in the *Reference MOL*.

For design purposes, it is hypothesized that biogas flow would be considered reasonably unrestricted when θ_a is greater than $\theta_{a\text{-}pocc}$. Therefore, a practical definition of LUGM would be the length, taken horizontally, from the top of the slope to the point where θ_a becomes equal to $\theta_{a\text{-}pocc}$. Beyond this point, gas flow becomes somehow restricted and, when it reaches a value of $\theta_a \approx \theta_{a\text{-}occ}$, it is considered blocked. It is reasonable to consider that biogas would prefer to migrate laterally - and find easier escape points – rather than try to flow through a partially restricted area (where $\theta_a \approx \theta_{a\text{-}pocc}$). Changes in dry density due to settlement or swelling were ignored during numerical simulations.

Knowing the initial dry density and porosity of the MOL material, one can calculate the θ_w associated with $\theta_{a\text{-}pocc}$ and $\theta_{a\text{-}occ}$ and compare them with θ_w values obtained from the numerical simulations. For simulations No. 1 and No. 7 (Table 4-1), whose porosities are equal to 0.665, θ_w associated with $\theta_{a\text{-}pocc}$ ($\theta_{w\text{-}pocc}$) is equal to 50.5% and θ_w associated with $\theta_{a\text{-}occ}$ ($\theta_{w\text{-}occ}$) is equal to 61.5%. The van Genuchten parameters that define the WRC of the MOL material in simulations No. 3 and No. 9, a = 4.2 and n = 1.28, are associated with the *Reference MOL* compacted to ρ_d = 0.930 kg/m^3 (porosity equal to 0.584) [AhouGhalandari et al., 2015]. Although the value of $k_{sat\text{-}MOL}$ may change due to compaction, for the case with ρ_d = 0.930 kg/m^3, it remained within the same magnitude as that of the *Reference MOL* (data not presented). Therefore, it seems reasonable to use $\theta_{a\text{-}pocc}$ and $\theta_{a\text{-}occ}$ shown in Figure 4-3 for simulations No. 3 and No. 9, where $k_{sat\text{-}MOL} = 9\times10^{-6}$ m/s, a = 4.2 and n = 1.28. For these simulations, $\theta_{w\text{-}pocc}$ and $\theta_{w\text{-}occ}$ are equal to 42.4% and 53.4%, respectively. Since the porosities associated with all other simulations in Table 4-1 are unknown, $\theta_{w\text{-}occ}$ and $\theta_{w\text{-}pocc}$ cannot be calculated for these simulations and therefore, LUGM cannot be determined. For these cases, only the influence of variables a, n and $k_{sat\text{-}MOL}$ on the distribution of θ_w along the GDL-MOL interface was evaluated.

4.2.4. Numerical Simulations

For the purpose of this study, the finite element software SEEP/W (2010) was adopted. SEEP/W can mathematically simulate the real physical process of water flowing through a particulate medium.

The SEEP/W simulation with *Reference MOL* is herein denominated *Reference simulation* (simulation No. 1 in Table 4-1). For all simulations, the thickness of MOL is 80 cm and the thickness of GDL is 40 cm. Figure 4-4 shows the dimensions, meshing and boundary conditions adopted for the simulations. In order to avoid boundary effects, the length of PMOB in all simulations was considered equal to 100 m. The finite element mesh contains 10,000 elements. The mesh density is higher near the GDL-MOL interface. Two types of boundary conditions were considered for the simulations: 1) unit flux function to assign the seepage reaching the top of the MOL, and 2) zero total flux boundary condition with potential

seepage face review at the toe of the simulations in both layers to represent the drainage system.

The transient state analysis performed lasted 246 days. The initial θ_w at points located 1 cm above the GDL-MOL interface (herein denominated "*interface points*") were set equal to 35% for all simulations. Water balance components based on climatic data of September 2006 to August 2007 in Quebec [Cabral et al., 2010a] show that the average annual amount of water that seeps into the landfill is equal to 22% of precipitation. Since SEEP/W does not include a soil-atmosphere interaction module (evapotranspiration), the daily seepage rate into the PMOB is therefore considered as 22% of the daily rate of precipitation from March to November 2009 (Figure 4-5).

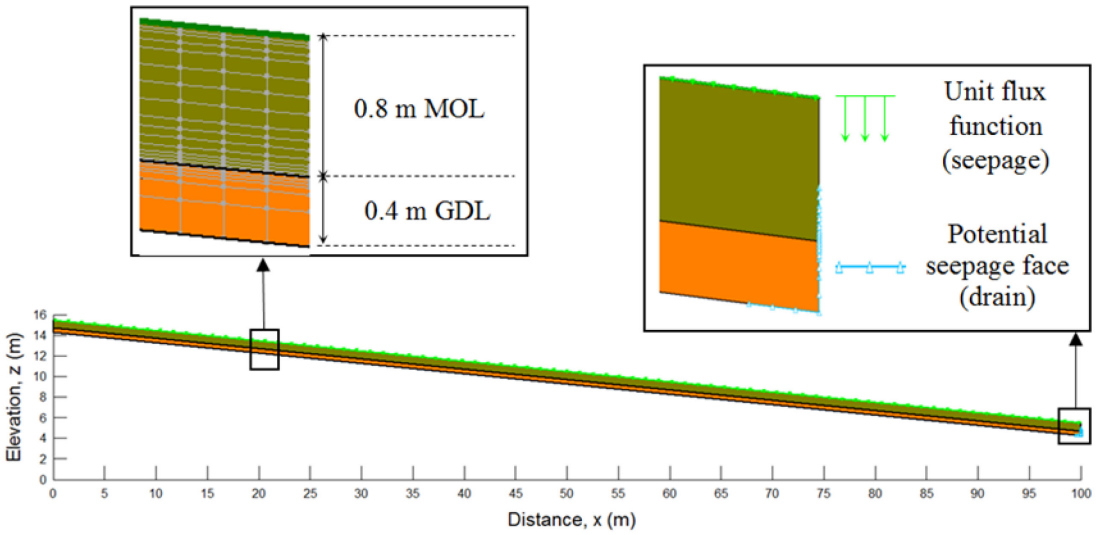

Figure 4-4: Dimensions and boundary conditions of the SEEP/W simulations (slope is variable)

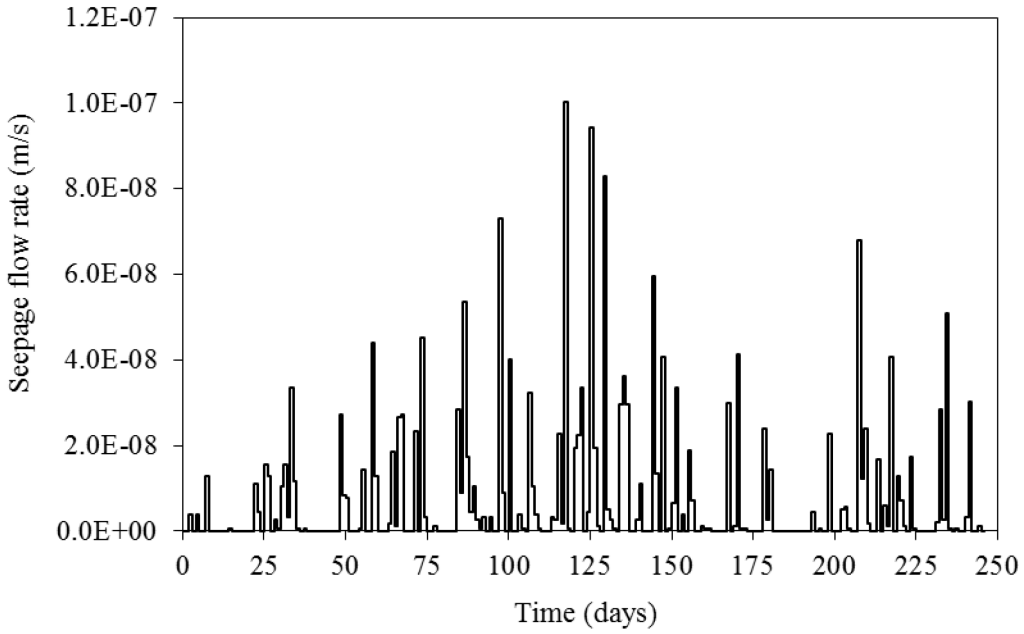

Figure 4-5: The daily rate of seepage into the PMOB2 during 246 days, from March to November

4.3. Results

Data presented in all the figures were obtained from *interface points*. The nodes located in the first and last 5 meters of the modelled PMOBs were not considered in the analyses, in order to avoid potential boundary effects.

4.3.1. *Reference simulation*

Figure 4-6 shows θ_w values of the *interface points* at several time steps during the *Reference simulation*, which lasted 246 days. The initial θ_w = 35.0% is associated with S_r = 53% and gravimetric water content (w) equal to 47%, which means compaction on the dry side of the line of optima.

θ_w increased towards the bottom of the slope, but the difference in θ_w values from the top to the bottom were quite small. The difference between maximum and minimum values of θ_w along the interface, referred to as $\Delta\theta_w$, increased with time. This parameter gives an idea of the level of uniformity of θ_w along the interface, and the higher it is, the greater the chance of

a non-uniform interface, as far as moisture is concerned. The opposite is rather straightforward: the lower $\Delta\theta_w$ is, the greater the uniformity in distribution of moisture.
During the simulation period, the maximum $\Delta\theta_w$ (1.5%) occurred on day 208, when θ_w of the *interface points* had already reached $\theta_{w\text{-}pocc}$, i.e. upward gas migration was already partially restricted. Prior to the onset of $\theta_{w\text{-}pocc}$, which was equal to 50.5% and occurred on day 141, the maximum value of $\Delta\theta_w$ was equal to 8.8×10^{-3} %. This very small value leads to the conclusion that the interface had become uniform, as far as volumetric water content was concerned. Therefore, once the $\theta_{w\text{-}pocc}$ was attained, LUGM abruptly became equal to zero, considering the practical definition of LUGM (distance from top to the point where $\theta_{w\text{-}pocc}$ is attained).

During the last 105 days of the *Reference simulation,* $\theta_w > \theta_{w\text{-}pocc}$, meaning that upward biogas flow was restricted along the interface. Biogas would therefore migrate within the GDL towards the top of the slope or escape through preferential pathways, such as cracks on the final cover. The CH_4 in the biogas transported through these preferential flow paths would less likely be submitted to biotic oxidation [Chanton et al., 2011].

The maximum value of θ_w ($\theta_{w\text{-}max}$) was equal to 53.3%, which was lower than $\theta_{w\text{-}occ}$ (61.5%) but greater than $\theta_{w\text{-}pocc}$ (50.5%). Therefore, despite the fact that the pores at the interface of the *Reference simulation* never became completely occluded ($\theta_w > \theta_{w\text{-}occ}$), it is suggested to use a conservative approach and consider restricted gas migration due to the fact that $\theta_w > \theta_{w\text{-}pocc}$.

Before attainment of $\theta_{w\text{-}max}$, the value of θ_w at the *interface points* increased continuously, independent of the transient seepage rate. After that, θ_w may have fluctuated depending on the seepage rate.

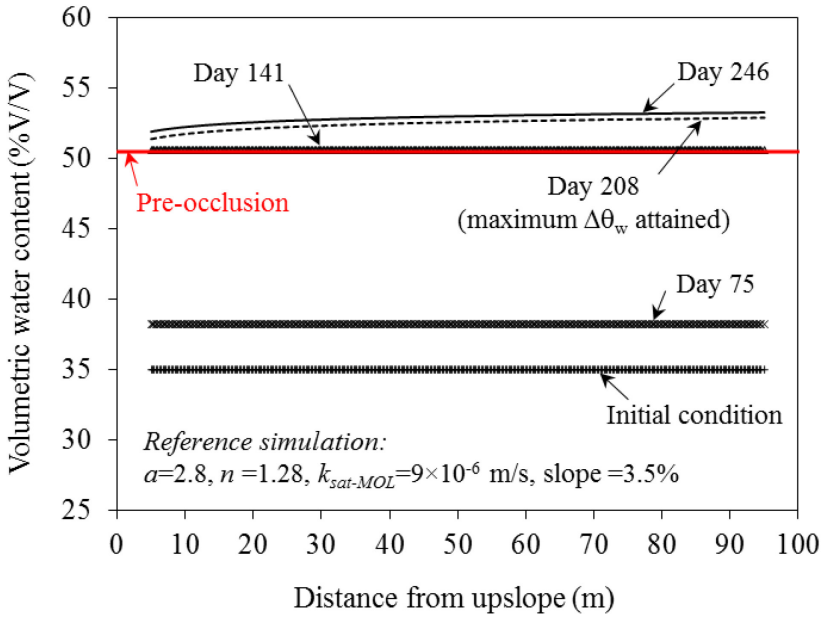

Figure 4-6: Distribution of θ_w in *interface points* at several time steps in simulation No. 1 (*Reference simulation*)

Figure 4-7 presents the K values of the *interface points*, at several time steps during the *Reference simulation*. K decreased continuously with time and, on day 141, all K values of the *interface points* fell below the pre-occlusion value, i.e. $K = 2.1\times10^{-12}$ m^2. The lowest value of K during the simulation period was 1.4×10^{-12} m^2.

Prior to the pre-occlusion, the maximum value of K_{max}/K_{min} occurred on day 129 and it was equal to 1.0007. In other words, there was very little variability in K along the interface up to this time. This is expected, given the small variation in moisture content along the interface. During the analysis, the maximum value of K_{max}/K_{min} was equal to 1.25, and occurred on day 208.

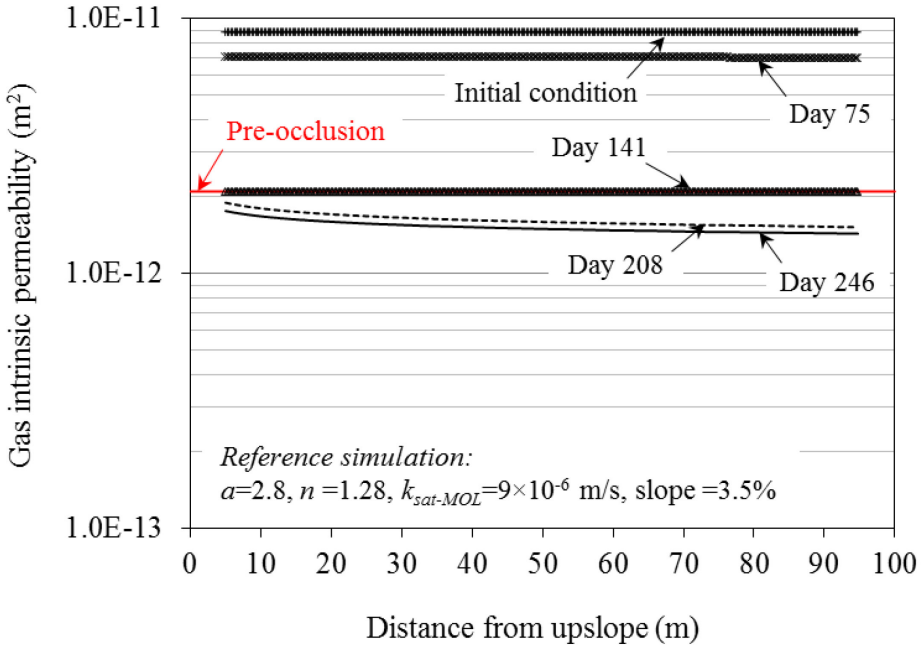

Figure 4-7: Distribution of K in *interface points* at several time steps, for simulation No. 1

4.3.2. Effect of the pore size distribution

The parameter *n* in the Van Genuchten [1980] equation represents the rate of desaturation of the soil. The greater the value of *n*, the steeper the slope of WRC, and the easier to drain (desaturate) the soil [Fredlund et al., 2002]. Since the shape of the grain size distribution (GSD) curve is similar to the shape of the WRC, the former is often used to estimate the latter [e.g. Arya and Paris, 1981; Fredlund et al., 2002]. In practical terms, the steeper the GSD, the steeper the slope of the desaturation zone of the WRC.

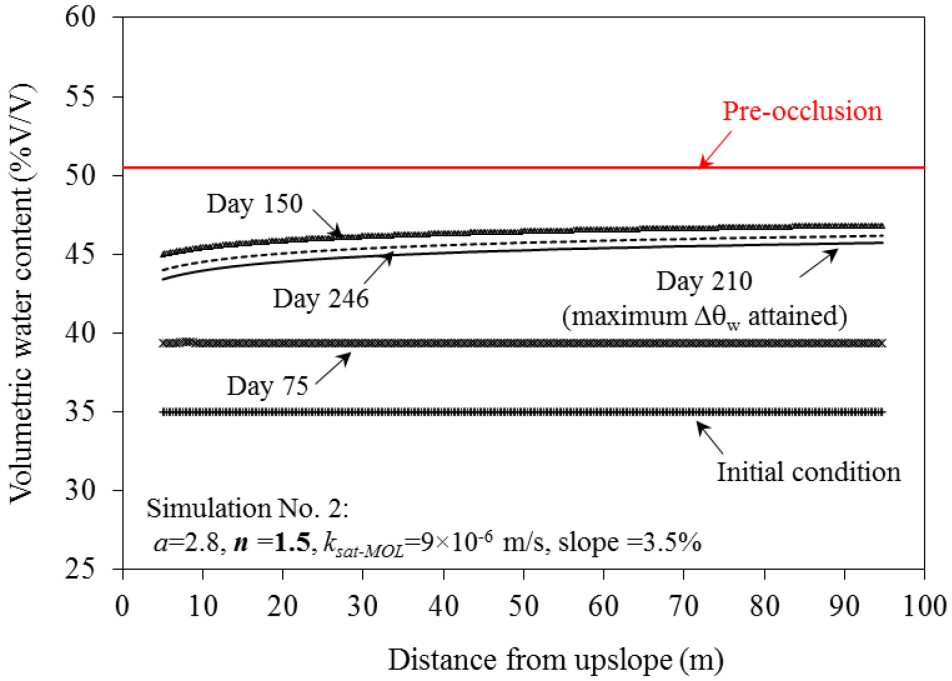

Figure 4-8: Distribution of θ_w in *interface points* at several time steps, for simulation No. 2

For simulation No. 2, the value of the van Genuchten parameter *n* of the *Reference MOL* was increased from 1.28 to 1.5, while the values of *a*, $k_{sat\text{-}MOL}$ and initial θ_w remained constant. The variation of θ_w with distance is presented in Figure 4-8. In this case, in order to evaluate whether or not there was pre-occlusion, a value of $\theta_{w\text{-}pocc}$ had to be adopted, since it was not obtained in the laboratory for this simulated MOL. For simulations No. 2 and No. 8 the same $\theta_{w\text{-}pocc}$ value of the *Reference MOL* was adopted.

The results of the simulation showed that the maximum $\Delta\theta_w$ occurred on day 210 and an increase in *n* led to a reduction in the value of θ_w and therefore, to an unrestricted gas flow across the interface. Indeed, $\theta_{w\text{-}max}$ attained 47.0%, which is lower than $\theta_{w\text{-}pocc}$. However, the validity of these results relies on the presupposition that it was reasonable to adopt the same $\theta_{w\text{-}pocc}$ value of the *Reference MOL*. This hypothesis was verified as discussed in the remainder of this section.

In Figure 4-9, WRC of *Reference MOL* is compared with WRC of two other materials from other studies, whose shapes of gas permeability function (shown in Figure 4-10) are similar (see Figure 4-3 for the *Reference MOL*). The shapes are similar insofar as one can clearly identify the occurrence of pre-occlusion. In the case of the clay, $\theta_{a\text{-}pocc}$ was equal to ~12%

(Figure 4-10a), whereas for the silty sand it was ~17% (Figure 4-10b) ($\theta_{a\text{-}pocc} \approx 16$ % for the *Reference MOL*). According to Figure 4-9, the steepest slope of desaturation zone was associated with the clay studied by Jucá and Maciel [2006], followed by the silty sand tested by Springer et al. [1998], and the sand-compost mixture of the *Reference MOL*. Therefore, the clay possessed the greatest value of *n*. The results presented in Figure 4-9 and Figure 4-10 showed that materials with different textures and desaturation slopes (as expressed by *n*) may exhibit rather similar values of $\theta_{a\text{-}pocc}$. Based on this limited analysis, it was assumed that changing the value of *n* from 1.28 (adopted for the *Reference MOL*) to 1.5 would not lead to much of a difference in $\theta_{a\text{-}pocc}$.

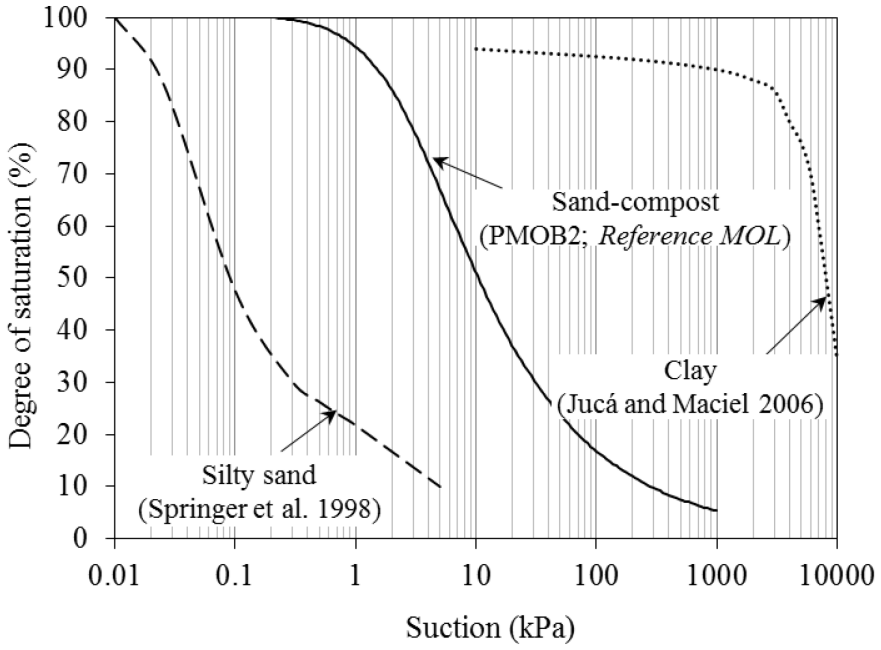

Figure 4-9: The WRC of the *Reference MOL* and materials from other studies

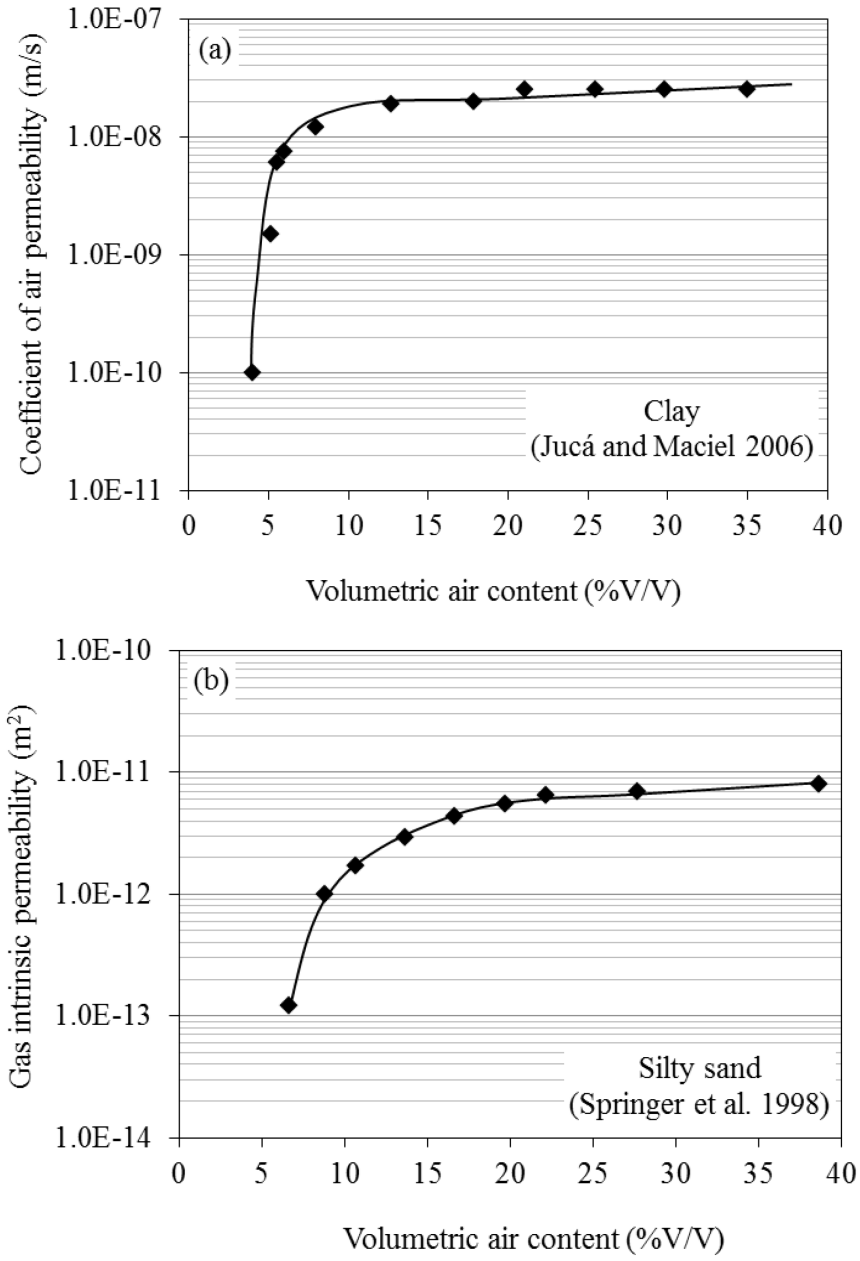

Figure 4-10: variation of (a) coefficient of air permeability and (b) gas intrinsic permeability with θ_a in materials from other studies [Springer et al., 1998; Jucá and Maciel, 2006]

In Figure 4-11, two GSD curves were derived from the WRCs: one for the *Reference MOL* (a = 2.8 and n =1.28) and the other for the modified *Reference MOL* (a = 2.8 and n = 1.5). In order to obtain the material with n = 1.5, the amount of compost whose particles have a diameter less than 0.4 mm had to be artificially decreased and substituted by a granular soil, such as sand. It is as if there was more sand in the mixture. Such substitution entails a slight change in G_s and saturated volumetric water content (θ_s, which is equal to porosity). Since the

initial dry density, $\theta_{a\text{-}pocc}$ and the porosity of the material remained similar, $\theta_{w\text{-}pocc}$ remained almost unaltered. Consequently, increasing *n* to 1.5 resulted in only a slight change in $\theta_{w\text{-}pocc}$, the control parameter based on which the results of the simulations are analyzed.

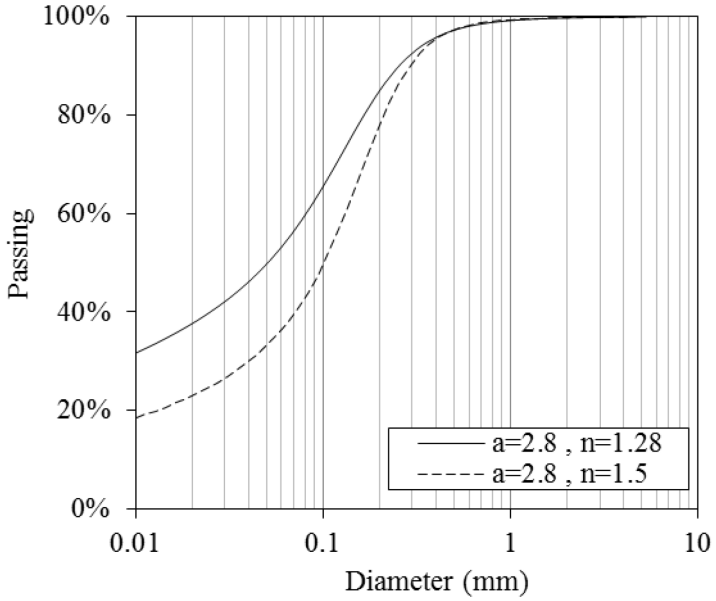

Figure 4-11: The corresponding grain size distribution curves of WRCs of MOL materials with *a*=2.8 and *n* equal to 1.28 or 1.5, using the Fredlund et al. equation *[2002]*

4.3.3. Effect of Initial dry density

The effect of compaction on the value of gas permeability has been the subject of several studies both in soil mechanics [e.g. Tang et al., 2011; Leroueil and Hight, 2013] and dealing with methane oxidation efficiency of passive methane oxidation biosystems [e.g. Gebert et al., 2011a; Rachor et al., 2011]. It can be expected that an increase in dry density results in a higher air entry value (AEV), therefore greater values of *a*, while the slope of the desaturation zone of the WRC (*n*) remains unchanged [Nuth and Laloui, 2008; Mirzaii and Yasrobi, 2012]. The same behavior was observed in the material constituting the *Reference MOL* [AhouGhalandari et al., 2015]. Therefore, the results obtained from simulations where the value of *a* was increased from 2.8 to 4.2, are expected to incorporate the effect of a higher initial dry density of the MOL on the distribution of θ_w values along the GDL-MOL interface.

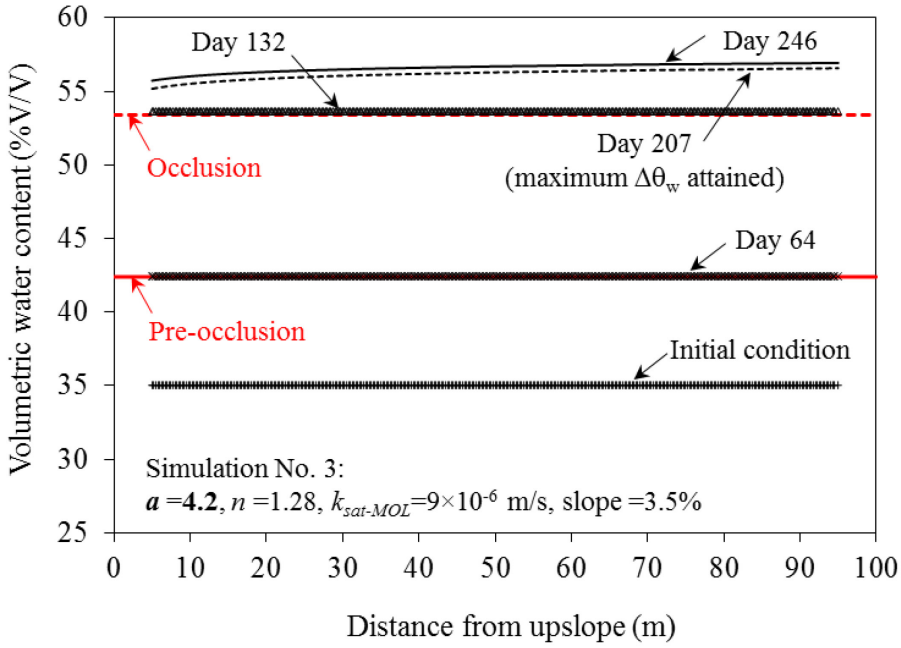

Figure 4-12: Distribution of θ_w in *interface points* at several time steps, for simulation No. 3

Figure 4-12 shows the results of simulation No. 3, for which the initial θ_w was equal to 35.0%. The initial θ_w corresponds to S_r = 60% and w = 38%, indicating that the material was compacted dry of optima. As a result of increasing the initial dry density of the MOL material, θ_w at the *interface points* exceeded both $\theta_{w\text{-}pocc}$ (42.7%) and $\theta_{w\text{-}occ}$ (53.4%) on days 64 and 132, respectively. It is noteworthy to recall that $\theta_{w\text{-}occ}$ was not attained during the *Reference simulation*. Prior to the onset of pre-occlusion, the maximum $\Delta\theta_w$ was equal to 0.0049%; by all means a nearly negligible difference in moisture content between the top and the bottom of the slope. Therefore, the value of LUGM abruptly became equal to zero when $\theta_{w\text{-}pocc}$ was attained. The maximum $\Delta\theta_w$ occurred on day 207.

4.3.4. Effect of $k_{sat\text{-}MOL}$

Figure 4-13 shows θ_w values at the *interface points* for several time steps of simulations No. 4 to No. 6. For these simulations, the $k_{sat\text{-}MOL}$ was 9×10^{-4} m/s, i.e. 100 times greater than the $k_{sat\text{-}MOL}$ of the *Reference MOL*. Since the materials corresponding to simulations No. 4 to No. 6 were not characterized, the values of $\theta_{w\text{-}pocc}$ and $\theta_{w\text{-}occ}$ are unknown. Consequently, it was not possible to clearly evaluate whether or not the *interface points* ever reached pre-occlusion or occlusion.

The results in Figure 4-13 show that, at each time step, the increase in $k_{sat\text{-}MOL}$ led to greater variations in θ_w along the interface, towards the bottom of the slope. In other words, $\Delta\theta_w$ for these simulations were greater than those obtained with the corresponding simulations with $k_{sat\text{-}MOL}$ = 9×10^{-6} m/s, i.e. *Reference simulation* and simulations No. 2 and No. 3. The maximum values of $\Delta\theta_w$ during simulations No. 4 to No. 6 occurred on day 207. The evolution of θ_w with time in simulations No. 4 to No. 6 was consistent with the variation in seepage rate with time (Figure 4-5), a clear indication of the sensitivity of the modeled system to the seepage rate, due to the value of $k_{sat\text{-}MOL}$.

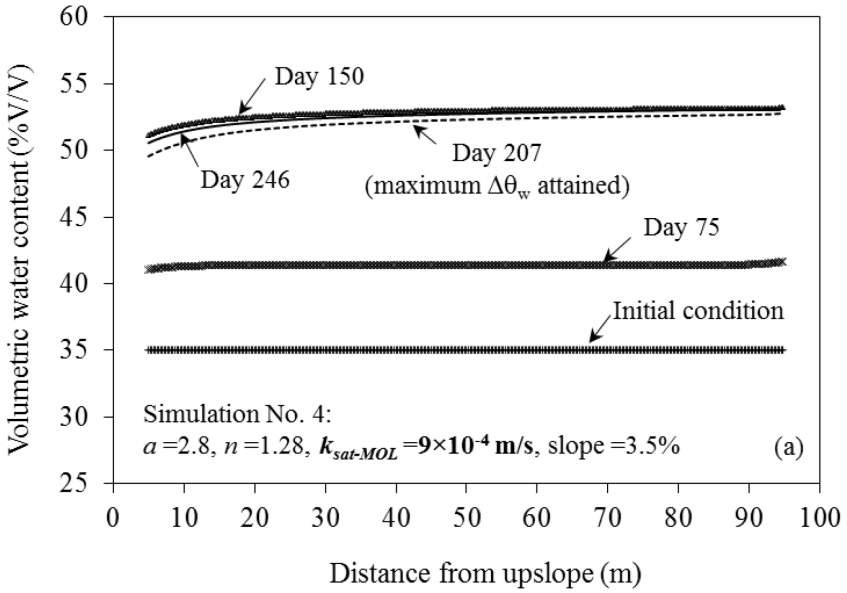

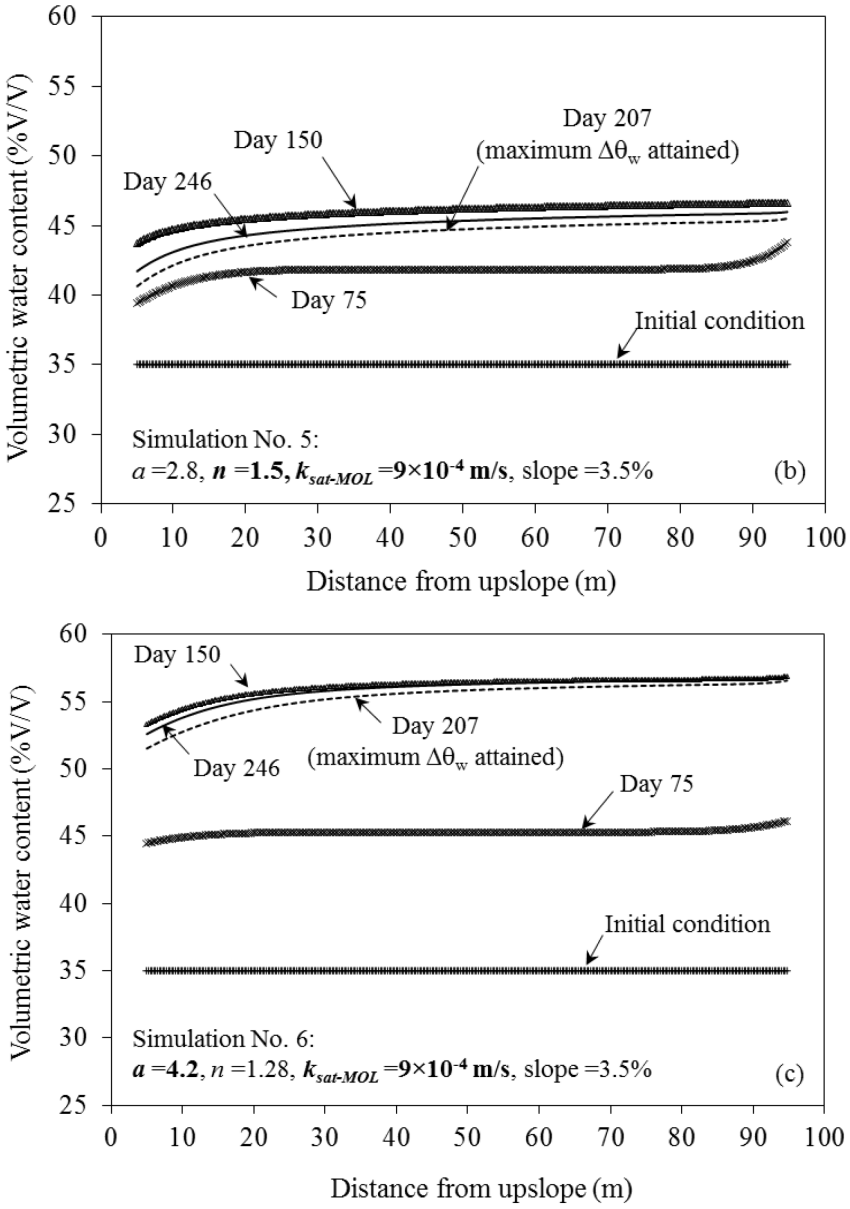

Figure 4-13: Distribution of θ_w in *interface points* at several time steps, for (a) simulation No. 4, (b) simulation No. 5, and (c) simulation No. 6

4.3.5. Effect of slope

Figure 4-14, shows the results of simulations No. 7 to No. 9, which used the same materials as simulations No. 1 to No. 3, respectively (Table 4-1). However, in these cases, the model was built with a steeper slope (10%). Simulation No. 7 (Figure 4-14a) was quite similar to the *Reference simulation*, insofar as the value of LUGM became equal to zero quite abruptly; and both on day 141. LUGM abruptly became equal to zero on day 64 in simulation No. 9 (Figure 4-14c), and on day 132 the interface had become completely occluded. The change in

slope from 3.5% to 10% led to very slight changes in θ_w along the interface. This is valid when comparing simulations No. 1 and No. 7, No. 2 and No. 8 and No. 3 and No. 9.

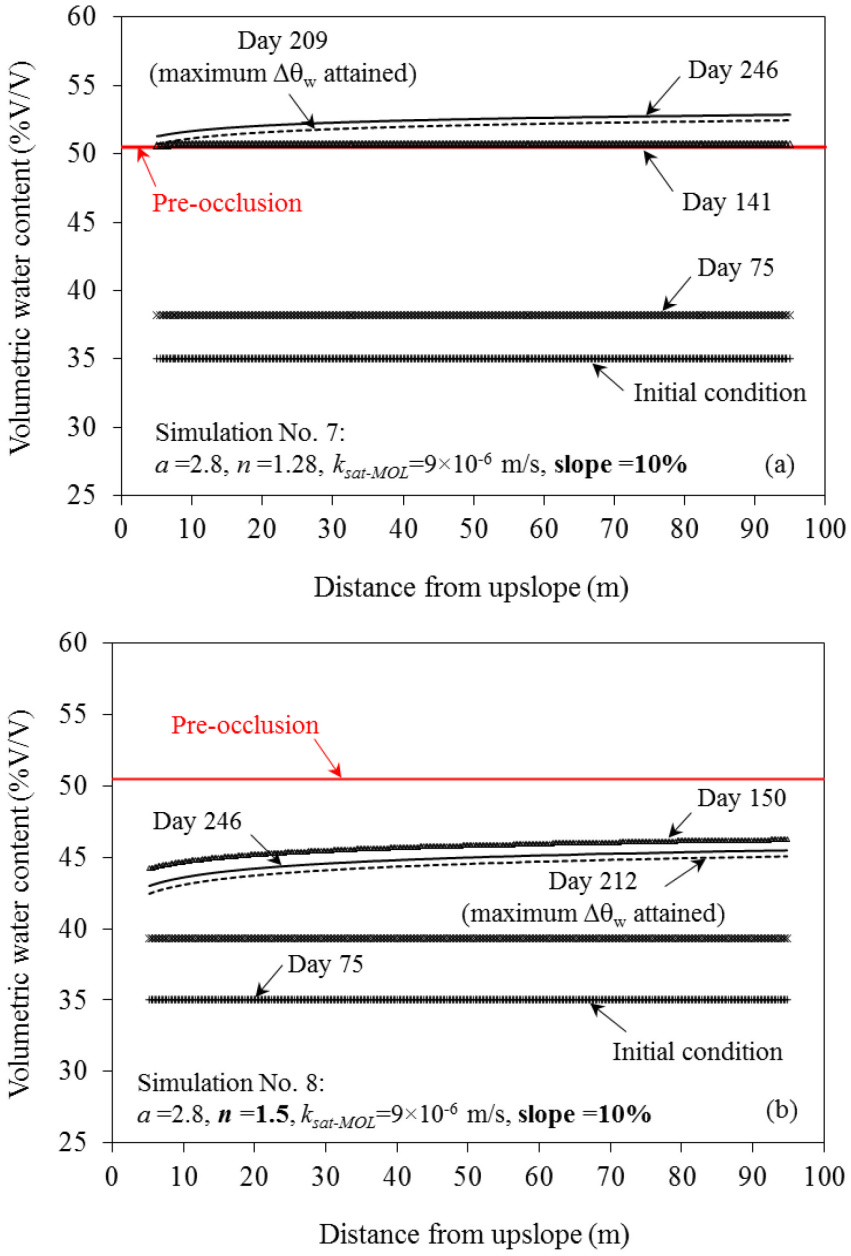

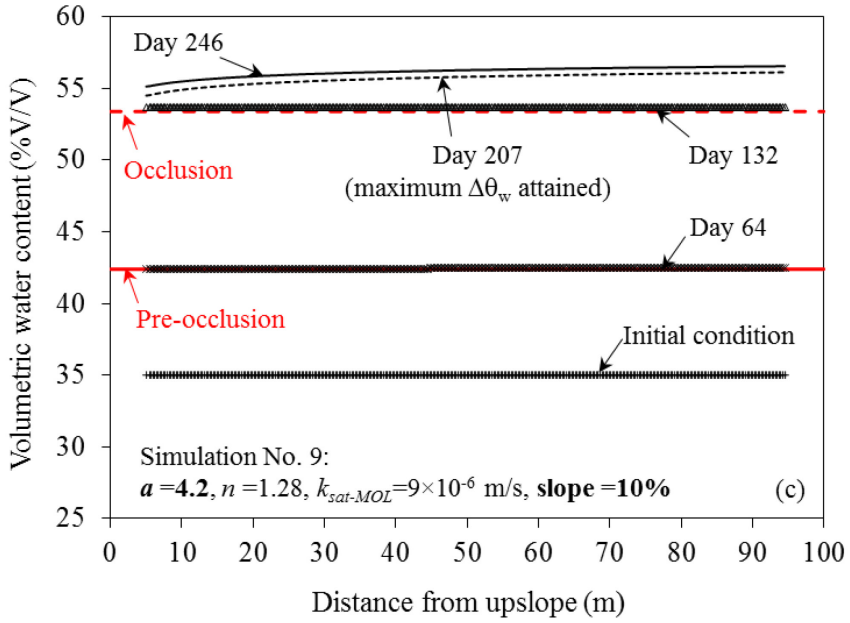

Figure 4-14: Distribution of θ_w in *interface points* at several time steps, for (a) simulation No. 7, (b) simulation No. 8, and (c) simulation No. 9

Figure 4-15 shows the results of simulations No. 10 to No. 12, whose interfaces were steeper than interfaces in simulations with the same materials (No. 4 to No. 6; see Table 4-1). As can be observed in Figure 4-15, at each time step, increasing the slope of the interface resulted in a radically greater variation in θ_w along the interface.

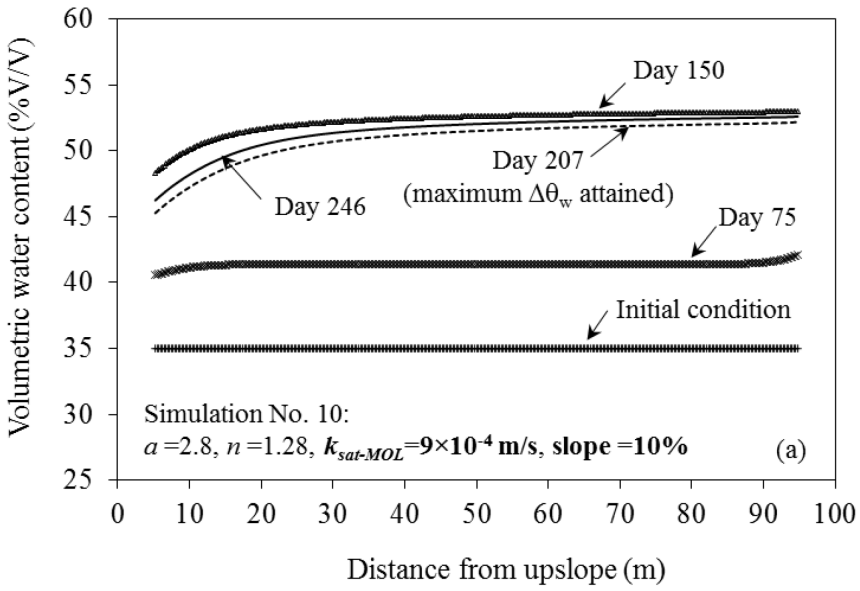

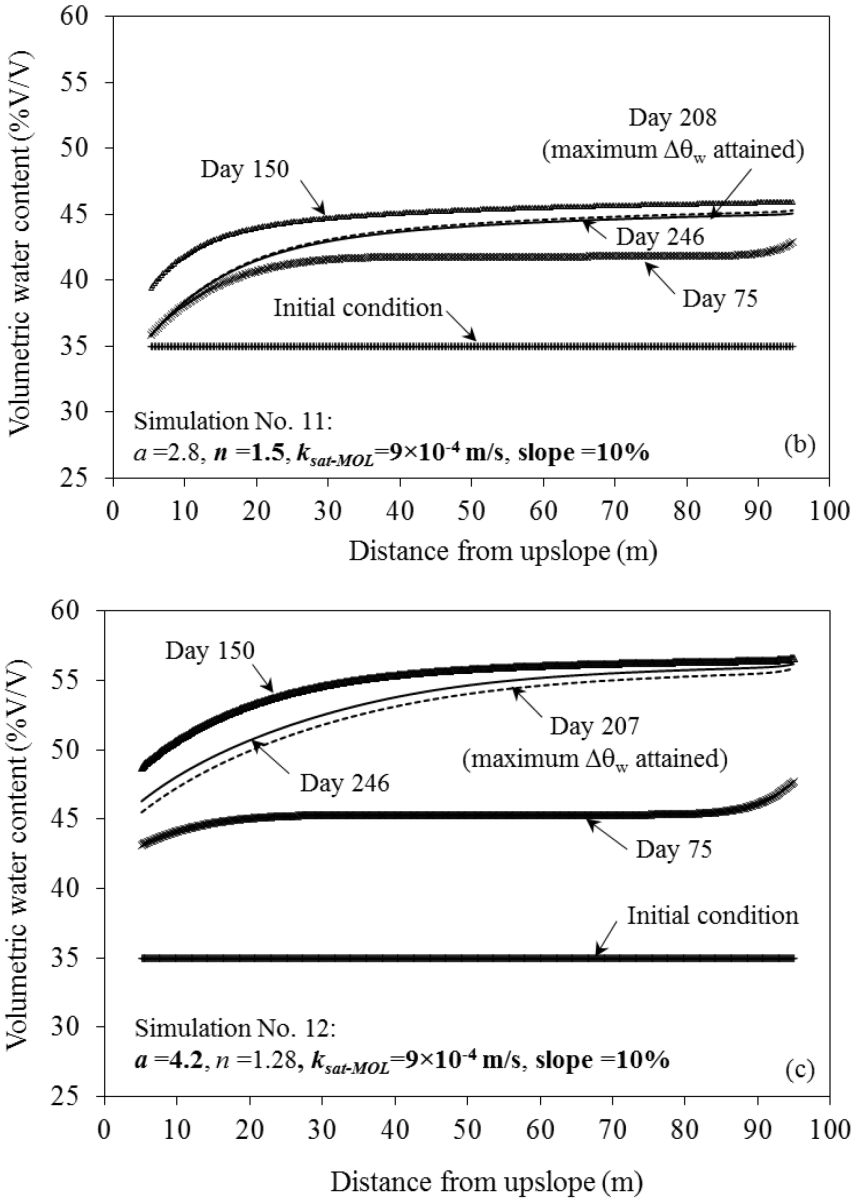

Figure 4-15: Distribution of θ_w in *interface points* at several time steps, for (a) simulation No. 10, (b) simulation No. 11, and (c) simulation No. 12

4.4. Discussion

Figure 4-16 presents the effect of slope, $k_{sat\text{-}MOL}$, a and n on $\theta_{w\text{-}max}$ at the *interface points* of simulations No. 1 to No. 12. It can be observed that the values of $\theta_{w\text{-}max}$ decreased very slightly with the increase in slope of the interface. However, when it comes to the van Genuchten parameter a, regardless of the value of the slope and $k_{sat\text{-}MOL}$, increasing a (which can be attributed to greater compaction) results in a large increase in $\theta_{w\text{-}max}$, i.e. the air-filled pores at *interface points* would become more likely to reach $\theta_{w\text{-}pocc}$ or $\theta_{w\text{-}occ}$.

For each value of *a*, *n* and slope, increasing the $k_{sat\text{-}MOL}$ very slightly increased the value of $\theta_{w\text{-}max}$. However, important drops in the values of θ_w and $\theta_{w\text{-}max}$ at *interface points* were observed following an increase in the value of *n*. For example, increasing the *n* of the *Reference MOL* (Simulation No. 2; Figure 4-8) led to a value of LUGM equal to the total length of the interface, i.e. it remained completely unrestricted throughout the duration of the simulation, whereas in the actual *Reference simulation*, LUGM had become equal to 0 on day 141.

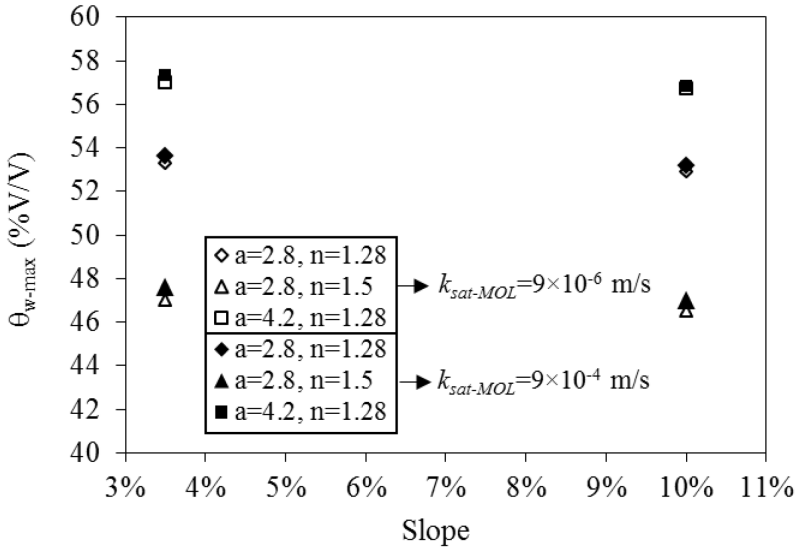

Figure 4-16: $\theta_{w\text{-}max}$ values in *interface points*, for several values of *a*,*n*, $k_{sat\text{-}MOL}$ and slope

It stems from these analyses that, among the variables evaluated in the present study, *n* is the one that most influenced $\theta_{w\text{-}max}$, therefore the response of the PMOB to upward gas migration. In simpler terms, *n* is a fundamental parameter in PMOB design, since it is determinant in reducing the risk of attaining pore occlusion (or pre-occlusion), which restricts upward gas migration across the GDL-MOL interface. When partial occlusion occurs, biogas flows laterally within the GDL towards the top of the slope, where it can escape to the atmosphere. Of course, biogas can also escape through preferential pathways, such as cracks within the final cover (tension cracks are common near the top of slopes) or voids around protruding instrumentations and collection wells. In all these cases, hotspots, a recurring problem in landfills, are created.

In Figure 4-17 the maximum values of $\Delta\theta_w$ are plotted as a function of slope, $k_{sat\text{-}MOL}$, a and n. For simulations with $k_{sat\text{-}MOL} = 9.4\times10^{-6}$ m/s, increasing a and slope had a minor effect on the maximum $\Delta\theta_w$. However, increasing n led to important variations of θ_w (greater $\Delta\theta_w$). For certain types of designs, such as the jagged interface proposed by Kjeldsen et al. [2013], it is important to maintain θ_w at the top of each segment sufficiently lower than at the bottom to increase the chances that a sufficiently large "channel" allows upward migration of CH_4 to be oxidized within the MOL.

In the cases where $k_{sat\text{-}MOL}$ was 100 times greater (9.4×10^{-4} m/s), increasing a, n and slope, considerably increased the maximum $\Delta\theta_w$. Accordingly, depending on the value of $k_{sat\text{-}MOL}$, the other 3 variables (a, n and slope) may have an important role in controlling the pattern of upward flow of biogas, and reducing the chances of localized emissions (hotspots).

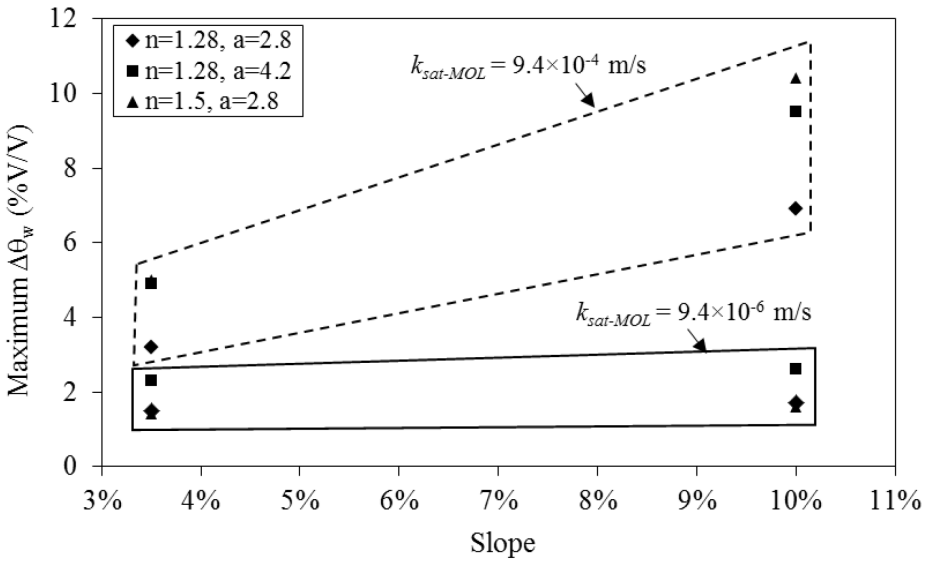

Figure 4-17: Maximum $\Delta\theta_w$ in *interface points*, for several values of a, n, $k_{sat\text{-}MOL}$ and slope

Figure 4-18 shows the day when $\theta_{w\text{-}max}$ was attained for several simulations. As presented in the previous section, the time associated with the onset of maximum $\Delta\theta_w$ was quite similar for all simulations, i.e. days 207-212. According to Figure 4-18, for simulations with n or slope greater than those of the *Reference simulation*, $\theta_{w\text{-}max}$ was attained earlier than maximum $\Delta\theta_w$. In other words, from the moment when $\theta_{w\text{-}max}$ is attained until the onset of maximum $\Delta\theta_w$ the *interface points* are continuously drained, particularly towards the top of the slope. The

temporary drainage of *interface points* may be considered as an advantageous effect, as far as unrestricted upward flow of biogas is concerned. For the simulations with *n* or slope equal to those of the *Reference simulation*, $\theta_{w\text{-}max}$ was attained later than maximum $\Delta\theta_w$ (gray area in Figure 4-18). Therefore, between the onset of $\theta_{w\text{-}max}$ and the moment when the maximum $\Delta\theta_w$ was attained, the interface became wetter.

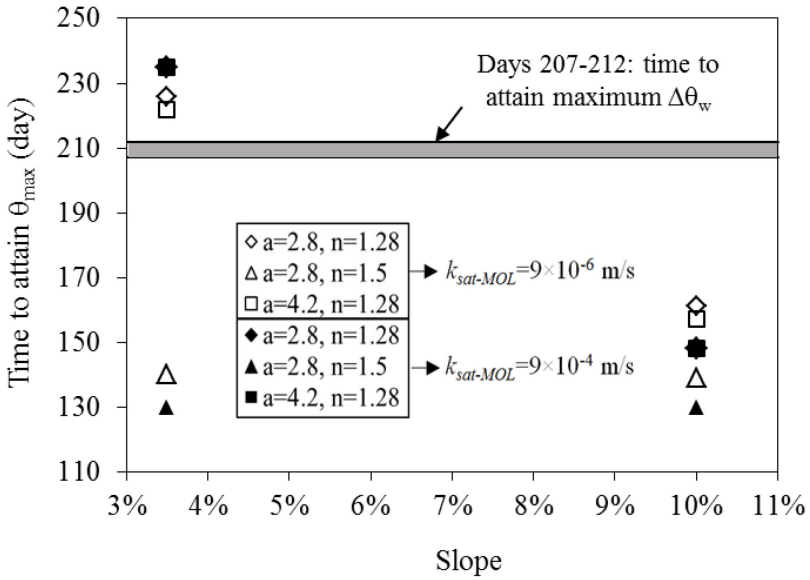

Figure 4-18: The time associated with attaining the $\theta_{w\text{-}max}$ in *interface points*, for several values of *a*, *n*, $k_{sat\text{-}MOL}$ and slope

4.5. Conclusions

This study and the simulations thereof aimed at evaluating how variations in the main hydraulic parameters affected the behavior of a modelled PMOB, as far as biogas migration and loading distribution at the base of the MOL is concerned. Ideally, the values of $\theta_{w\text{-}pocc}$ and/or $\theta_{w\text{-}occ}$ (or $\theta_{a\text{-}pocc}$ and/or $\theta_{a\text{-}occ}$) would have been known for all simulations, i.e. all the simulated MOL materials would have been characterized to obtain their hydraulic parameters and gas flow properties. Analysis of the performance would therefore be straightforward: the distance from the top to the point where $\theta_{w\text{-}pocc}$ occurred (i.e. LUGM) would be determined from the simulations. Designs would be based on an optimization of the value of LUGM. It is not necessary to seek for the maximum value of LUGM, which is equal to the entire length of the interface. Good practice calls for a compromise between CH_4 oxidation efficiency and the cost of materials to construct the PMOB. Unfortunately, it was beyond the scope of this study

to determine the hydraulic and gas flow parameters of all the materials considered in the simulations presented herein. The value of this study relies on the identification of the relative importance of the main variables involved.

Increasing any of three parameters, i.e. n, $k_{sat\text{-}MOL}$ and slope of the interface, led to greater differences in volumetric water content along the interface, which in designs as in the present study may result in a LUGM shorter than the total length of the interface. Regarding the van Genuchten parameter a, the greater its value, the greater are the chances that the pores in *interface points* become occluded enough to restrict upward gas flow.

The maximum suction values in all simulations were sufficiently high to prevent seepage of water from the MOL into the GDL for a capillary barrier with the MOL acting as a moisture retaining layer and the GDL as a capillary block layer (data not presented). However, these suction levels were low enough to allow the air-filled pores of MOL to be in a state of occlusion or pre-occlusion, and therefore to divert upward migrating biogas upslope. If the biogas eventually escapes to the atmosphere in a concentrated point upslope it can potentially decrease the methane oxidation efficiency of a passive biosystem, which needs to be avoided by design.

Acknowledgements

This study received financial support from the Natural Science and Engineering Research Council of Canada (NSERC) and Waste Management (WM Quebec Inc.), under the collaborative research and development grant # CRD 379885-08, from the Consortium de recherche et innovations en bioprocédés industriels du Québec (CRIBIQ) and from Discovery Grant #170226. The invaluable help of Jean-Guy Lemelin, technician, and of Philippe Tétrault, formerly with the Geoenvironmental Group at University of Sherbrooke, must also be acknowledged.

CHAPTER 5. EVALUATION OF THE UPWARD FLOW OF BIOGAS AT THE BASE OF METHANE OXIDATION LAYER OF THREE PMOBS

5.1. Introduction

The objective of this chapter is to analyse the upward flow of biogas at the base of methane oxidation layer (MOL) of three passive methane oxidation biosystems (PMOBs), influenced by unsaturated flow of meteoric seepage and ensuing capillary barrier effect. Chapter 5 presents, indeed, the application of design criteria and the considerations in the design of PMOBs introduced in previous chapters, using transient-state simulations in SEEP/W. The results presented in this chapter will be submitted to a journal, before the final thesis deposit.

5.2. Materials and methods

5.2.1. Site configurations

The first design, named herein *German design*, is a large-scale experimental PMOB with a slope of 1V:10H, constructed in Germany. Several years of field investigations showed the persistent presence of a hotspot upslope [Bohn and Jager, 2009]. It consisted of the following layers from top to the bottom: a 30-cm layer of compost and loamy clay mixture (top soil), a 70-cm layer of clayey silt (subsoil), a 40-cm layer of sand, and a 20-cm layer of gravel. The latter two layers were constructed to control the infiltration and act as gas distribution layer (GDL). The first two layers together, denominated *recultivation layer*, create the MOL of the PMOB.

The second design (*Danish design*-combination 1) is also an experimental PMOB situated in Denmark, designed and constructed by Kjeldsen et al. [2013]. This 42-m length PMOB

consisted of a MOL with 80-90 cm thickness and a GDL of 30-50 cm thickness. Compost material (CL) and coarse gravel were used to construct the MOL and the GDL, respectively. The GDL-MOL interface had a jagged form, which was assumed to provide a permanent available passage for upward flow of biogas at top of each segment (see Figure 5-4), while the bottom parts may become restricted by accumulated seepage, due to the capillary barrier effect. The slope of the jagged interface and the width of each segment were equal to 7% and 4 m, respectively.

For the last design, denominated as *Danish design*-combination 2, the configuration of the *Danish design*-combination 1 was adapted; however, the MOL was subdivided into two layers: a 15-cm layer of sand-compost mixture and a 45-60 cm layer of fine sand. Very high methane oxidation efficiencies, both in laboratory-scale column experiments and in 90×90 cm experimental field plots, were reported by Ndanga et al. [2015] for the latter layout of MOL. The main characteristics of the fine sand and the sand-compost mixture are presented in chapter 3. The reasoning for substituting the MOL material of *Danish design*-combination 1 with a two-layer-MOL as in *Danish design*-combination 2 will be discussed in section 5.3.

5.2.2. Hydraulic properties of the materials

The water retention curves (WRC) and hydraulic conductivity functions (*k-fct*s) of the materials used in simulations are presented in Figure 5-1 and Figure 5-2. The WRCs of the materials for *German design* was obtained from grain size distribution curves, using the Arya and Paris model [1981]. In order to define the materials in SEEP/W, the van Genuchten model [1980] was used as the fitting equations for WRCs, and hydraulic conductivity functions (*k-fct*s) were obtained using the van Genuchten [1980] model, based on the Mualem formulation [1976] (Equations 4-1 and 4-2). The subsoil and the topsoil layers had very similar hydraulic properties. Therefore, only one material was used as MOL material.

Since the actual properties of the materials used to construct the *Danish design*-combination 1 were unknown, the constituting materials of MOL and GDL of an experimental PMOB at the St-Nicepohre landfill (Quebec, Canada), entitled PMOB2, were used to build the simulations. Similar to the *Danish design*-combination 1, compost material was used in MOL of PMOB2. The details of obtaining the WRCs and *k-fct*s of the GDL and MOL materials of PMOB2

were presented in chapter 3 and chapter 4. A summary of the hydraulic properties of the materials used in numerical simulations is shown in Table 5-1.

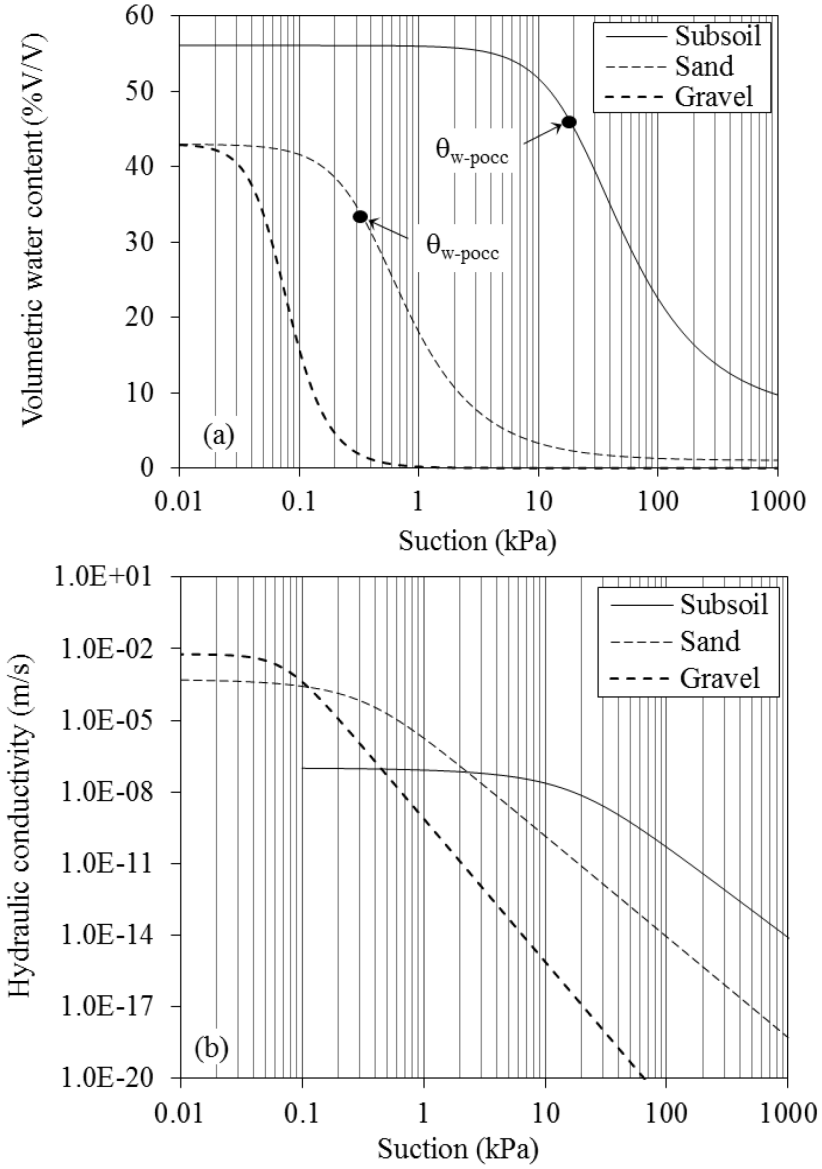

Figure 5-1:(a) WRCs, and (b) *k-fcts*, used in simulation of *German design*

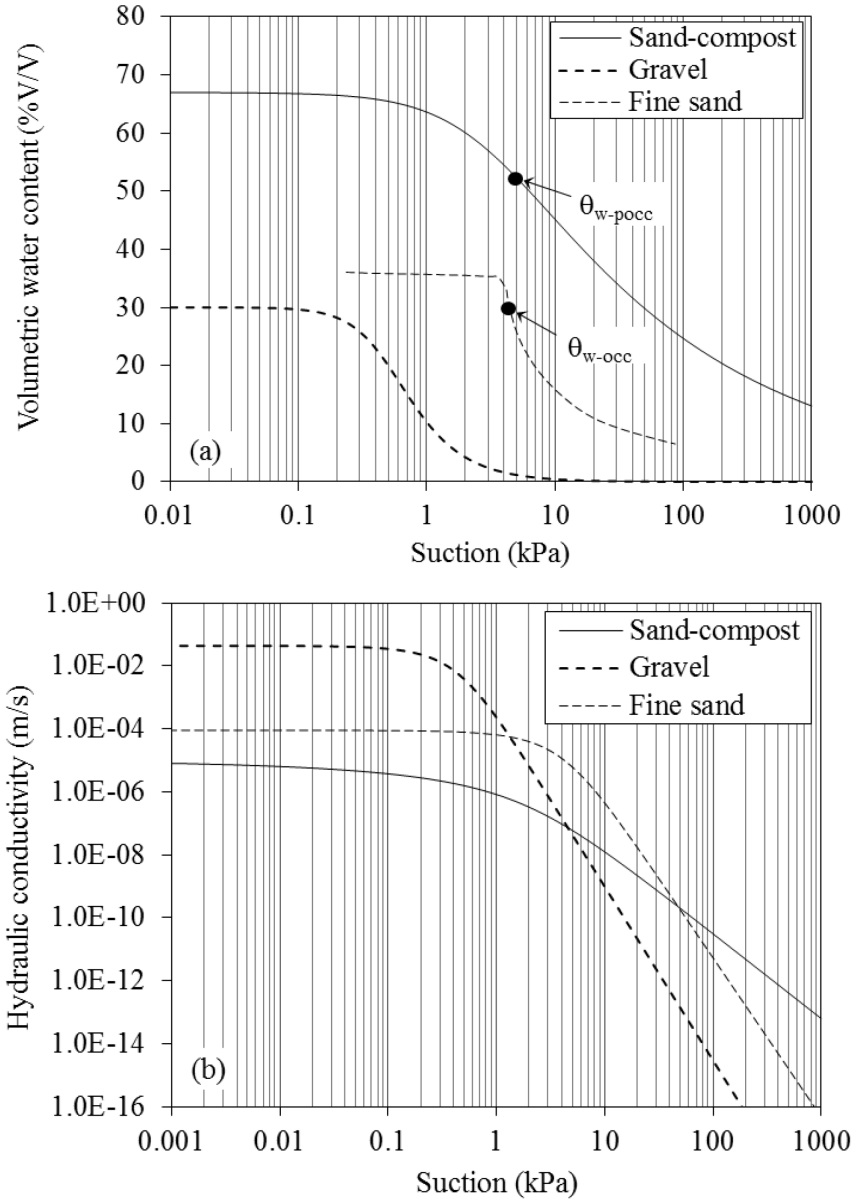

Figure 5-2: (a) WRCs, and (b) *k-fcts*, used in *Danish design*-combination 1 and *Danish design*-combination 2

Table 5-1: Hydraulic properties of the materials used in the numerical simulations

Parameters	*German design*			*Danish design*-combination 1 and *Danish design*-combination 2		
	subsoil	sand	gravel	sand-compost	fine sand	gravel
a (kPa)	22.5	0.4	0.066	2.8	-	0.5
n	1.747	1.9	3	1.28	-	2.4
θ_s (%V/V)	56.1	43	43	67	36.6	30
θ_r (%V/V)	6.83	1	0	0.1	5	0
k_{sat} (m/s)	1.0×10^{-7}	5.0×10^{-4}	6.0×10^{-3}	9.0×10^{-6}	9.0×10^{-5}	4.3×10^{-2}

5.2.3. Design parameters for flow of biogas at the base of MOL

According to Figure 5-1 and Figure 5-2, the capillary barrier effect can be formed along the interface between subsoil and sand, and/or sand and gravel in *German design*. Between sand-compost mixture and gravel for *Danish design*-combination 1, and between sand-compost mixture and fine sand, and/or fine sand and gravel in *Danish design*-combination 2 as well, the capillary barrier can be identified. Therefore, the design parameters for the constituting materials of the upper layer of each interface, i.e. subsoil and sand in *German design*, sand-compost in *Danish design*-combination 1, and sand-compost and fine sand in *Danish design*-combination 2, should be defined.

As discussed in chapter 3, the design parameters for flow behavior of biogas at the base of MOL, i.e. $\theta_{a\text{-}occ}$ and $\theta_{a\text{-}pocc}$, could be obtained using k_a-function, WRC and Standard Proctor curve. For the materials used to construct the *German design*, design parameters should be obtained using the WRCs, as the only available information. Adapting the van Genuchten model [1980] to fit the WRCs results in creating a transition zone around the air entry values (AEVs) of all materials, regardless their actual unsaturated hydraulic behavior. Therefore, a $\theta_{a\text{-}pocc}$ value is expected for both subsoil and sand. Assuming that the S_r (therefore θ_w under constant dry density condition) associated with the AEV provides a reasonable estimation of S_r (and θ_w) at $\theta_{a\text{-}occ}$, the S_r (and θ_w) at $\theta_{a\text{-}pocc}$ is considered as 10% lower than the S_r (and θ_w)

corresponding to the $\theta_{a\text{-}occ}$ value. This latter percentage coincides with the point at which the transition zone around the AEV is connected to the desaturation zone (singled out by circles in Figure 5-1a). Consequently, the θ_w at $\theta_{a\text{-}pocc}$ ($\theta_{w\text{-}pocc}$) is equal to 32% and 46% for sand and subsoil, respectively.

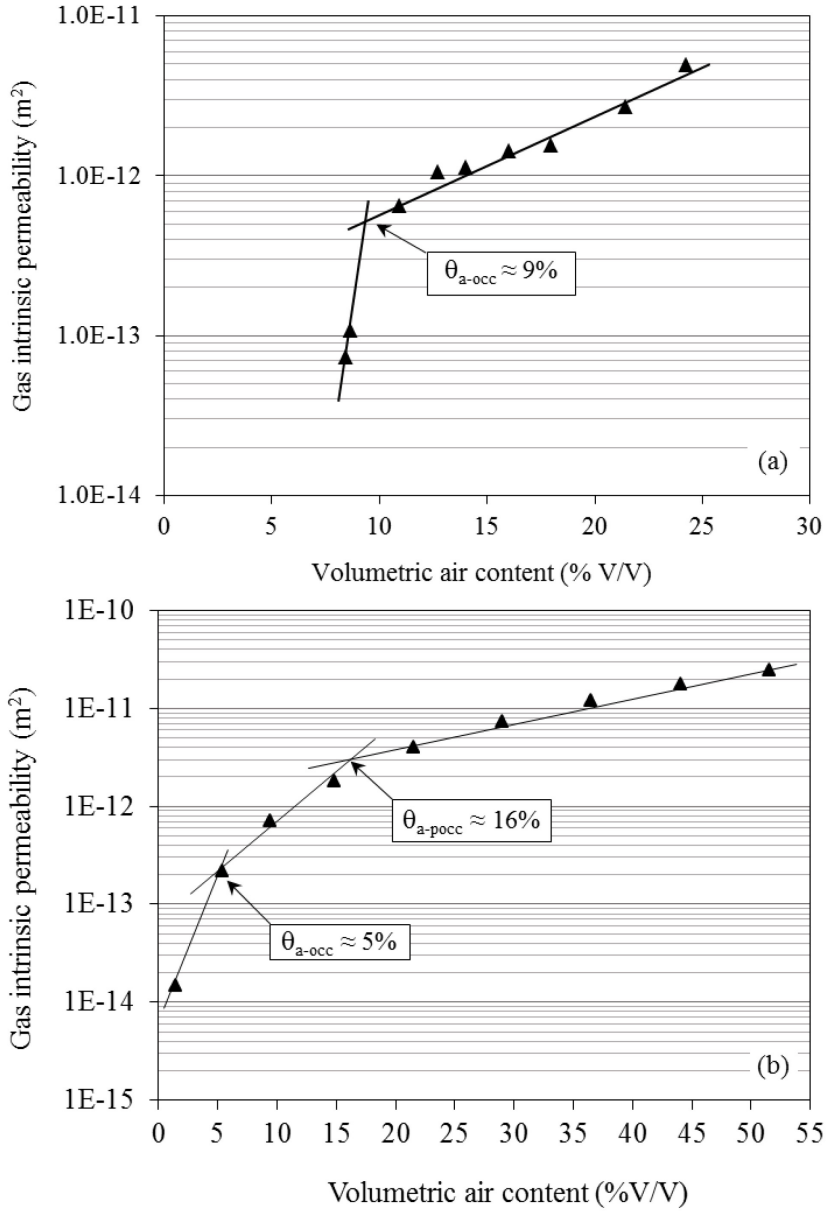

Figure 5-3: Gas intrinsic permeability function of (a) fine sand, and (b) sand-compost, and the corresponding design parameters

Since the k_a-functions of the fine sand and the sand-compost mixture used in *Danish design*-combination 1 and *Danish design*-combination 2 were obtained in the laboratory, the design parameters can be identified more precisely. As shown in Figure 5-3, $\theta_{a\text{-}occ} \approx 9\%$ and $\theta_{a\text{-}pocc} \approx 16\%$ are the design parameters in fine sand and sand-compost mixture, respectively. The installation dry density is assumed as 1650 kg/m^3 in fine sand and 750 kg/m^3 in sand-compost. Therefore, $\theta_{w\text{-}occ}$ (θ_w at $\theta_{a\text{-}occ}$) = 30% for fine sand and $\theta_{w\text{-}pocc}$ = 50.5% for sand-compost mixture. $\theta_{w\text{-}occ}$ in sand-compost is equal to 61.5%.

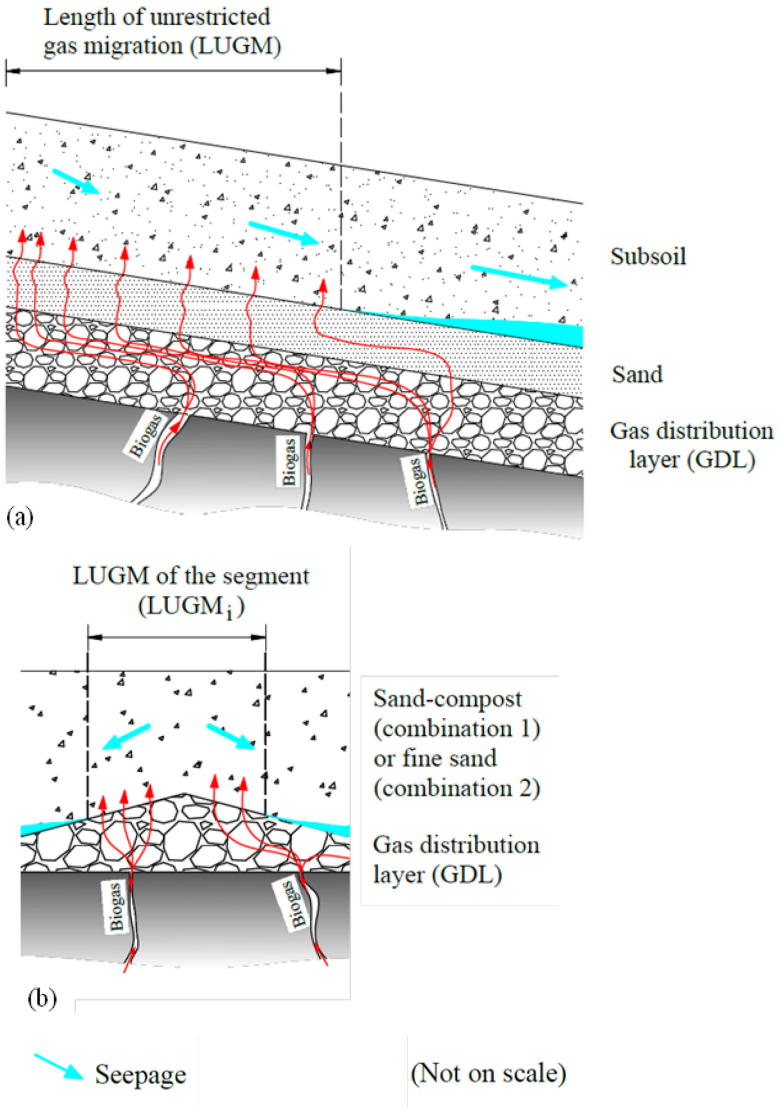

Figure 5-4: Definition of (a) LUGM in German design, and (b) one segment and the LUGM$_i$ in *Danish design*-combination 1 and *Danish design*-combination 2

In *German design*, the LUGM would be the length from upslope, taken horizontally, along which θ_a value is greater than the value of $\theta_{a\text{-}pocc}$ in subsoil or sand, whichever is shorter. The LUGM for *Danish design*-combination 1 is defined as the sum of the LUGMs at each segment, denominated herein as $LUGM_i$, which is the length within a segment, taken horizontally, along which $\theta_a > \theta_{a\text{-}pocc}$ in sand-compost (Figure 5-4). For the *Danish design*-combination 2, however, two LUGMs should be defined: 1) a LUGM for the sand-compost layer ($LUGM_{sc}$), and 2) a LUGM for the fine sand layer ($LUGM_i$). $LUGM_{sc}$ is the length along the interface between sand-compost and gravel layers, taken horizontally, where $\theta_a > \theta_{a\text{-}pocc}$ in the sand-compost, and the LUGM for fine sand is similar to the $LUGM_i$ in *Danish design*-combination 1 while $\theta_a > \theta_{a\text{-}occ}$ in fine sand (Figure 5-4).

5.2.4. Numerical simulations

In order to build the simulations, the geometry and the thickness of the constituting layers were respected according to the site configurations presented in section 5.2.1. The length of PMOB in all simulations was considered 100 m to avoid boundary effects. The mesh density was higher near the interfaces. Two types of boundary conditions were considered for the simulations: 1) unit flux function to assign the seepage reaching the top of the PMOB, and 2) zero total flux boundary condition with potential seepage face review to represent the drainage systems. Figure 5-5 shows the meshing and boundary conditions adapted for the simulations.

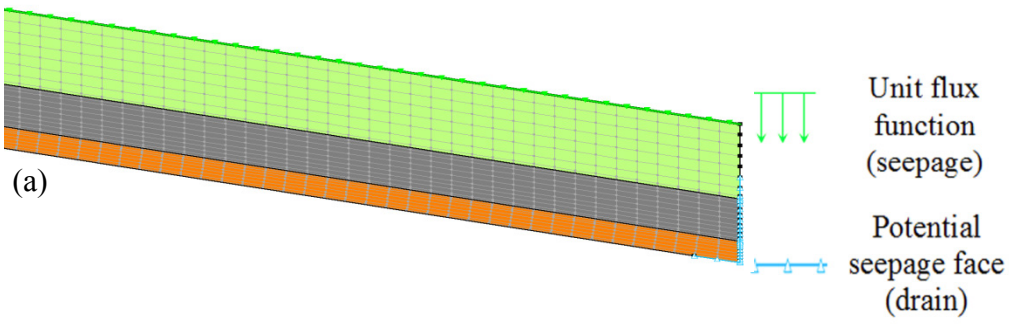

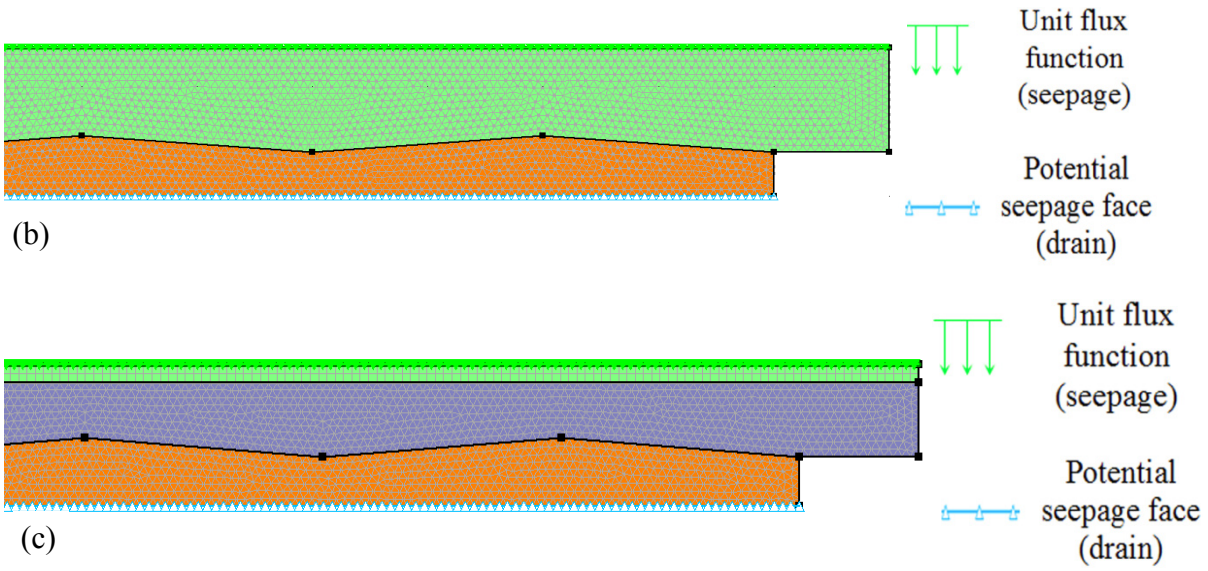

Figure 5-5: Meshing and boundary conditions of SEEP/W simulations for (a) *German design*, (b) *Danish design*-combination 1, and (c) *Danish design*-combination 2

A reasonable percentage (20%) of the total precipitation was assumed to seep through the PMOBs and reach the GDL-MOL interfaces, in order to overcome in part the lack of consideration of evapotranspiration in SEEP/W. For the *Danish design*-combination 1 the precipitation of Quebec was considered, since the actual data were not available. The daily rates of seepage for the 3 designs studied are presented in Figure 5-6. The transient state analyses performed lasted 365 days for *German design* and 246 days for *Danish design*-combination 1 and *Danish design*-combination 2.

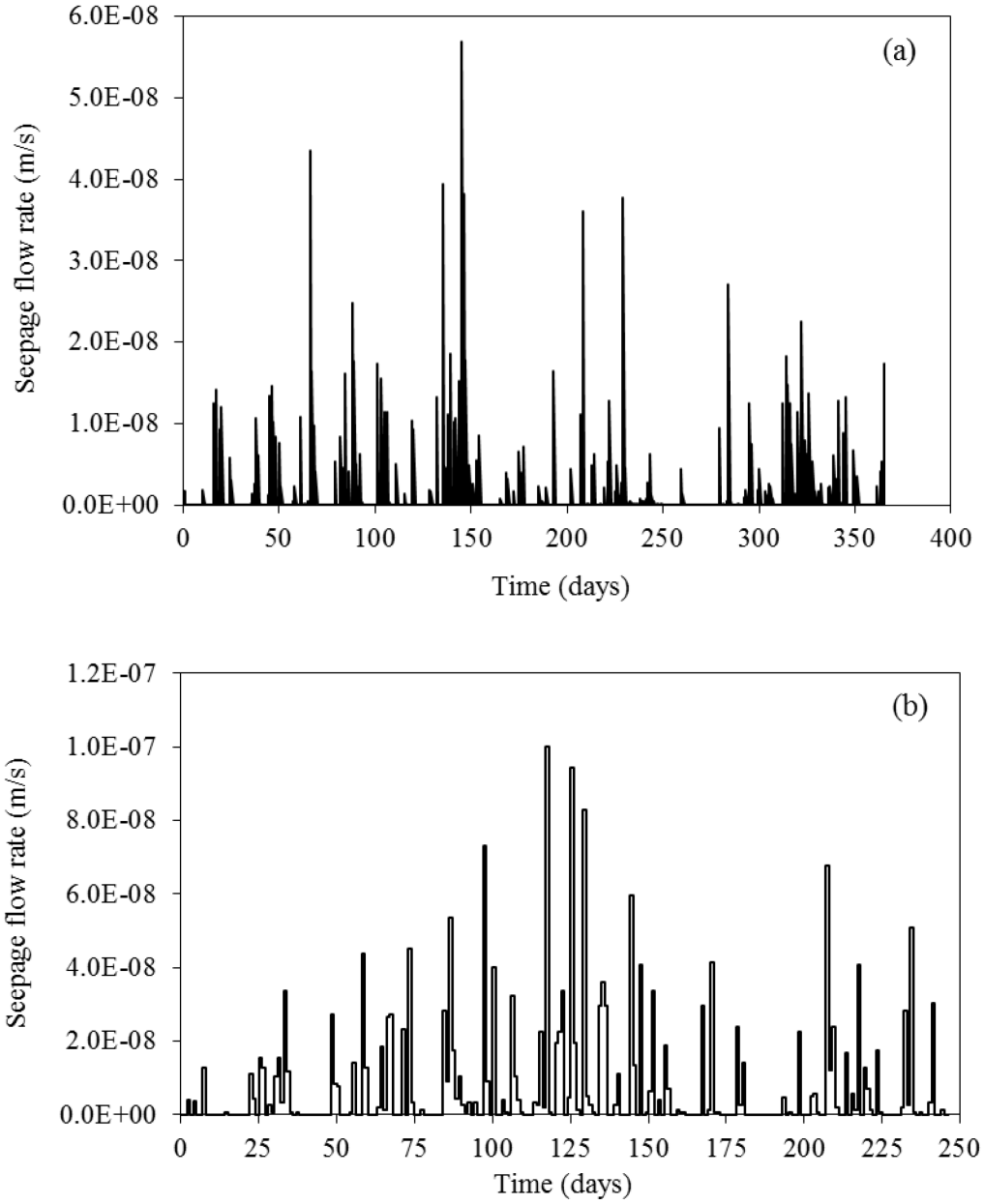

Figure 5-6: The daily rate of seepage into (a) *German design*, and (b) *Danish design*-combination 1 and *Danish design*-combination 2

In *German design*, the initial θ_w was set to 32% in subsoil and 1.59% in sand. The initial θ_w in sand-compost mixture for *Danish design*-combination 1 and *Danish design*-combination 2 was equal to 35%. For fine sand used in MOL of *Danish design*-combination 2 the initial θ_w was 25%.

5.3. Results

Nodes located 1 cm above the interface are herein denominated "*interface points*" whose θ_w values were obtained from the simulations. Data presented in all figures belong to the *interface points*. Since the design parameters are obtained in the constituting materials of the MOL, the effect of the capillary barrier along the interface was studied evaluating the θ_w values in MOL close to the interface.

5.3.1. *German design*

Figure **5-7** presents θ_w values of *interface points* of *German design*, which are associated with the points in subsoil layer and sand layer. The nodes located in the first and last 5 meters of the modelled PMOB were not considered in the analysis, in order to avoid potential boundary effects. The results presented in Figure 5-7a show that the distribution of θ_w in the *interface points* of subsoil layer was quite uniform. On day 334, θ_w values exceeded simultaneously the $\theta_{w\text{-}pocc}$ and LUGM became abruptly equal to zero. In other words, during the last 31 days the interface was restricted, which may provoke the migration of biogas toward the top of slope and creating the reported upslope hotspots by Bohn and Jager [2009]. As shown in Figure 5-7b, after 365 days, θ_w values in *interface points* of sand layer remained rather similar to the initial value, i.e. 1.59%. This latter value was considerably lower than the $\theta_{w\text{-}pocc}$ value of sand, which is equal to 32% (Figure 5-1). Therefore, the interface between GDL and sand layer of MOL was unobstructed during the period of analysis and the biogas can flow unrestrictedly upwards across this interface.

These results were consistent with the results of steady-state simulations performed by Tétreault et al. [2013] for *German design*, i.e. full saturation of the interface between sand and subsoil, while the degrees of saturation along the sand-gravel interface were low enough to avoid the occlusion of air-filled pores. They assumed the degree of saturation equal to 85% for the occlusion of air-filled pores.

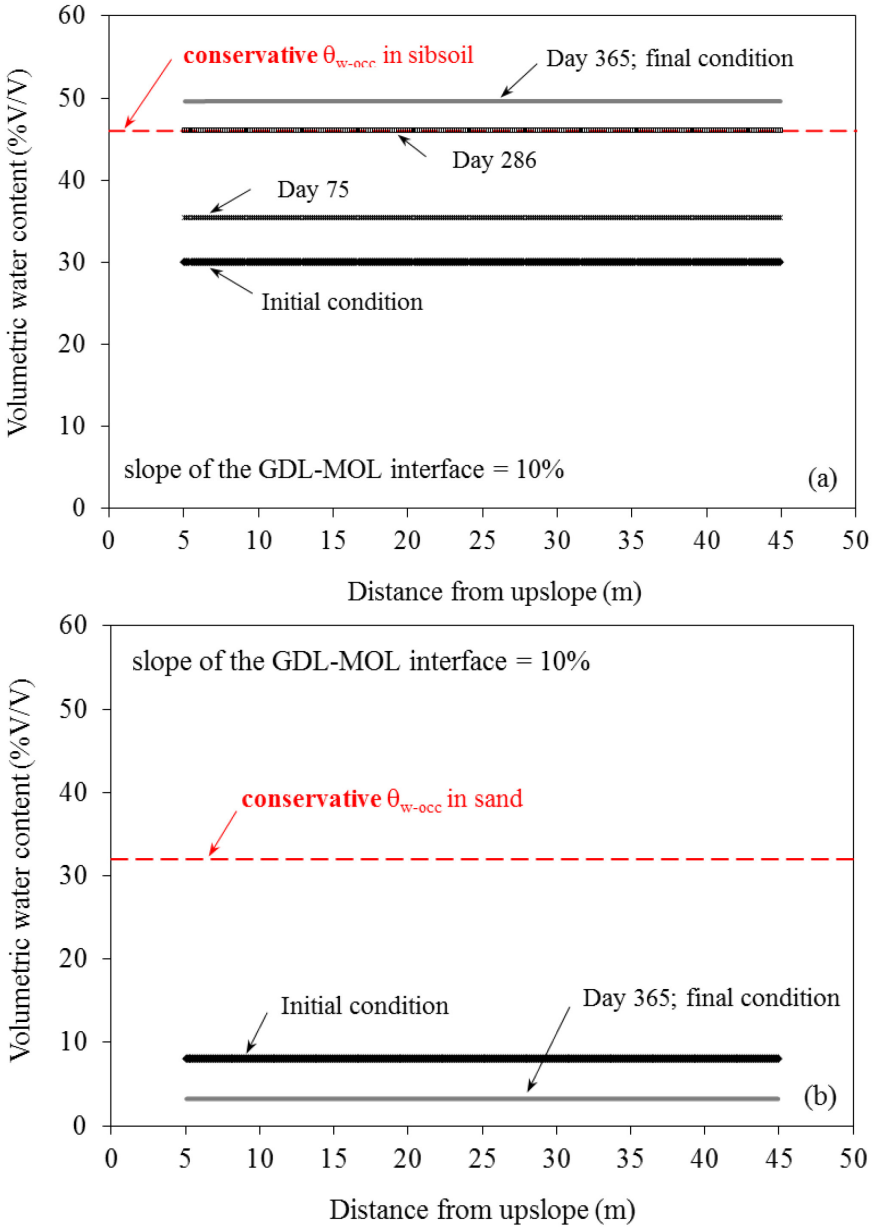

Figure 5-7: Evolution of θ_w with time in *interface points* of (a) upper interface (within subsoil), and (b) lower interface (within sand), in *German design*

5.3.2. *Danish design*-combination 1

Figure 5-8a presents θ_w values of *interface points* in *Danish design*-combination 1. Since the global slope of MOL was equal to zero, the same pattern for distribution of θ_w along the interface was obtained within all segments (data not presented). Therefore, in Figure 5-8a the data associated with only one of the segments are shown. On day 136, θ_w values of *interface*

points, located at lower part of the segment, started to exceed the $\theta_{w\text{-}pocc}$, and on day 143 all the θ_w values were greater than $\theta_{w\text{-}pocc}$. The difference between maximum and minimum values of θ_w along the interface, which represents the level of uniformity and referred to as $\Delta\theta_w$, increased with time. Maximum value of $\Delta\theta_w$ was equal to 2.9% − a very low value − and it occurred on day 199 where the interface was completely restricted.

Figure 5-8b shows the evolution of $LUGM_i$ (LUGM within one segment) in *Danish design*-combination 1. On day 136, $LUGM_i$ started to decrease gradually, and on day 143 it became equal to zero. In other words, during these 8 days, the jagged form of the interface helped the interface to be unrestricted within the top of the segment when the bottom parts are restricted. However, during the last 103 days the $LUGM_i$ was equal to zero.

The results of simulations of *Danish design*-combination 1 (Figure 5-8) showed that the suggested configuration and the materials used to construct the MOL do not yield the required low enough level of uniformity in distribution of θ_w along the interface. Such great level of non-uniformity is necessary to provide the longest possible $LUGM_i$ and to reduce the risk of creating hotspots during the long term performance of PMOB.

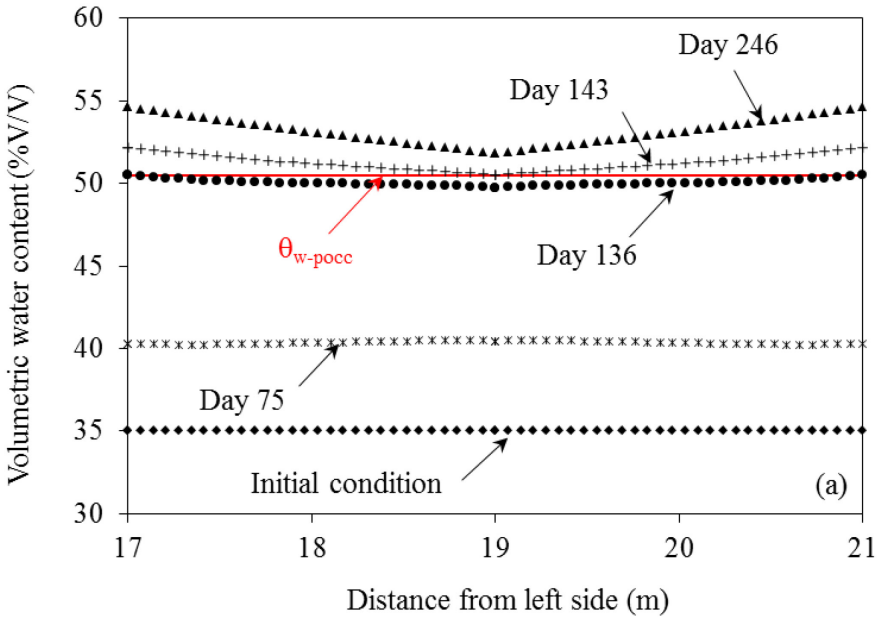

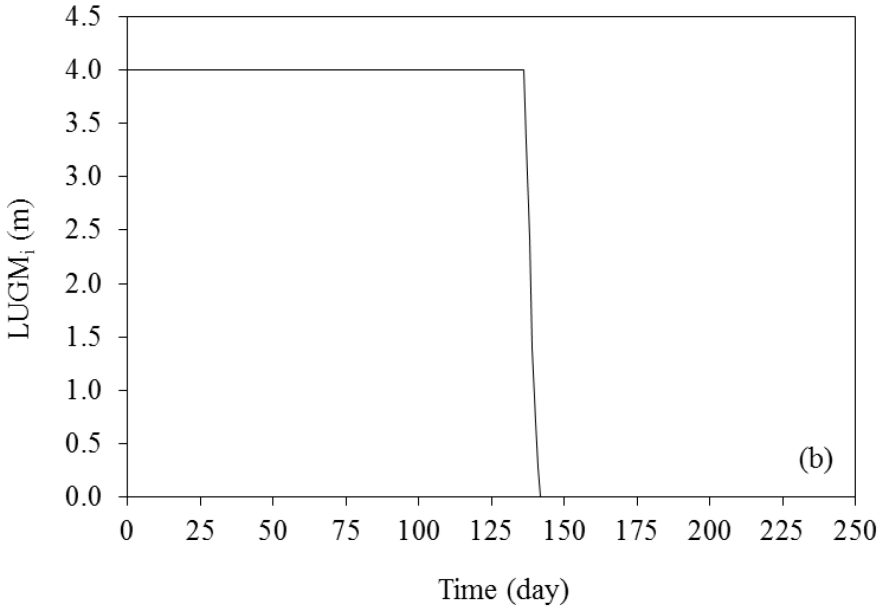

Figure 5-8: Evolution of (a) θ_w in *interface points*, and (b) $LUGM_i$ with time in *Danish design*-combination 1

In chapter 4, the slope of interface was introduced as one of the influencing parameters in uniformity of distribution of θ_w. As a prompt solution for the insufficient non-uniformity in distribution of θ_w in *Danish design*-combination 1, the slope of the interface at each segment was increased to 14% and numerical simulations were performed. Figure 5-9 shows the evolution of $LUGM_i$ and distribution of θ_w in this **modified** *Danish design*-combination 1. As shown in Figure 5-9a, on day 132, θ_w values of *interface points* at lower parts of the segment exceeded for the first time the $\theta_{w\text{-}pocc}$. The interface remained partially unrestricted until the end of the simulation period. Therefore, the time associated with partial restriction of interface in **modified** *Danish design*-combination 1 (114 days) was longer than the time given by actual *Danish design*-combination 1 (47 days). Maximum value of $\Delta\theta_w$ was equal to 5.1%, which occurred on day 198, and on this day the interface was still partially restricted. Therefore, increasing the slope of each segment resulted in greater non-uniformity in distribution of θ_w when the interface is not completely blocked.

Based on Figure 5-9b, the $LUGM_i$ of **modified** *Danish design*-combination 1 decreased gradually from day 132. From day 139 until the last day of the analysis, cycles of increase and decrease in $LUGM_i$ were observed. Throughout the simulation period, the $LUGM_i$ remained greater than zero. Therefore, increasing the slope of each segments to 14% helped to enhance

the biogas flow of the system in terms of providing a greater $LUGM_i$ during a longer period of time.

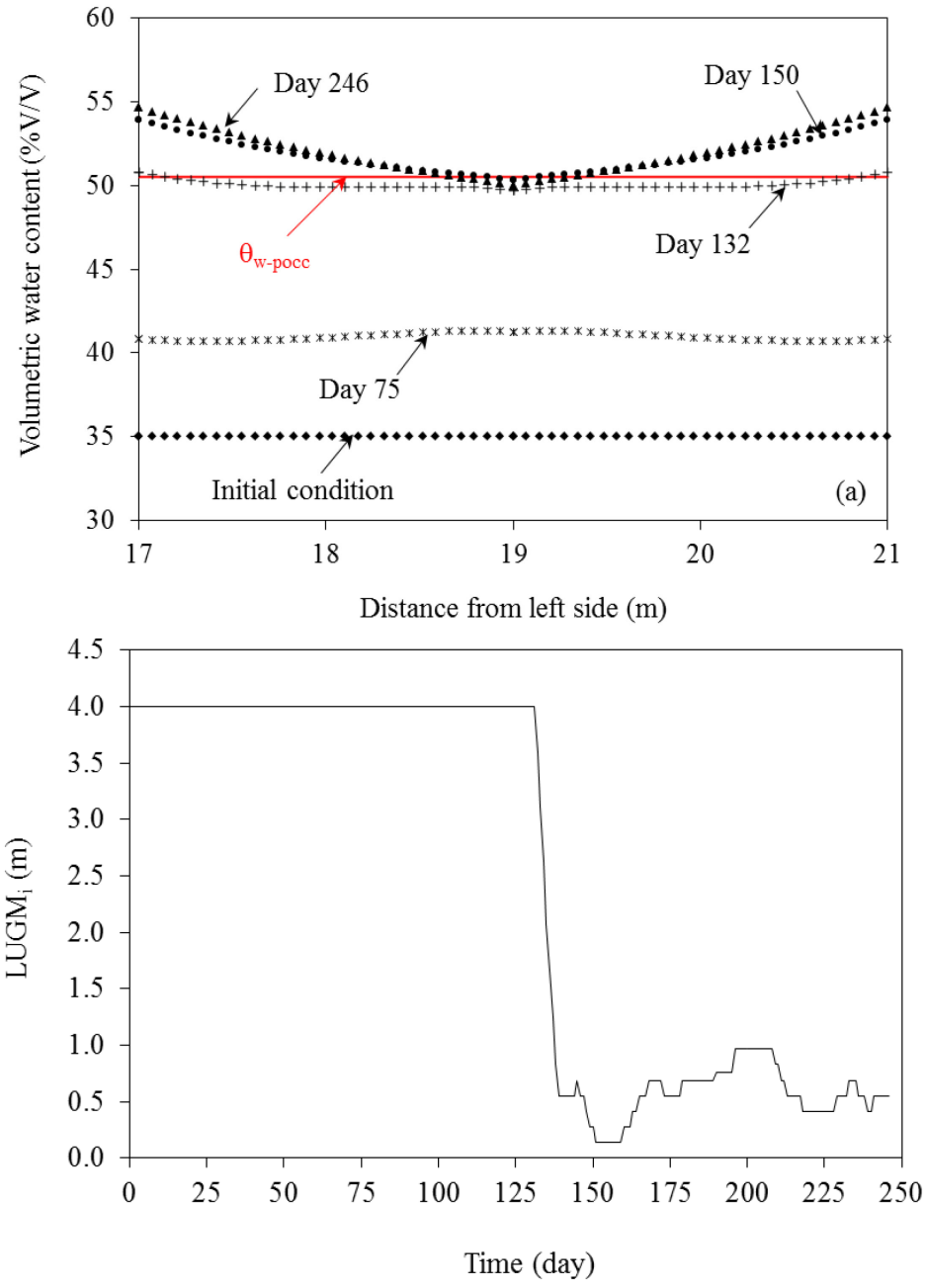

Figure 5-9: Evolution of (a) θ_w in *interface points*, and (b) $LUGM_i$ with time in **modified** *Danish design*-combination 1 (14% slope of interface at each segment)

5.3.3. *Danish design*-combination 2

In section 5.3.2, it was shown that increasing the slope of each segment can be an improving parameter to increase the magnitude of $LUGM_i$. However, as shown in Figure 5-9b, from day 135 until the end of the simulation period (45% of the simulation period), the $LUGM_i$ of **modified** *Danish design*-combination 1 was much shorter than 2 m, i.e. half of the total width of the segment.

According to the results presented in chapter 4, greater *n* value of van Genuchten and unsaturated hydraulic conductivity of MOL material provide lower value and level of uniformity in distribution of θ_w along the interface. Therefore, the multi-layer MOL in *Danish design*-combination 2 was considered as a convenient choice to substitute the MOL of the *Danish design*-combination 1, in order to provide longer $LUGM_i$. The fine sand possesses greater unsaturated hydraulic conductivity and *n* value of van Genuchten than those given by sand-compost mixture. In addition, the variation of *K* (gas intrinsic permeability) with θ_a (and therefore θ_w under constant dry density condition) for $\theta_a > \theta_{a\text{-}occ}$ in fine sand is greater than that associated with sand-compost mixture when $\theta_a > \theta_{a\text{-}pocc}$ (Figure 5-3). Subsequently, using fine sand, the distribution of biogas flow along the interface would be more non-uniform, which is required in designs with jagged interface. The compost material in 15-cm sand-compost layer would help the metanotrophic bacteria to oxidize CH_4 into CO_2. It is noteworthy to recall that this configuration showed high efficiencies in oxidation of methane [Ndanga et al., 2015].

Figure 5-10 presents the evolution of θ_w along 2 interfaces of *Danish design*-combination 2, within one segment. As shown in Figure 5-10a, the distribution of θ_w in *interface points* of sand-compost layer was quite uniform and the θ_w values never attained the $\theta_{w\text{-}pocc}$ value of sand-compost (50.5%). Therefore, the interface between sand-compost layer and fine sand layer was always unrestricted for upward flow of biogas, and $LUGM_{sc}$ was equal to the width of the segment.

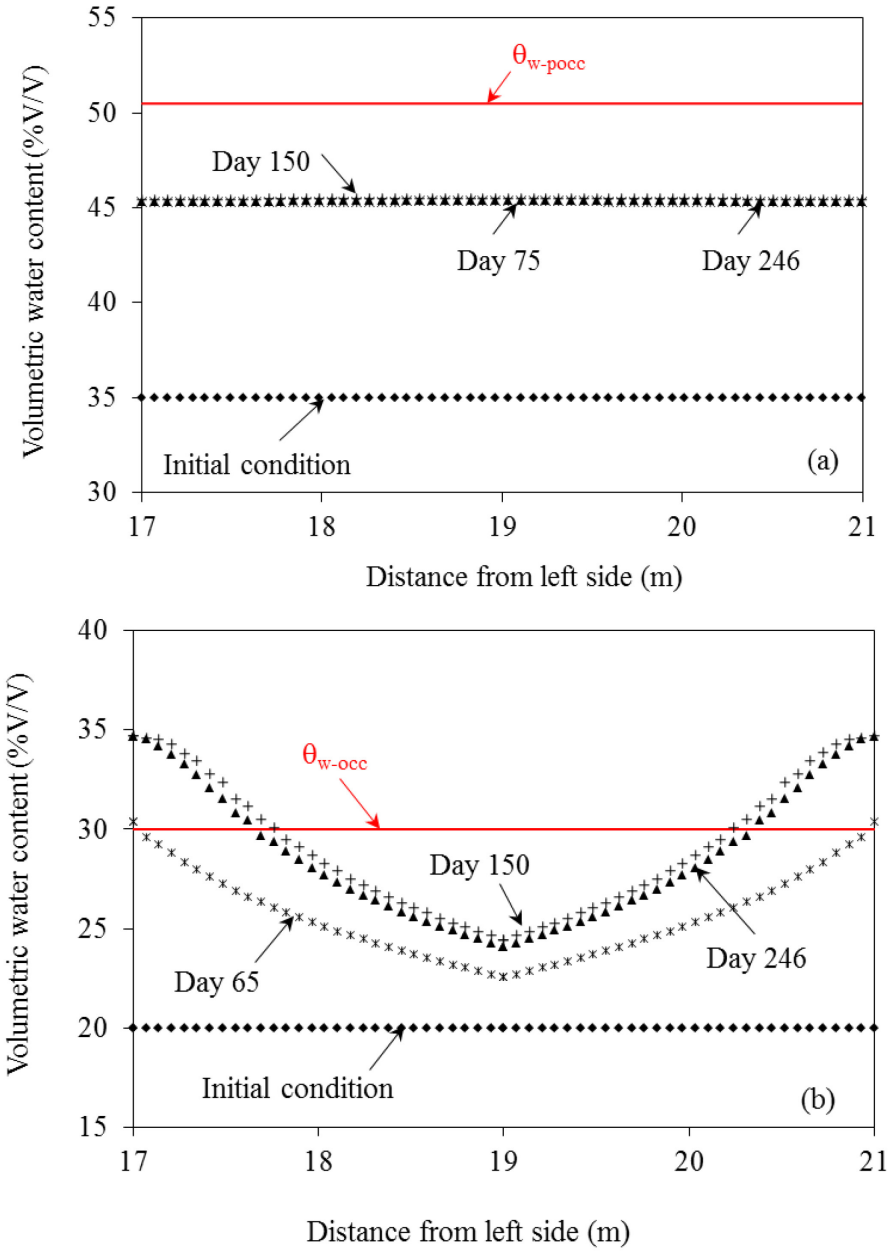

Figure 5-10: Evolution of θ_w with time in *interface points* of *Danish design*-combination 2 in (a) upper interface (within sand-compost layer), and (b) lower interface (fine sand layer)

Figure 5-10b shows that on day 65 the θ_w values in *interface points* of fine sand layer started to exceed the $\theta_{w\text{-}occ}$ value of fine sand, i.e. 30%. However, during the simulation period the interface never became completely restricted ($\theta_w > \theta_{w\text{-}occ}$). The maximum $\Delta\theta_w$ was equal to 10.7%, which is considerably greater than maximum $\Delta\theta_w$ in actual and **modified** *Danish design*-combination 1. When the maximum $\Delta\theta_w$ was attained (day 191), the interface was partially restricted.

The evolution of $LUGM_i$ in *Danish design*-combination 2 is shown in Figure 5-11. The $LUGM_i$ underwent cycles of increase and decrease, depending on the seepage flow rate. During the simulation period, the $LUGM_i$ was always greater than 50% of the total with of the segment, i.e. 2 m. Therefore, half of the segment was always an unrestricted passage for upward flow of biogas.

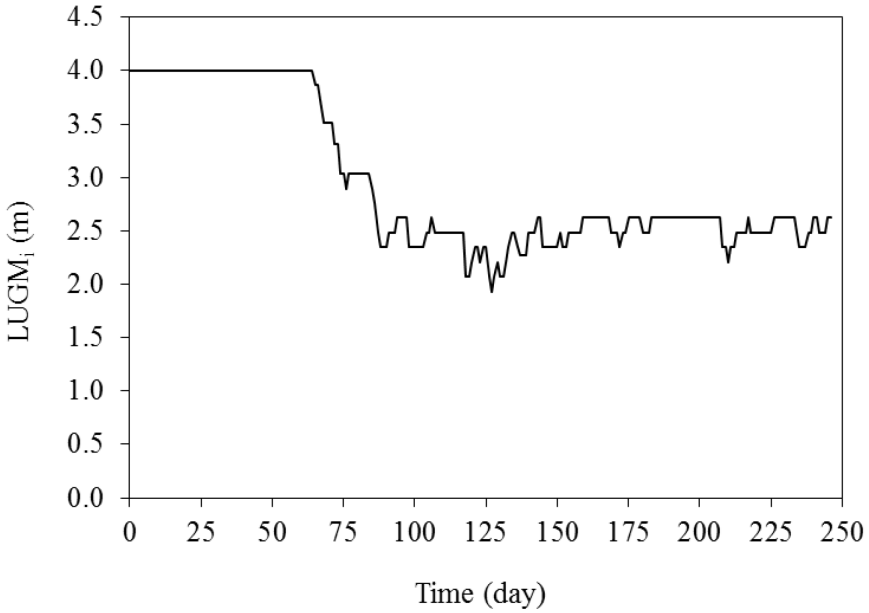

Figure 5-11: Evolution of $LUGM_i$ with time in *Danish design*-combination 2

Consequently, using the convenient configuration and materials to construct the MOL, as in *Danish design*-combination 2, a greater and more permanent passage for upward flow of biogas was provided. Moreover, the suction values were sufficiently high to avoid the percolations into the GDL (data not presented).

5.4. Conclusions

Sets of transient-state numerical simulations were performed to analyze the upward flow of biogas across the interface between the constituting layers of 3 PMOBs. In the first design (*German design*), the simultaneous restriction of all air-filled pores of the MOL material along the GDL-MOL interface was considered as the reason for migration of biogas toward the top of slope and creating the reported hotspots. The results of the second design (*Danish design*-combination 1) showed that the jagged form of the GDL-MOL interface was indeed, a clever idea that provides an unrestricted passage for the upward flow of biogas within the top of each segment. In order to increase the width ($LUGM_i$) and the presence time of the unrestricted passage, the slope of the interface at each segment was increased (**modified** *Danish design*-combination 1). The system was improved; however, the $LUGM_i$ was smaller than half of the total width of the segment during 45% of the simulation period. The *Danish design*-combination 2 with the same geometry as *Danish design*-combination 1, but with a two-layer MOL, was suggested. The results showed that more than 50% of the total width of the segment was unrestricted for the upward flow of biogas throughout the simulation period. Therefore, identifying conveniently the requirements of the design, in terms of the value and the level of the uniformity in distribution of θ_w, is one of the essential steps in design of PMOBs. A good design is the one that provides the longest possible length along which the biogas can flow unrestrictedly upwards.

CHAPTER 6. CONCLUSIONS AND RECOMMENDATIONS

6.1. Summary and conclusions

Reports of upslope hotspot, non-uniform distribution of surface methane concentrations and increasing moisture values toward the downslope of three experimental PMOBs constructed in Canada, Germany and Netherlands triggered the present Ph.D. research project. The main focus was the importance of considering the unsaturated hydraulic behavior of constituting materials and the ensuing capillary barrier effect along the interface between the main layers in the design of PMOBs, in order to provide sufficient ease and distribution of upward biogas flow at the base of methane oxidation layer.

The first step was the evaluation of gas flow behavior in unsaturated soils. Therefore, the air permeability functions of the MOL materials of two experimental PMOBs constructed at the St-Nicephore landfill (Quebec, Canada) were obtained. The onset of abrupt reduction in the coefficient of air permeability with volumetric air content was identified, and it was defined as the threshold of unrestricted gas migration. The corresponding degree of saturation was related to the degree of saturation at air entry value and at the line of optima so that the design parameter (threshold of unrestricted gas migration) can be identified even in the absence of air permeability function. Using the latter design parameter, a design criterion was introduced that represents the available surface for unrestricted upward gas migration at the base of methane oxidation layer (MOL). This design criterion was denominated the *length of unrestricted gas migration* (LUGM) whose boundaries are defined by the threshold of unrestricted gas migration (the design parameter). A good design of PMOB is the one that provides the longest LUGM possible. Using the introduced design criterion and parameter, a parametric study through the SEEP/W numerical simulations was performed to evaluate the effect of the slope of interface and the parameters defining the water retention curve (WRC) and hydraulic conductivity function of MOL material on value and the distribution of moisture along the interface.

Based on the results of laboratory experiments, $\theta_{a\text{-}occ}$ (volumetric air content at occlusion) and $\theta_{a\text{-}pocc}$ (volumetric air content at pre-occlusion) were defined as the threshold of unrestricted upward flow of biogas. Depending on the form of air permeability function and/or WRC of MOL material, the flow of biogas was considered reasonably unrestricted when $\theta_a > \theta_{a\text{-}occ}$ or $\theta_a > \theta_{a\text{-}pocc}$. These latter two situations define the end of the LUGM. The results of the parametric study showed that increasing slope of the interface, saturated hydraulic conductivity and the slope of desaturation zone in WRC of MOL material lead to greater differences in volumetric water content (and therefore flux of biogas) along the interface. In addition, regarding the parameter that defines the water entry value of WRC, the greater its value, the greater the chances of occlusion of air-filled pores and restriction of upward gas flow would be.

Referring to the conclusions presented herein, one can design a PMOB that incorporates the capillary effect into considerations associated with the methane oxidation efficiency. Indeed, the PMOB would be designed based on the introduced design parameter (the threshold of unrestricted gas migration) and design criterion (LUGM) to provide the most sufficient possible ease and distribution of upward flow of biogas.

6.2. Limitations and recommendations for future studies

The present study is a beginning required to enhance the methane oxidation efficiency of PMOBs, influenced by capillary barrier effect. Therefore, the study undergoes some limitations that arise from the number of materials studied, or the boundary conditions used in numerical simulations. However, using the data in the technical literature or making reasonable assumptions, it was attempted to minimize the effect of the limitations. In the remaining of the section, the limitations and the corresponding recommendations for future studies with fewer limitations are presented:

1) The materials studied to obtain the design parameter were extremes, in the sense that the commencement of significant reduction in coefficient of air permeability with

volumetric air content was in the form of a very wide zone of transition or a point. Other materials from the technical literature were also studied to validate the suggestions based on the tested materials in the present study. However, due to the limited number of data, the simultaneous evaluation of air permeability functions, WRCs and Standard proctor curves of all of the materials was not possible. Therefore, it is recommended to obtain the air permeability function, WRC and Standard Proctor curve of more various types of soils to suggest more comprehensive steps in obtaining the design parameter, using the air permeability function or the accessible geotechnical tools, such as WRC and Standard Proctor curve.

2) SEEP/W is an efficient tool to study the seepage flow in saturated or unsaturated media. However, it does not include the effect of temperature, water generation during the microbial activies, pore occlusion by micro-organisms, and a soil-atmosphere interaction module (evapotranspiration). In numerical simulations of the present research project, the daily precipitation rate was reduced to incorporate the average rate of regional evapotranspiration. In addition, the upward flow of biogas at the base of PMOB cannot be simulated in SEEP/W, and all the interpretations herein were made based on the value and the distribution of moisture along the interface. For future studies, using multiyphysics and multiphase algorithms is recommended to consider the evapotranspiration in MOL and the interaction between biogas flow with unsaturated seepage flow at the base of MOL.

3) The experimental PMOB with jagged interface constructed in Denmark was analyzed using the meteorological data and MOL and GDL material of PMOB2 (St-Nicephore landfill, Quebec, Canada). Performing sets of numerical simulations with actual data is suggested, in order to analyze and eventually enhance the performance of this innovative design more precisely.

APPENDIX A. MEASURING THE COEFFICIENT OF AIR PERMEABILITY IN LABORATORY

1. Background

The coefficient of air permeability (k_a) can be measured in field or in the laboratory. Two main categories of methods for obtaining the k_a in laboratory are defined: 1) steady-state methods, and 2) unsteady-state methods. However, the most precise results are obtained performing the steady-state method [Benson and Gribb, 1997].

In order to calculate k_a in the laboratory, two different types of air flow regulations, i.e. mass flow control and pressure control, are used. In any case, the assembly of the test includes three main parts: air supply, permeameter and flow measurement system. The air flows through the sample from the air supply and the flow measurements are conducted using a burette (flowmeter) connected to the permeameter. Some equipments may be added to measure the suction value, the hydraulic conductivity and the deformations.

The permeameter can be flexible wall permeameter [Rodeck et al., 1994; Samingan et al., 2003; Kamiya et al., 2006; Marinho and Teixeira, 2013], or rigid wall permeameter [ex. Klute, 1965; Fleureau and Taibi, 1994; Springer et al., 1998]. In tests with flexible wall permeameter, a confining pressure is applied. The value of the confining pressure may be selected according to the overburden of the site [ASTM-D6539-13, 2006], or sufficient enough to avoid any gas leakage around the sample and to fill the surface irregularities between the membrane and the sample [McPhee and Arthur, 1991]. However, it should be low enough to minimize the influence of confining pressure on porosity reduction and therefore, on the k_a value of some specific samples [McPhee and Arthur, 1991; ASTM-D6539-13, 2006].

2. Permeameter used in present study

The air permeability tests of the present study were performed by installing the sample on a triaxial apparatus. An innovative and easy-to-use mold with dimensions precisely adapted to the pedestal of the triaixal apparatus was designed[1] to be used during sample preparation and also as the permeameter (Figure A-1a). Two holes were implemented on both sides of the mold to apply the vacuum during the sample preparation. These latter holes can also be used to apply air, instead of water, as the confining pressure for the cases where the lateral pressure due to the overburden is required, or there is the risk of rigid wall effects.

For sample preparation, a membrane is placed on the pedestal and then, the mold is installed to surround firmly the sample membrane (Figure A-1b). The vacuum is applied during the whole time of sample preparation to ensure the complete filling of the irregularities between the mold and the membrane. The sample with given initial water content is compacted at

[1] The mold was designed by Jean-Guy Lemelin, the technician of Soil Mechanics Laboratory at Université de Sherbrooke.

given initial dry density in the mold, using the rammer designed specifically for the mold (Figure A-1c).

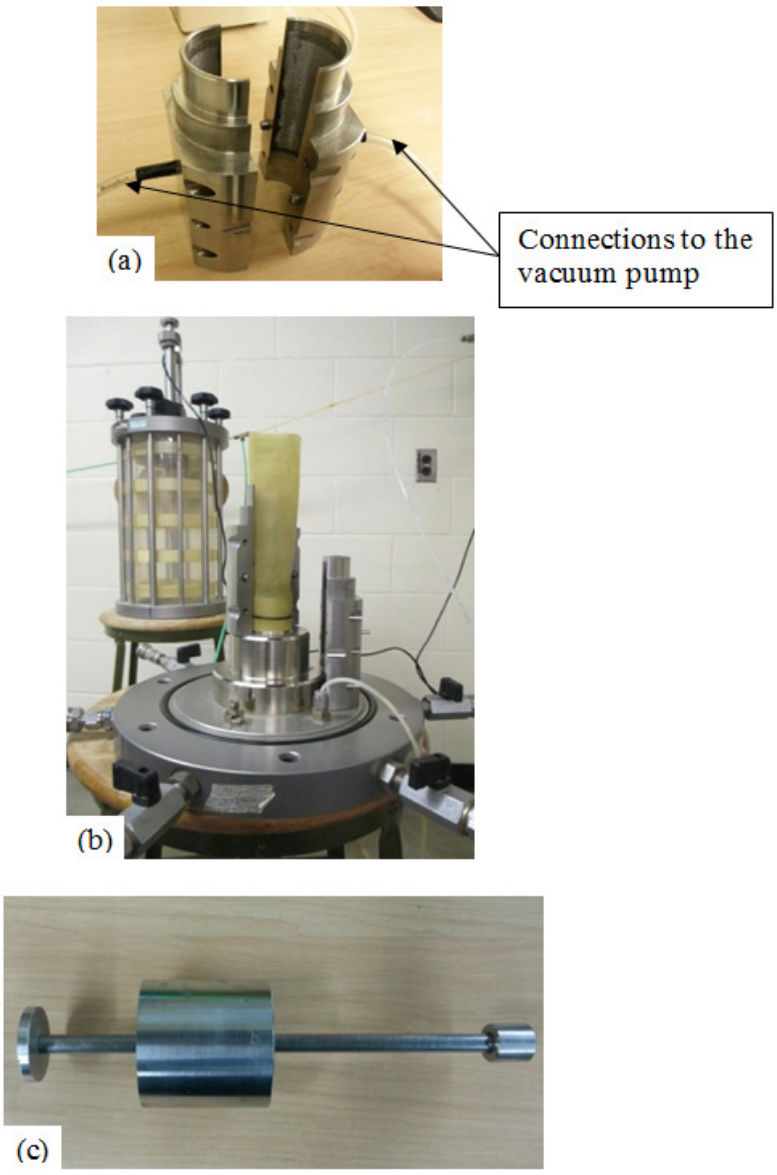

Figure A-1: (a) sampling mold (permeameter), (b) the mold surrounding the membrane, and (c) compaction rammer

At the end of compaction, the cap of the sample was placed and the vacuum is discontinued (Figure A-2a). The triaxial cylinder is then installed and the axial load piston was carefully placed on the cap of the sample to touch the cap without applying any pressure (Figure A-2b). The axial load piston helps avoiding the upward movements of cap, due to the inlet air pressure. After these preoperational steps, the air permeability tests can be performed as in the literature.

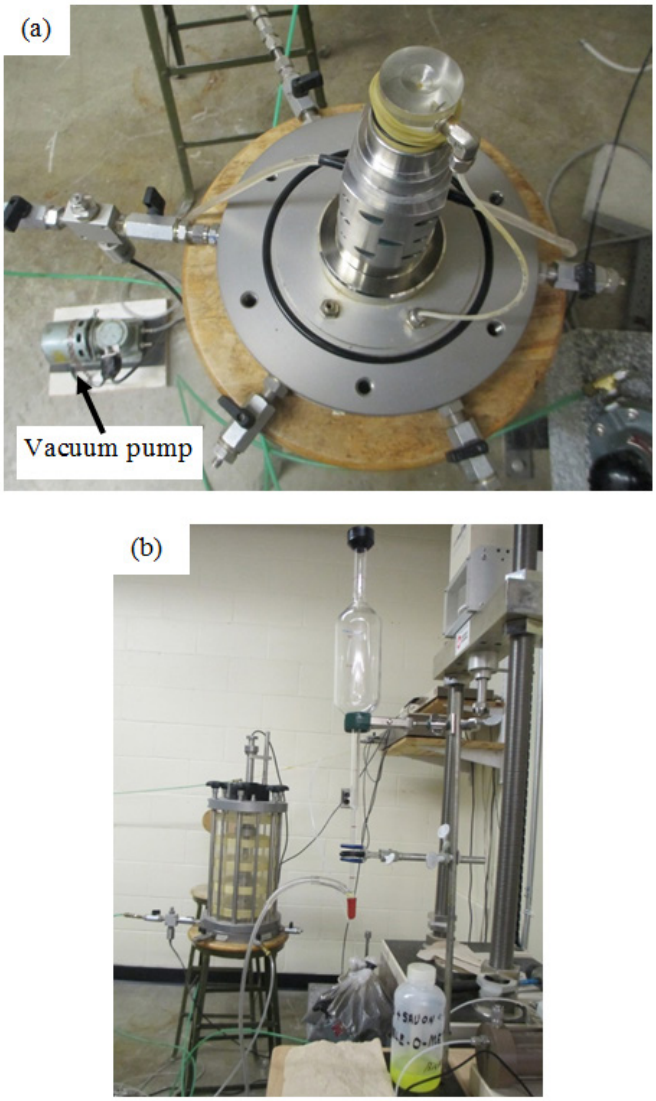

Figure A-2: (a) the permeameter and the sample after the sample preparation process, and (b) the assembly ready to run an air permeability test

APPENDIX B. ASSESSMENT OF BIOGAS DISTRIBUTION AT THE BASE OF PASSIVE METHANE OXIDATION BIOSYSTEMS

Titre: Assessment of biogas distribution at the base of passive methane oxidation biosystems

Auteurs et affiliation:

Bahar Ahoughalandari: étudiante au doctorat, Université de Sherbrooke, Faculté de génie, Département de génie civil

Alexandre R. Cabral: professeur titulaire, Université de Sherbrooke, Faculté de génie, Département de génie civil

Serge Leroueil: professeur titulaire, Université Laval, Département de génie civil et de génie des eaux

Date de soumission: 10 juin 2015

État de la soumission: Accepté sans correction

Conférence: The XV Panamerican Conference on Soil Mechanics and Geotechnical Engineering, Buenos Aires, Argentina

Référence : [AhouGhalandari et al., 2015]

Titre français : l'évaluation de la distribution du biogaz à la base des biosystèmes d'oxydation passive du méthane

Contribution au document:
This paper presents the results of a preliminary analysis, which was performed to identify the threshold of unrestricted gas migration of the MOL material of PMOB2. Indeed, it provided an opportunity to assess the performance of the new permeameter and evaluate the gas flow behavior of the material used to construct the MOL of PMOB2. Further development of the methodology created the results and the resulting journal paper presented in chapter 3.

Abstract: Passive methane oxidation biosystems (PMOB) are implemented as part of final cover systems and can be cost-effective means of controlling fugitive CH_4 emissions from landfills. The efficiency of a PMOB increases with increasing uniformity of CH_4 loading at the interface between its main components, i.e. methane oxidation layer (MOL) and gas distribution layer (GDL). Concentrated – or non-uniform - distribution increases the risk of surface emissions higher than acceptable, particularly upslope. This study is part of a larger project that aims to evaluate the length along the MOL-GDL interface where gas can migrate unrestricted upwards through the cover. The first step is to perform proper characterization of the materials, which includes determination of the water retention curve and the coefficient of air permeability of the MOL material used for the construction of the PMOB installed at the St-Nicephore landfill (Quebec, Canada). Both were determined at several initial water contents and dry densities. The subsequent determination of the onset of the air permeability drop as water content and dry density changed was one of the main outputs of the present study and is a fundamental step in the determination of unrestricted gas migration within PMOBs.

Keywords: Passive methane oxidation biosystems, coefficient of air permeability, non-uniform gas distribution, unsaturated hydraulic behavior, degree of saturation, landfills

1. Introduction

Construction of a landfill cover is one of the final activities upon termination of waste landfilling. It has several purposes, including the control of infiltration into the landfill and biogas emissions to the atmosphere. Passive methane oxidation biosystems (PMOBs) have been considered as a cost-effective technology to minimize the emissions of methane, a greenhouse gas with global warming potential of 25 times greater than that of carbon dioxide [IPCC, 2001]. PMOBs are part of the final cover and are installed near the surface. Reduction in methane emissions results from the action of a group of natural bacteria in soils called methanotrophs, which oxidize CH_4 into CO_2. Biosystems contain two main layers: the methane oxidation layer (MOL), where methane oxidation occurs, particularly near the surface where atmospheric O_2 is available, and the gas distribution layer (GDL), composed mainly of coarse-grain materials whose permeability is higher than MOL. The GDL usually sits on top of the MOL within the final cover system. Its purpose is to intercept fugitive emissions that flow through cracks within the low permeability layer and to distribute them uniformly at the base of the MOL.

As a result of the capillary barrier effect, infiltration of meteoric water into sloped PMOB may result in non-uniform distribution of the degree of saturation along the MOL-GDL interface. Depending on the extent of this phenomena, upward migrating biogas may eventually flow towards the drier (upslope) parts of the biosystem and eventually be emitted on very concentrated areas, creating what is known as hot spots [Abdolahzadeh et al., 2010; Cabral et al., 2010a; Tétreault et al., 2013], which is detrimental to the PMOB.

The main mechanisms of flow of gas, i.e. advection and diffusion, are partly dominated by soil parameters, such as dry density, water content (w) and degree of saturation (S_r) [Fredlund and Rahardjo, 1993; Lu and Likos, 2004]. In some unsaturated soils, the air phase becomes continuous at suctions larger than air entry value (AEV) [Springer et al., 1998; Jucá and

Maciel, 2006]. In addition, according to the review paper of Leroueil and Hight [2013], the results of tests conducted by Langfelder show that on the dry side of the compaction curves the air phase is continuous, whereas on wet side it is occluded. The transition of air phase status from continuous to occluded, on compaction curves can be observed in air permeability test results where abrupt decreases in the coefficient of air permeability occur [Langfelder et al., 1968; Springer et al., 1998; Maciel and Jucá, 2000; Ba-Te et al., 2005; Jucá and Maciel, 2006; Kamiya et al., 2006; Marinho and Teixeira, 2013].

The methane oxidation efficiency of a PMOB increases with increasing uniformity of CH_4 loading at the interface between its main components, i.e. the MOL and the gas distribution layer (GDL). Uniformity increases with the increase in the length along the MOL-GDL interface where gas can migrate unrestricted upwards, wherein referred to as *length of unrestricted gas migration*, or LUGM.

In order to determine the LUGM of a PMOB it is necessary to assess how gas and water migrate within its unsaturated MOL and how – and where - water accumulates along the MOL-GDL interface. This requires determination of the water retention curve and the air permeability at several initial water contents and dry densities. The LUGM is then evaluated by monitoring changes in air permeability and, particularly, the onset of the air permeability drop as water content and dry density change. The Standard Proctor curve of the MOL is the reference on the basis of which results must be interpreted.

We present herein an assessment of one of the PMOBs installed at St-Nicephore (Quebec, Canada) in regards to its air permeability behavior as a function of density and moisture content. We expect the testing methodology proposed herein and the analysis thereof to eventually be considered for PMOB design in the future.

2. Materials and methods

2.1. Materials

The material considered in the study has been used to build the MOL of the experimental biocover (namely PMOB-2), constructed in the middle of a capped area of the Saint-Nicephore landfill, Quebec, Canada. Full description of PMOB-2 is given by Cabral et al. [2010b] and Roncato and Cabral [2012]. The MOL material results from a mixture of five volumes of compost and one volume of sand with total relative density, G_s, equal to 2.24. In addition, the in situ dry density and porosity of the MOL are 750 kg/m^3 and 0.66, respectively.

2.2. Laboratory tests

A series of laboratory tests, including Standard Proctor test, air permeability tests and determination of the WRC were conducted.

Two paths for initial water contents and dry densities selection were chosen: 1) *Standard Proctor path (SPP)*, which follows the Standard Proctor curve from the dry to the wet side; and 2) *Field density path (FDP)*, which follows the horizontal line of constant in-situ dry density from lower to higher water contents.

2.2.1. Air permeability test

Cylindrical samples of 3.8 cm diameter and 7.3 cm height, at different initial water contents and dry densities were prepared in a rigid mold placed on the pedestal of a triaxial cell. Two dry coarse porous stones were placed at the bottom and the top of the sample and any gas leakage was avoided using four O-rings at both ends. The constant differential pressure method was adopted to conduct the air permeability tests. The exit pressure at the top of the sample was always atmospheric. The air flow velocity was measured using a soap film flow meter (Bubble-O-Meter; 1-10-500 ml), while the above-mentioned mold confined the sample to avoid preferential air flow. The air permeability was calculated using equation (B-3) below [Maciel and Jucá, 2000]:

$$k_a = \frac{2 \times q \times \mu \times \Delta x \times P_s \times g}{\left(P_e^2 - P_s^2\right) \times \nu} \qquad \text{(B-3)}$$

where: k_a = coefficient of air permeability (m/s)
q = apparent flow velocity (m/s)
Δx = sample's height (m)
P_e = absolute inflow pressure (Pa)
P_s = absolute outflow pressure (Pa)
μ = dynamic viscosity of air at ambient temperature (Pa.s)
g = acceleration of gravity (m/s^2)
ν = cinematic viscosity of air at ambient temperature (m^2/s)

2.2.2. Water retention curve

The WRC was obtained by means of the HYPROP system (UMS), which is based on the evaporation method proposed by Wind [Wind, 1968] and determines the drying water retention curve of a vertical soil column. Samples were prepared according to the manual provided with the apparatus [HYPROP-UMS, 2013], at the same initial water contents and dry densities of the samples tested for air permeability. All samples were initially inundated in water at least for 7 days to attain the highest possible degree of saturation.

3. Results

The results of Standard Proctor test, in situ sand-cone test and the test points at which the coefficient of air permeability and the water retention curve have been obtained are shown in Figure B-1. The optimum water content (w_{opt}) and maximum dry density were equal to 43% and 1080 kg/m^3, respectively. The field water content was 50.8% and dry density obtained from in situ sand-cone test was 750 kg/m^3. According to Figure B-1, the optimum is situated on an isoline where the degree of saturation (S_r) is equal to ~ 90%. The path along the horizontal line defined by field dry density at varying water contents is called herein the FDP.

All test points of the FDP were located on left side of the line of optima. In other words, all samples were compacted dry of their respective optimum.

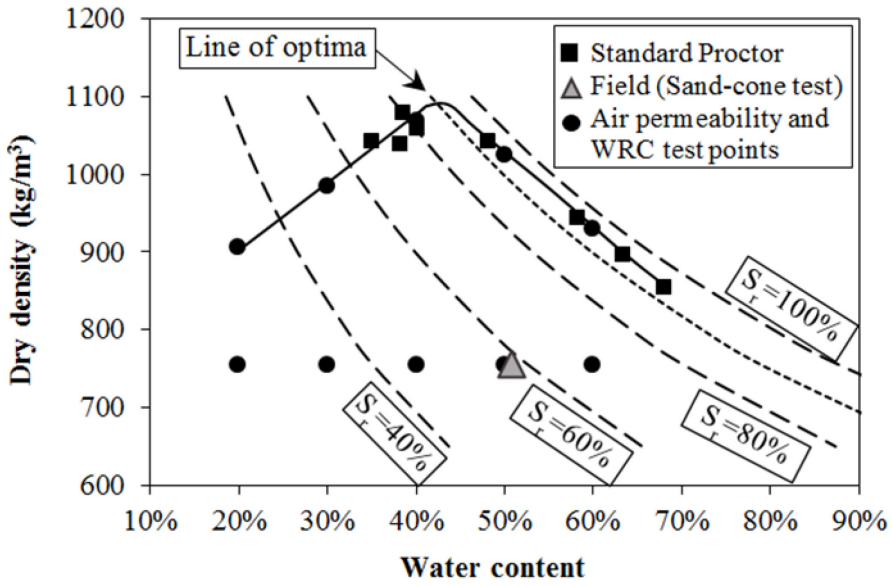

Figure B-1: The curve of Standard Proctor test, in-situ condition and air permeability and HYPROP test points

Figure B-2 shows the variations of volumetric water content (θ_w) and volumetric air content (θ_a) with suction for samples prepared at field dry density and varying water contents (FDP). The curve shown in Figure B-2a is known as the soil-air characteristic curve (SACC).

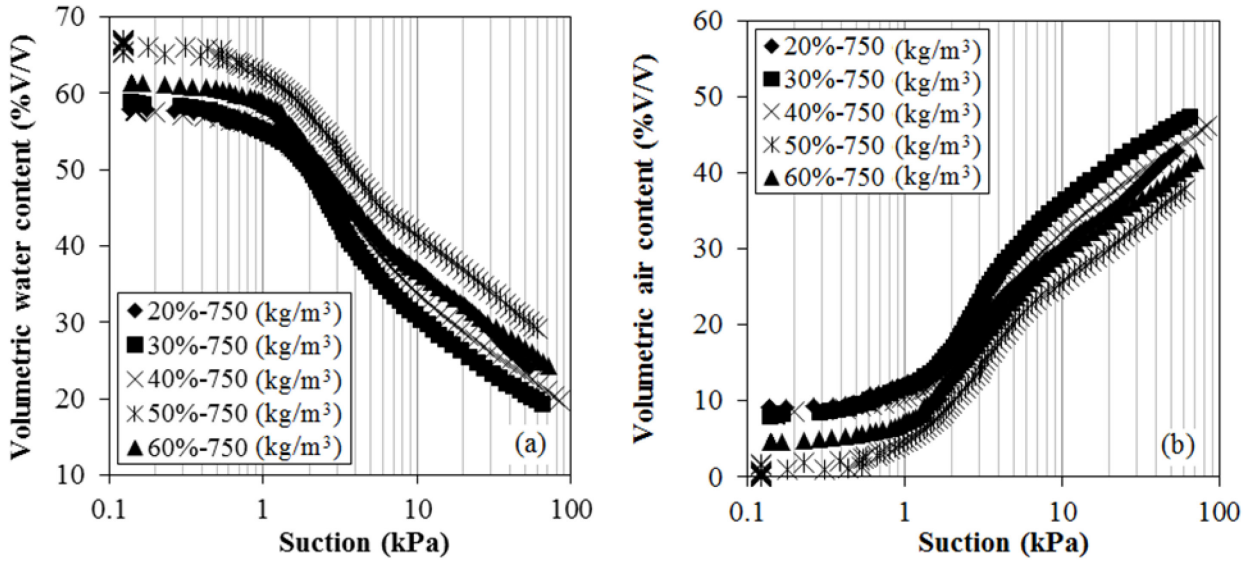

Figure B-2: WRC (a) and SACC (b) of samples on field density path.

In Figure B-2a, the S_r at which the tests started ranged from 86% to 99% and corresponding θ_w values were between 57% and 67%. The results show that the AEV is approximately 1.5 kPa. The volumetric air content (θ_a) is the difference between porosity and θ_w, with porosity being calculated using the dry density and the G_s value of the sample. Figure B-2b shows

that, at AEV, θ_a is approximately equal to 7% (S_r=89%) for the samples whose test started at nearly full saturation. It can be assumed that this characterizes the inflection point for all the tests.

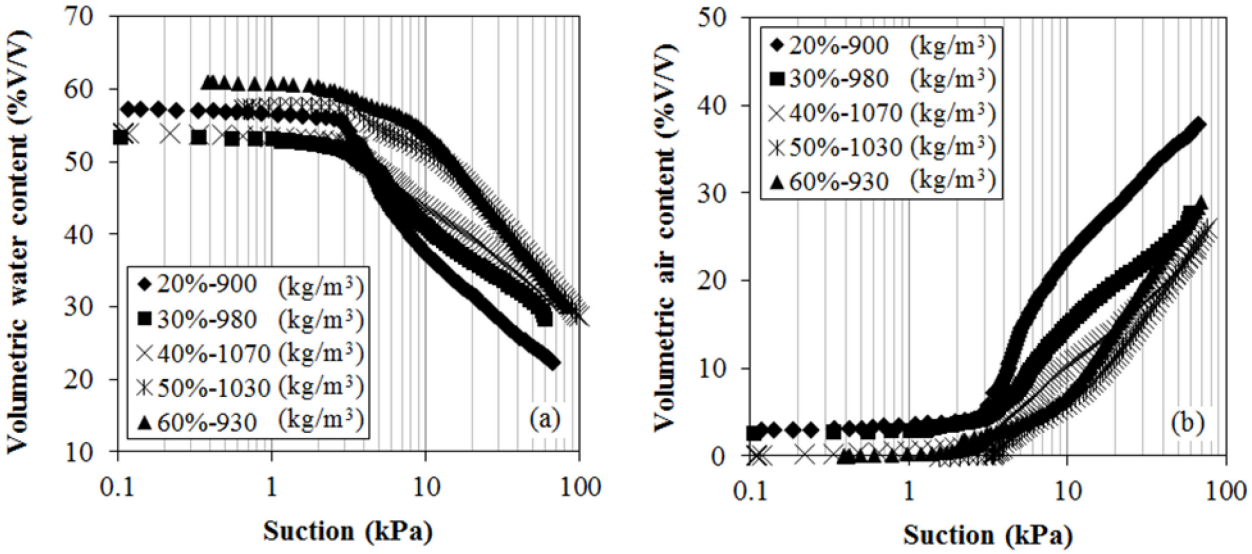

Figure B-3: The WRC (a) and SACC (b) of samples on Standard Proctor path.

The WRCs of the samples prepared with initial water content and dry density on SPP are shown in Figure B-3a. The initial degrees of saturation of the samples varied from 92% to 99%. Accordingly, θ_w values ranged from 53% to 61%. Two families of curves can be observed: one for the tests carried out at water contents lower than optimum (dry side) and one for the tests performed at water contents greater than optimum (wet side). The AEV is approximately 3 kPa on the dry side and close to 7 kPa on the wet side, which is consistent with the conclusions of Leroueil & Hight [2013]. This reflects the fact that the fabric is aggregated with large pores on the dry side. The corresponding SACCs are shown in Figure B-3b. The θ_a values at AEV (taken from their respective WRCs - Figure B-3a) for the curves starting from nearly full-saturation vary between 2% and 5% (in fact 93% < S_r < 97%), which are the inflection points.

The values of coefficient of air permeability (k_a) associated with the samples in Figure B-1 are presented in Figure B-4 as a function of air flow rate. The samples were subjected to differential pressure values varying from 0.5 to 5 kPa, except for samples at 50% and 60% water content on the SPP. For the latter, the differential pressures varied between 5 to 12 kPa. These higher values were necessary in order to be able to form soap bubbles in the soap film flowmeter.

As shown on the top-right side of Figure B-4, for each sample along the FDP, k_a increases with decreasing air flow rate. It can be observed that for the same air flow rate, the drier the sample the greater the k_a value. Despite the preceding, the value of k_a remains within the same order of magnitude ($1x10^{-6}$ m/s - $7x10^{-6}$ m/s). For the SPP, there are 3 distinct behaviors. The 1st is associated with samples prepared at 20% and 30% water content (therefore dry of optimum) whose variation of k_a with air flow rate were quite similar to those obtained for the

FDP. The 2nd behavior is associated with the samples compacted at 50% and 60% water content, i.e. wet of optimum. Their k_a (~$1x10^{-8}$ m/s) was virtually not influenced by changes in air flow rate, remaining 40 times lower than the k_a value associated with the sample compacted close to w_{opt} (40%). The 3rd behavior is associated with the sample prepared at ~w_{opt}. In this case, for all practical purposes, the value of k_a (~$3x10^{-7}$ m/s), which did not vary with air flow rate, was one order of magnitude lower than the values obtained from drier samples (20% and 30%).

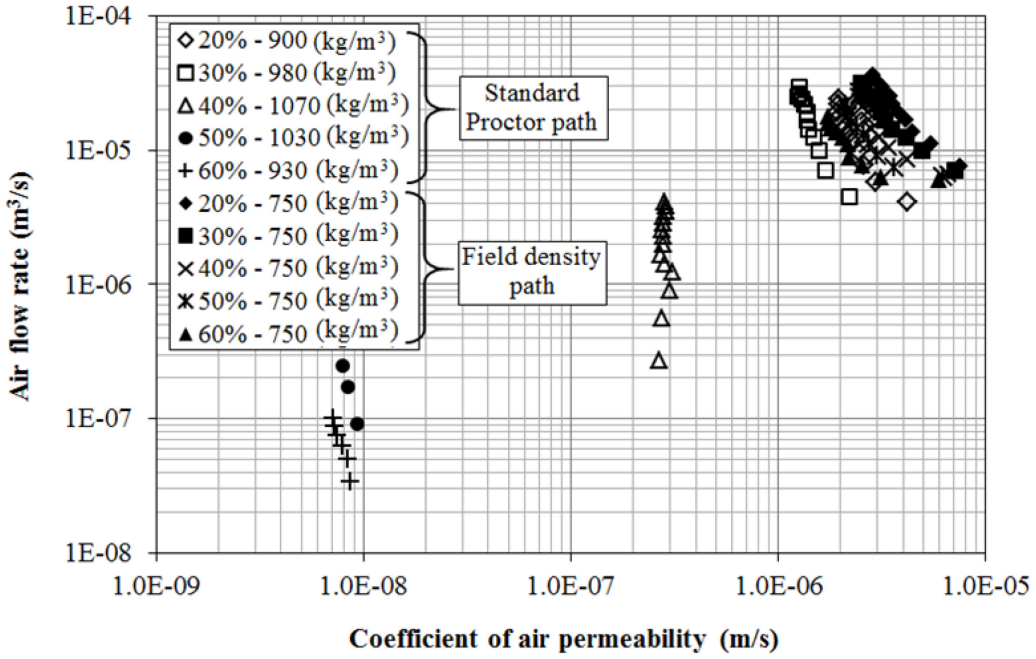

Figure B-4: Relationship between the coefficient of air permeability and air flow rate for samples at field density path and Standard Proctor path, submitted to several differential pressure values.

A very important observation concerning the results in Figure B-4 is that k_a values obtained for samples compacted dry of their respective optimum - which includes all the FDP samples and samples dry of optimum along the SPP - are more than two orders of magnitude higher than the k_a values obtained for samples compacted wet of optimum. Between these two opposite poles is the sample compacted close to w_{opt}.

The results presented above reflect the fact that the air phase is continuous on the dry side of w_{opt}, with larger pores, and occluded, with smaller pores, on the wet side. Similar abrupt decreases of k_a associated with compaction on the wet side of optimum have been reported in the literature [Springer et al., 1998; Maciel and Jucá, 2000; Jucá and Maciel, 2006; Kamiya et al., 2006; Marinho and Teixeira, 2013]. These studies did associate the drops in k_a with occluded air phase, in opposition to continuous air phase on the dry side of optimum.

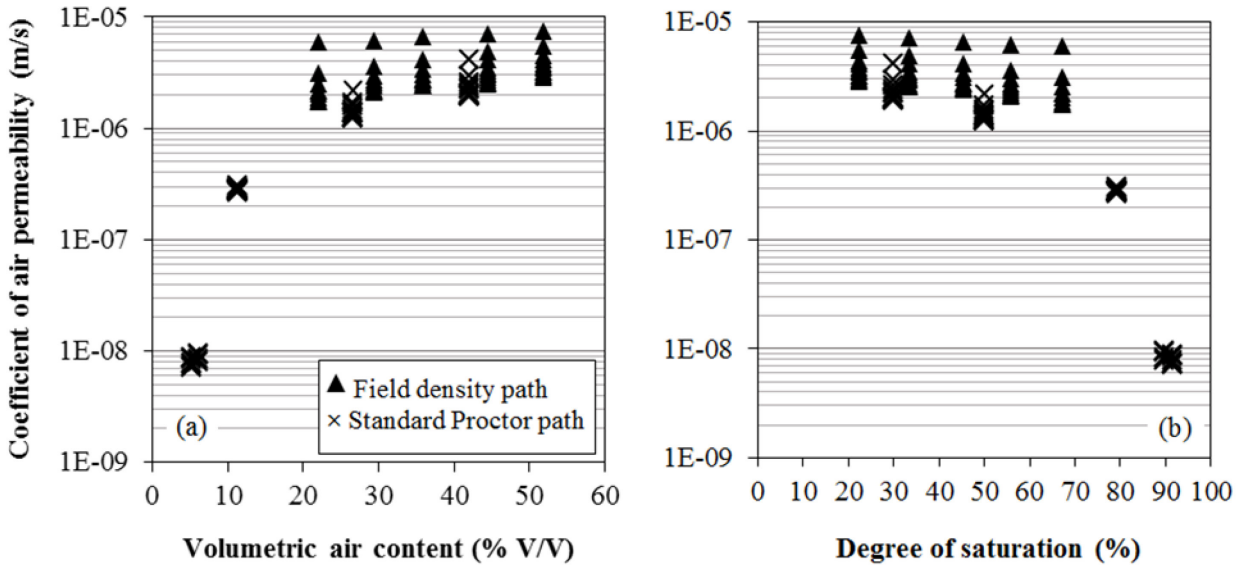

Figure B-5: Relationship between the coefficient of air permeability at several differential pressure values and (a) volumetric air content; (b) degree of saturation.

Figure B-5a presents the relationship between θ_a and k_a. These results show that an abrupt change in k_a occurred when the θ_a was approximately 12%. According to the results presented in Figure B-5b, the corresponding S_r was in the vicinity of 80%. The critical θ_a value of 12% is far greater than the 4% and 7% (inflection points) found in Figure B-2 and Figure B-3. This seems to indicate that inflection points obtained from SACC is not necessarily the most reliable criteria to indicate the onset of air occlusion within compacted soils.

3. Concluding remarks

A well-designed PMOB ensures that surface emissions are lower than allowed by regulation (ideally close to nil). The PMOB has to allow upward migration of CH_4 in such a manner that the residence time of this gas within the MOL is sufficient for its biotic oxidation into CO_2. In the end, a good design is tributary of the placement conditions of the materials forming the PMOB, in particular the MOL. Depending on the coefficient of air permeability of the material under expected placement (compaction) conditions (i.e. dry density and water content), gas migration through the MOL may be well distributed or concentrated, leading to hot spots at the surface. The latter are related to non-uniform distribution of biogas at the base of the MOL-GDL interface, which, in turn, is caused by the creation of a capillary barrier that results from a contrast in hydraulic properties between the two materials.

The focus of this paper was on how the coefficient of air permeability of the material used to construct the MOL of an experimental PMOB varied with variations in compaction conditions. More precisely, the onset of an abrupt change in the coefficient of air permeability needed to be defined. It was shown that the soil-air characteristic curve is not the best curve to identify the transition between continuous and occluded pores. Instead, the transition depends on the fabric that is formed during compaction.

Based on tests performed on samples compacted at several dry densities and water contents along the Standard Proctor curve and at the field dry density, it was shown that the onset of an

abrupt change in the coefficient of air permeability occurs near the optimum degree of saturation. The results also showed that compaction dry of optimum creates a fabric that can ensure proper migration of CH_4 within the MOL, irrelevant of the fact that the material may become saturated due to infiltration.

REFERENCES

Abdolahzadeh, A. M. (2011). *Geotechnical and Hydraulic Behaviour of Cover with Capillary Barrier Effect Combined with a Seepage Control Barrier Made-up of Recycled Materials*. Ph.D. Thesis, Université de Sherbrooke, Sherbrooke.

Abdolahzadeh, A. M., Cabral, A., Lafond, J. and Allaire, S. (2010). Hydraulic Aspects of the Design of a Passive Methane Oxidation Biocover. In *GeoFlorida 2010: Advances in Analysis, Modeling & Design*, Florida, USA, ASCE, GeoInstitute.

Adu-Wusu, C. and Yanful, E. K. (2006). Performance of Engineered Test Covers on Acid-Generating Waste Rock at Whistle Mine, Ontario. *Canadian Geotechnical Journal*, volume 43, number1, p. 1-18.

AhouGhalandari, B., Cabral, A. R. and Leroueil, S. (2015). Assessment of Biogas Distribution at the Base of Passive Methane Oxidation Biosystems. In *The XV Panamerican Conference on Soil Mechanics and Geotechnical Engineering*, Buenos Aires, Argentina.

Ahuja, L. R., Naney, J. W., Green, R. E. and Nielsen, D. R. (1984). Macroporosity to Characterize Spatial Variability of Hydraulic Conductivity and Effects of Land Management. *Soil Science Society of America Jouranl*, volume 48, p. 699-702.

Ait-Benichou, S., Jugnia, L.-B., Greer, C. W. and Cabral, A. R. (2009). Methanotrophs and Methanotrophic Activity in Engineered Landfill Biocovers. *Waste Management*, volume 29, number 9, p. 2509-2517.

Arya, L. M. and Paris, J. F. (1981). A Physicoempirical Model to Predict the Soil Moisture Characteristic from Particle-Size Distribution and Bulk Density Data. *Soil Science Society of America Journal*, volume 45, p. 1023-1030

ASTM-D698 (2012). Standard Test Methods for Laboratory Compaction Characteristics of Soil Using Standard Effort (12,400 ft-lbf/ft3 (600 kN-m/m3)). West Conshohocken, PA, ASTM International. ASTM D698-12e1.

ASTM-D2434-68 (2006). Standard Test Method for Permeability of Granular Soils (Constant Head). West Conshohocken, PA, ASTM International. ASTM D2434-68.

ASTM-D6539-13 (2006). Standard Test Method for Measurement of the Permeability of Unsaturated Porous Materials by Flowing Air. West Conshohocken, PA, ASTM International. ASTM-D6539-13.

Aubertin, M., Cifuentes, E., Martin, V., Apithy, S., Bussiere, B., Molson, J., Chapuis, R. P. and Maqsoud, A. (2006). An Investigation of Factors that Influence the Water Diversion Capacity of Inclined Covers with Capillary Barrier Effects. *Geotechnical Special Publication, American Society of Civil Engineers*, volume 147, p. 613-624.

Ba-Te, Zhang, L. and Fredlund, D. (2005). A General Air-phase Permeability Function for Airflow through Unsaturated Soils. In *Slopes and Retaining Structures Under Seismic and Static Conditions*, p. 1-15.

Ball, B. C., O'Sullivan, M. F. and Hunter, R. (1988). Gas Diffusion, Fluid Flow and Derived Pore Continuity Indices in Relation to Vehicle Traffic and Tillage. *Journal of Soil Science*, volume 39, p. 327-339.

Barlaz, M. A., Chanton, J. P. and Green, R. B. (2009). Controls on Landfill Gas Collection Efficiency: Instantaneous and Lifetime Performance. *J. Air Waste Manag. Assoc*, volume 59, number12, p. 1399-1404.

Barral, C., Oxarango, L. and Pierson, P. (2010). Characterizing the Gas Permeability of Natural and Synthetic Materials. *Transport in Porous Media*, volume 81, number 2, p. 277-293.

Benson, C. H. and Gribb, M. M. (1997). Measuring Unsaturated Hydraulic Conductivity in the Laboratory and Field. In *Unsaturated soil engineering practice*, American Society of Civil Engineers, p. 113-168.

Berger, J., Fornés, L. V., Ott, C., Jager, J., Wawra, B. and Zanke, U. (2005). Methane Oxidation in a Landfill Cover with Capillary Barrier. *Waste Management*, volume 25, p. 369-373.

Blackwell, P. S., Ringrose-Voase, A. J., Jayawardane, N. S., Olssons, K. A., Mckenzie, D. C. and Mason, W. K. (1990). The Use of Air-filled Porosity and Intrinsic Permeability to Air to Characterize Structure of Macropore Space and Saturated Hydraulic Conductivity of Clay Soils. *Journal of Soil Science*, volume 41, p. 215-228.

Bohn, S. and Jager, J. (2009). Microbial Methane Oxidation in Landfill top Covers - Process Study on an MBT Landfill. In *12th International Waste Management and Landfill Symposium*, Margherita di Pula, Italy, CISA.

Bohn, S. and Jager, J. (2011). Low Gas Emissions of Mechanically and Biologically Treated Waste and Microbial Methane Oxidation as an Adapted Method for Mitigation of Emissions. In *XIII International Waste Management and Landfill Symposium* S. Margherita di Pula, Italy, CISA Publisher

Bussière, B., Apithy, S., Aubertin, M. and Chapuis, R. P. (2003a). Diversion Capacity of Sloping Covers with Capillary Barrier Effect. In *The 56th Annual Canadian Geotechnical Conference, 4th Joint IAH-CNC, and CGS Groundwater Specialty Conference & 2003 NAGS Conference*, Winnipeg, Manitoba, Canada.

Bussière, B., Aubertin, M. and Chapuis, R. P. (2003b). The Behavior of Inclined Covers Used as Oxygen Barriers. *Canadian Geotechnical Journal*, volume 40, p. 512-535.

Cabral, A., Racine, I., Burnotte, F. and Lefebvre, G. (2000). Diffusion of Oxygen through a Pulp and Paper Residue Barrier. *Canadian Geotechnical Journal*, volume 37, p. 201-217.

Cabral, A. R. (2012). Biorecouvrements d'oxydation passive du méthane pour les sites d'enfouissement, 3RVE. 7.

Cabral, A. R., Létourneau, M., Yanful, E., Song, Q., McCartney, J. S. and Parks, J. (2010a). Geotechnical Issues in the Design and Construction of PMOBs. In *UNSAT 2010*, Barcelona.

Cabral, A. R., Moreina, J. F. V. and Jungia, L. B. (2010b). Biocover Performance of Landfill Methane Oxidation: Experimental Results. *Journal of Environmental Engineering*, volume 136, p. 785-793.

Capanema, M. A. and Cabral, A. R. (2012). Evaluating Methane Oxidation Efficiencies in Experimental Landfill Biocovers by Mass Balance and Carbon Stable Isotopes. *Water Air Soil Pollut*, volume 223, number 9, p. 5623-5635.

Chanton, J., Abichou, T., Langford, C., Hater, G., Green, R., Goldsmith, D. and Swan, N. (2011). Landfill Methane Oxidation Across Climate Types in the U.S. *Environ. Sci. Technol.* , volume 45, p. 313-319.

Chapuis, R. P. (2004). Predicting the Saturated Hydraulic Conductivity of Sand and Gravel Using Effective Diameter and Void Ratio. *Can. Geotech. J.*, volume 41, p. 787-795.

Chi, Z. F., Lu, W. J., Li, H. and Wang, H. T. (2012). Dynamics of CH_4 Oxidation in Landfill Biocover Soil: Effect of O_2/CH_4 Ratio on CH_4 Metabolism. *Environmental Pollution*, volume 170, p. 8-14.

Chiemchaisri, C., Chiemchaisri, W., Chittanukul, K., Soontornlerdwanich, W. and Tanthachoon, N. (2010). Effect of Leachate Irrigation on Methane Oxidation in Tropical Landfill Cover Soil. *J Mater Cycles Waste Manag*, volume 12, p. 161-168.

Dagenais, A.-M., Aubertin, M., Bussiere, B. and Cyr, J. (2005). Performance of the Lorraine Mine Site Cover to Limit Oxygen Migration In *2005 SME Annual Meeting: Got Mining* Salt Lake City, UT, United States Annual Meeting: Got Mining - Preprints, Society for Mining, Metallurgy and Exploration, Littleton, CO 80127-4102, United States,.

Einola, J.-K. M., Kettunen, R. H. and Rintala, J. A. (2007). Responses of Methane Oxidation to Temperature and Water Content in Cover Soil of a Boreal Landfill. *Soil Biology & Biochemistry*, volume 39, p. 1156-1164.

Estes, R. K. and Fulton, P. F. (1956). Gas Slippage and Permeability Measurements. *Petroleum Transactions, AIME*, volume Technical Note 370, p. 338-342.

Fleureau, J. M. and Taibi, S. (1994). A New Apparatus for the Measurement of Polyphasic Permeabilities. In *the 1st International Conference on Environmental Geotechnics (ICEG)*, Edmonton, Alberta, Canada, BiTech Publishers, p. 227-232.

Fredenslund, A. M., Scheutz, C. and Kjeldsen, P. (2010). Tracer Method to Measure Landfill Gas Emissions from Leachate Collection Systems. *Waste Management*, volume 30, p. 2146–2152.

Fredlund, D. G. and Rahardjo, H. (1993). *Soil Mechanics for Unsaturated Soils*, John Wiley & Sons, Inc.

Fredlund, D. G., Rahardjo, H. and Fredlund, M. D. (2012). Air Flow through Unsaturated Soils. In *Unsaturated Soil Mechanics in Engineering Practice*. Hoboken, NJ, USA, volume, John Wiley & Sons, Inc., p. 450-486.

Fredlund, M. D., Wilson, G. W. and Fredlund, D. G. (2002). Use of the Grain-Size Distribution for Estimation of the Soil-Water Characteristic Curve. *Canadian Geotechnical Journal*, volume 39, p. 1103-1117.

Gebert, J., Groengroeft, A. and Pfeiffer, E. M. (2011a). Relevance of Soil Physical Properties for the Microbial Oxidation of Methane in Landfill Covers. *Soil Biol Biochem*, volume 43, p. 1759-1767.

Gebert, J., Röwer, I. U., Scharff, H., Roncato, C. D. L. and Cabral, A. R. (2011b). Can Soil Gas Profiles be Used to Assess Microbial CH_4 Oxidation in Landfill Covers? *Waste Management*, volume 31, p. 987-994.

Geck, C., Gebert, J., Scharff, H., Streese-Kleeberg, J. and Pfeiffer, E.-M. (2012). Heterogeneous Gas Distribution within a Biocover Designed for Methane Oxidation. In *7th Intercontinental Landfill Research Symposium (ICLRS)*, Luleä, Sweden, Poster presentation.

GEO-SLOPE (2010). Seepage Modeling with SEEP/W 2007. G.-S. I. Ltd.

He, R., Wang, J., Xia, F., Mao, L. and Shen, D. (2012). Evaluation of Methane Oxidation Activity in Waste Biocover Soil During Landfill Stabilization. *Chemosphere*, volume 89, p. 672-679.

Hettiarachchi, H., Meegoda, J. and Hettiaratchi, P. (2009). Effects of Gas and Moisture on Modeling of Bioreactor Landfill Settlement. *Waste Management*, volume 29, p. 1018-1025.

Hrad, M., Huber-Humer, M., Wimmer, B. and Reichenauer, T. G. (2012). Design of top Covers Supporting Aerobic in Situ Stabilization of Old Landfills – An Experimental Simulation in Lysimeters. *Waste Management* volume 32 p. 2324-2335.

Huber-Humer, M., Amann, A., Bogolte, T., Dos Santos, M., Hagenauer, I., Pauliny, W., Reichenauer, T., Watzinger, A. and Wimmer, B. (2008). Technischer Leitfaden Methanoxidationsschichten, Leitfaden Methanoxidationsschichten, ÖVA Arbeitsgruppe.

Huber-Humer, M., Röder, S. and Lechner, P. (2009). Approaches to Assess Biocover Performance on Landfills. *Waste Management*, volume 29, p. 2092-2104.

HYPROP-UMS (2013). HYPROP-UMS User's Manual. Art. no. HYPROP Version 02, UMS GmbH München.

IPCC (2001). Intergovernmental Panel on Climate Change: The scientific Basis. Cambridge, UK.

Jucá, J. and Maciel, F. (2006). Gas Permeability of a Compacted Soil Used in a Landfill Cover Layer. In *Fourth International Conference on Unsaturated Soils*, Carefree, Arizona, United States, American Society of Civil Engineers, p. 1535-1546.

Jugnia, L.-B., Cabral, A. R. and Greer, C. W. (2008). Biotic methane oxidation within an instrumented experimental landfill cover. *Ecological Engineering*, volume 33, number 2, p. 102-109.

Jung, Y., Imhoff, P. T., Augenstein, D. C. and Yazdani, R. (2009). Influence of High-Permeability Layers for Enhancing Landfill Gas Capture and Reducing Fugitive Methane Emissions from Landfills. *Journal of Environmental Engineering*, volume 135, number 3, p. 138-146.

Kamiya, K., Bakrie, R. and Honjo, Y. (2006). A New Method for the Measurement of Air Permeability Coefficient of Unsaturated Soil. In *Fourth International Conference on Unsaturated Soils*, Carefree, Arizona, United States, American Society of Civil Engineers, p. 1741-1752.

Khire, M. V., Benson, C. H. and Bosscher, P. J. (2000). Capillary barriers: Design variables and water balance. *Journal of Geotechnical and Geoenvironmental Engineering*, volume 126, number8, p. 695-708.

Kjeldsen, P., Skov, B., Cassini, F., Zishen, M. and Scheutz, C. (2013). Mitigation of Methane Emissions in a Pilot-Scale Biocover System at the Av Milo Landfill, Denmark: System Design and Gas Distribution. In *14th International Waste Management and Landfill Symposium* S. Margherita di Pula, Cagliari, Italy CISA Publisher

Klinkenberg, L. J. (1941). The Permeability of Porous Media to Liquids and Gases. *API Drilling and Production Practice*, volume, p. 200-213.

Klute, A. (1965). Laboratory Measurement of Hydraulic Conductivity of Unsaturated Soils. In *Method of soil analysis*, American Society of Agronomy, p. 253-261.

Lakhouit, A., Schirmer, W. N., Johnson, T. R., Cabana, H. and Cabral, A. R. (2014). Evaluation of the Efficiency of an Experimental Biocover to Reduce BTEX Emissions from Landfill Biogas. *Chemosphere*, volume 97, p. 98-101.

Langfelder, L. J., Chen, C. F. and Justice, J. A. (1968). Air Permeability of Compacted Cohesive Soils. *Journal of the Soil Mechanics and Foundations Division*, volume 94, number 4, p. 981-1002.

Leroueil, S. and Hight, D. W. (2013). Compacted Soils: From Physics to Hydraulic and Mechanical Behaviour. In *First Pan-American Conference on Unsaturated Soils*, Cartagena, Colombia.

Lu, N. and Likos, W. J. (2004). *Unsaturated Soil Mechanics*, John Wiley & Sons, Inc.

Maciel, F. and Jucá, J. (2000). Laboratory and Field Tests for Studying Gas Flow Through MSW Landfill Cover. In *Geo-Denver*, Denver, Colorado, United States, American Society of Civil Engineers, p. 569-585.

Maqsoud, A., Bussière, B., Aubertin, M., Chouteau, M. and Mbonimpa, M. (2011). Field Investigation of a Suction Break Designed to Control Slope-Induced Desaturation in an Oxygen Barrier. *Canadian Geotechnical Journal*, volume 48, p. 53-71.

Marinho, F. A. M., Andrade, M. C. J. and Jucá, J. F. T. (2001). Air and Water Permeability of a Compacted Soil Used in a Solid Waste Landfill in Recife, Brazil. In *the Third BGA Geoenvironmental Engineering Conference*, Edinburg, Scotland, Thomas Telford Publishing, Thomas Telford Ltd., p. 437-442.

Marinho, F. A. M. and Teixeira, P. F. (2013). Air Permeability of Cover Soil from the Bandeirantes Landfill in São Paulo, Brazil. In *Advances in Unsaturated Soils*.

Mbonimpa, M., Aubertin, M., Aachib, M. and Bussière, B. (2003). Diffusion and Consumption of Oxygen in Unsaturated Cover Materials. *Canadian Geotechnical Journal*, volume 40, p. 916-932.

McPhee, C. A. and Arthur, K. G. (1991). Klinkenberg Permeability Measurements: Problems and Practical Solutions. In *Advances in Core Evaluation: Accuracy and Precision in Reserves Estimation*, p. 447-462.

Mirzaii, A. and Yasrobi, S. S. (2012). Influence of Initial Dry Density on Soil-Water Characteristics of Two Compacted Soils. *Géotechnique Letters*, volume 2, p. 193-198.

Mualem, Y. (1976). A New Model For Predicting the Hydraulic Conductivity of Unsaturated Porous Media. *Water Resources Research*, volume 12, p. 513-522.

Muskat, M. (1937). *The Flow of Homogeneous Fluids through Porous Media.* New York, McGraw-Hill.

Ndanga, É. M., Bradley, R. L. and Cabral, A. R. (2015). Does Vegetation Affect the Methane Oxidation Efficiency of Passive Biosystems? *Waste Management*, volume 38, p. 240-249.

Nuth, M. and Laloui, L. (2008). Advances in Modelling Hysteretic Water Retention Curve in Deformable Soils. *Computers and Geotechnics*, volume 35, p. 835-844.

Parent, S. E. and Cabral, A. (2006). Design of Inclined Covers with Capillary Barrier Effect *Geotechnical and Geological Engineering Journal,* volume 24, p. 689-710.

Pokhrel, D., Hettiaratchi, P. and Kumar, S. (2011). Methane Diffusion Coefficient in Compost and Soil-Compost mixtures in Gas Phase Biofilter. *Chem Eng J.,* volume 169, p. 200-206.

Rachor, I., Gebert, J., Gröngröft, A. and Pfeiffer, E. M. (2011). Assessment of the Methane Oxidation Capacity of Compacted Soils Intended for Use as Landfill Cover Materials. *Waste Management*, volume 31, p. 833-842.

Rajesh, S., Gourc, J. P. and Viswanadham, B. V. S. (2014). Evaluation of Gas Permeability and Mechanical Behaviour of Soil Barriers of Landfill Cap Covers through Laboratory Tests. *Applied Clay Science*, volume 97-98, p. 200-214.

Reichenauer, T. G., Watzinger, A., Riesing, J. and Gerzabek, M. H. (2011). Impact of Different Plants on the Gas Profile of a Landfill Cover. *Waste Management,* volume 31, p. 843-853.

Rodeck, S. A., DeVantier, B. A. and Das, B. M. (1994). Air-Permeability Measurement for Soil at Low and High Pressure. *Journal of Environmental Engineering*, volume 120, p. 1337-1343.

Roncato, C. D. L. and Cabral, A. R. (2012). Evaluation of Methane Oxidation Efficiency of Two Biocovers: Field and Laboratory Results. *Journal of Environmental Engineering*, volume 138, number 2, p. 164-173.

Ross, B. (1990). Diversion Capacity of Capillary Barriers. *Water Resources Research*, volume 26, number 10, p. 2625-2629.

Röwer, I. U., Gebert, J., Streese-Kleeberg, J., Kleinschmidt, V., Melchior, S., Scharff, H. and Pfeiffer, E.-M. (2012). Heterogeneous Emission from a Biocover Designed for Methane Oxidation. In *7th Intercontinental Landfill Research Symposium (ICLRS)*, Luleä, Sweden, Poster presentation.

Sadasivam, B. Y. and Reddy, K. R. (2014). Landfill Methane Oxidation in Soil and Bio-Based Cover Systems: a Review. *Rev Environ Sci Biotechnol*, volume 13, p. 79-107.

Samingan, A. S., Leong, E.-C. and Rahardjo, H. (2003). A Flexible Wall Permeameter for Measurements of Water and Air Coefficients of Permeability of Residual Soils. *Can. Geotech. J.*, volume 40, p. 559-574.

Scheutz, C., Fredenslund, A. M., Chanton, J., Pedersen, G. B. and Kjeldsen, P. (2011). Mitigation of Methane Emission from Fakse Landfill Using a Biowindow System. *Waste Management*, volume 31, p. 1018-1028.

Scheutz, C., Kjeldsen, P., Bogner, J. E., De Visscher, A., Gebert, J., Hilger, H. A., Huber-Humer, M. and Spokas, K. (2009a). Microbial Methane Oxidation Processes and Technologies for Mitigation of Landfill Gas Emissions. *Waste Management and Research*, volume 27, number 5, p. 409-455.

Scheutz, C., Pedersen, G. B., Costa, G. and Kjeldsen, P. (2009b). Biodegradation of Methane and Halocarbons in Simulated Landfill Biocover Systems Containing Compost Materials. *Journal of Environ. Quality*, volume 38, number 4, p. 1363-1371.

Spokas, K., Bogner, J., Chanton, J. P., Morcet, M., Aran, C., Graff, C., Golvan, Y. M.-L. and Hebe, I. (2006). Methane Mass Balance at Three Landfill Sites: What is the Efficiency of Capture by Gas Collection Systems? *Waste Management*, volume 26, number 5, p. 516-525.

Spokas, K. A. and Bogner, J. E. (2011). Limits and Dynamics of CH4 Oxidation on Landfill Cover Soils. *Waste Management*, volume 31, p. 823-832.

Springer, D. S., Loaiciga, H. A., Cullen, S. J. and Everett, L. G. (1998). Air Permeability of Porous Materials Under Controlled Laboratory Conditions. *Groundwater*, volume 36, number 4, p. 558-565.

Staub, M. J., Marcolina, G., Gourc, J.-P. and Simonin, R. (2011). An Incremental Model to Assess the Environmental Impact of Cap Cover Systems on MSW Landfill Emissions. *Geotextiles and Geomembranes*, volume 29, p. 298-312.

Steenhuis, T. S., Parlange, J. Y. and Kung, K. J. S. (1991). Comment on "the Diversion Capacity of Capillary Barriers" by Benjamin Ross (paper 91WR01366). *Water Resources Research*, volume 27, number 8, p. 2155.

Stormont, J. C. (1996). The Effectiveness of Two Capillary Barriers on a 10% Slope. *Geotechnical and Geological Engineering Journal*, volume 14, p. 243-267.

Tang, A. M., Cui, Y.-J., Richard, G. and Défossez, P. (2011). A Study on the Air Permeability as Affected by Compression of Three French Soils. *Geoderma*, volume 162, p. 171-181.

Tate, K. R. (2015). Soil Methane Oxidation and Land-Use Change - from Process to Mitigation. *Soil Biology & Biochemistry*, volume 80, p. 260-272.

Tétreault, P., Cabral, A. R. and Abdolahzadeh, A. M. (2013). Non-Uniform Distribution of Biogas under a Biocover due to Capillary Barrier Effect: Case Studies. In *GEOMontreal*, Montreal, Canada.

USEPA (2011). Inventory of U.S. Greenhouse Gas Emissions and Sinks: 1990 - 2009. Washington, U.S. Environmental Protection Agency**:** 459.

Vachon, B. L., Abdolahzadeh, A. M. and Cabral, A. R. (2015). Predicting the Diversion Length of Capillary Barriers Using Steady State and Transient State Numerical Modeling: Case Study of the Saint-Tite-des-Caps Landfill Final Cover. *Can. Geotech. J.*, volume 52, p. 2141-2148.

van Genuchten, M. T. (1980). A closed-form equation for predicting the hydraulic conductivity of unsaturated soils. *Soil Science Society of America Journal*, volume 44, p. 892-898.

Vangpaisal, T. and Bouazza, A. (2004). Gas Permeability of Partially Hydrated Geosynthetic Clay Liners. *Geotech. Geoenviron. Eng. ASCE*, volume 130, number5, p. 93-102.

Vaughan, P. R. (2003). Observations on the Behaviour of Clay Fill Containing Occluded Air Bubbles. *Géotechnique*, volume 53, number 2, p. 265-272.

Walter, M. T., Kim, J. S., Steenhuis, T. S., Parlange, J. Y., Heilig, A., Braddock, R. D., Selker, J. S. and Boll, J. (2000). Funneled Flow Mechanisms in a Sloping Layered Soil: Laboratory Investigation. *Water Resources Research*, volume 36, number 4, p. 841-849.

Williams, D. J., Wilson, G. W. and Currey, N. A. (1997). A Cover System for a Potentially Acid Forming Waste Rock Dump in a Dry Climate. In *4th International Conference on Tailings and Mine Waste 97,* Balkema, Rotterdam, Fort Collins, CO

Wilson, G. W., Barbour, S. L., Swanson, D. and O'Kane, M. (1995). Instrumentation and Modelling for Saturated/Unsaturated Performance of Soil Covers for Acid Generating Waste Rock. *Hydrogéologie,* volume 4, p. 99-108.

Wind, G. P. (1968). Capillary Conductivity Data Estimated by a Simple Method. In *R.E. Rijtema and H. Wassink (ed.) Water in the Unsaturated Zone: Proc. UNESCO/IASH Symp.*, Wageningen, the Netherlands, p. 181-191.

Wu, Y. S., Pruess, K. and Persoff, P. (1998). Gas Flow in Porous Media with Klinkenberg Effects. *Transport in Porous Media*, volume 32, p. 117-137.

Yanful, E. K. (1993). Oxygen Diffusion through Soil Covers on Sulphidic Mine Tailings. *Journal of Geotechnical Engineering*, volume 119, number 8, p. 1207-1228.

Zamoranoa, M., Pérezb, J. I. P., Pavésc, I. A. and Ridaoa, Á. R. (2007). Study of the Energy Potential of the Biogas Produced by an Urban Waste Landfill in Southern Spain. *Renewable and Sustainable Energy Reviews*, volume 11, number 5, p. 909-922.